LUND UNIVERSITY

Measurement Based Channel Characterization and Modeling for Vehicle-to-Vehicle Communications

Abbas, Taimoor

2014

Link to publication

LUND UNIVERSITY

PO Box 117
221 00 Lund
+46 46-222 00 00

Measurement Based Channel Characterization and Modeling for Vehicle-to-Vehicle Communications

–

Taimoor Abbas

Lund 2014

To my parents,
Ghulam Abbas,

&

Nusrat Parveen,
Without whom none of my success would be possible.

Abstract

Vehicle-to-Vehicle (V2V) communication is a challenging but fast growing technology that has potential to enhance traffic safety and efficiency. It can also provide environmental benefits in terms of reduced fuel consumption. The effectiveness and reliability of these applications highly depends on the quality of the V2V communication link, which rely upon the properties of the propagation channel. Therefore, understanding the properties of the propagation channel becomes extremely important. This thesis aims to fill some gaps of knowledge in V2V channel research by addressing four different topics. The first topic is channel characterization of some important safety critical scenarios (papers I and II). Second, is the accuracy or validation study of existing channel models for these safety critical scenarios (papers III and IV). Third, is about channel modeling (paper V) and, the fourth topic is the impact of antenna placement on vehicles and the possible diversity gains. This thesis consists of an introduction and six papers:

Paper I presents a double directional analysis of vehicular channels based on channel measurement data. Using SAGE, a high-resolution algorithm for parameter estimation, we estimate channel parameters to identify underlying propagation mechanisms. It is found that, single-bounce reflections from static objects are dominating propagation mechanisms in the absence of line-of-sight (LOS). Directional spread is observed to be high, which encourages the use of diversity-based methods.

Paper II presents results for V2V channel characterization based on channel measurements conducted for merging lanes on highway, and four-way street intersection scenarios. It is found that the merging lane scenario has the worst propagation condition due to lack of scatterers. Signal reception is possible only with the present LOS component given that the antenna has a good gain in the direction of LOS. Thus designing an antenna that has an omni-directional gain, or using multiple antennas that radiate towards different directions become more important for such safety critical scenarios.

Paper III presents the results of an accuracy study of a deterministic ray

tracing channel model for vehicle-to-vehicle (V2V) communication, that is compared against channel measurement data. It is found that the results from measurement and simulation show a good agreement especially in LOS situations where as in NLOS situations the simulations are accurate as far as existing physical phenomena of wave propagation are captured by the implemented algorithm.

Paper IV presents the results of a validation study of a stochastic NLOS pathloss and fading model named *VirtualSource11p* for V2V communication in urban street intersections. The reference model is validated with the help of independent channel measurement data. It is found that the model is flexible and fits well to most of the measurements with a few exceptions, and we propose minor modifications to the model for increased accuracy.

Paper V presents a shadow fading model targeting system simulations based on channel measurements. The model parameters are extracted from measurement data, which is separated into three categories; line-of-sight (LOS), LOS obstructed by vehicles (OLOS), and LOS blocked by buildings (NLOS), with the help of video information recorded during the measurements. It is found that vehicles obstructing the LOS induce an additional attenuation in the received signal power. The results from system level vehicular ad hoc network (VANET) simulations are also presented, showing that the LOS obstruction affects the packet reception probability and this can not be ignored.

Paper VI investigates the impact of antenna placement based on channel measurements performed with four omni-directional antennas mounted on the roof, bumper, windscreen and left-side mirror of the transmitter and receiver cars. We use diversity combining methods to evaluate the performance differences for all possible single-input single-output (SIMO), multiple-input single-output (MISO) and multiple-input multiple-output (MIMO) link combinations. This investigation suggests that a pair of antennas with complementary properties, e.g., a roof mounted antenna together with a bumper antenna is a good solution for obtaining the best reception performance, in most of the propagation environments.

In summary, this thesis describes the channel behavior for safety-critical scenarios by statistical means and models it so that the system performance can be assessed in a realistic manner. In addition to that the influence of different antenna arrangements has also been studied to exploit the spatial diversity and to mitigate the shadowing effects. The presented work can thus enable more efficient design of future V2V communication systems.

Preface

This doctoral thesis concludes my work as a Ph.D. student, and is comprised of two parts. The first part gives an overview of the research field in which I have been working during my Ph.D. studies and a brief summary of my contribution in it. The second part is composed of six included papers that constitute my main scientific work:

[1] T. Abbas, J. Karedal, F. Tufvesson, A. Paier, L. Bernadó, and A. F. Molisch, "Directional analysis of vehicle-to-vehicle propagation channels," in *Proc. IEEE* 73rd *Vehicular Technology Conference (VTC2011-Spring)*, Budapest, Hungary, pp. 01–05, May 2011.

[2] T. Abbas, L. Bernadó, A. Thiel, C. F. Mecklenbräuker and F. Tufvesson, "Radio channel properties for vehicular communication: Merging lanes versus urban intersections," in *IEEE Vehicular Technology Magazine (VTM)*, vol. 08, no. 04, pp. 27–34, Dec. 2013.

[3] T. Abbas, J. Nuckelt, T. Kürner, T. Zemen C. F. Mecklenbräuker, and F. Tufvesson, "Simulation and Measurement Based Vehicle-to-Vehicle Channel Characterization: Accuracy and Constraint Analysis," *Submitted to IEEE Trans. on Antennas and Propagation.*

[4] T. Abbas, A. Thiel, T. Zemen, C. F. Mecklenbräuker and F. Tufvesson, "Validation of a non-line-of-sight path-loss model for V2V communications at street intersections," in *Proc.* 13th *International Conference on ITS Telecommunications (ITST)*, Tampere, Finland, pp. 198–203, Nov. 2013.

[5] T. Abbas, K. Sjöberg, J. Karedal, and F. Tufvesson, "A measurement based Shadow Fading Model for Vehicle-to-Vehicle Network Simulations," *Submitted to IEEE Trans. on Intelligent Transportation Systems.*

[6] T. Abbas, J. Karedal, and F. Tufvesson, "Measurement-based analysis: The effect of complementary antennas and diversity on vehicle-to-vehicle com-

munication," in *IEEE Antennas and Wireless Propagation Letters (AWPL)*, vol. 12, no. 1, pp. 309–312, 2013.

During my Ph.D. studies, I have also contributed to the following publications. However, these publications are not included in the thesis:

[7] T. Abbas, and F. Tufvesson, "Line-of-Sight Obstruction Analysis for Vehicle-to-Vehicle Network Simulations in a Two Lane Highway Scenario," in *Hindawi International Journal of Antennas and Propagation, Special Issue on Radio Wave Propagation and Wireless Channel Modeling* vol. 2013, pp. 01–09, Nov. 2013.

[8] T. Abbas, and F. Tufvesson, "System Identification in GSM/EDGE Receivers Using a Multi-Model Approach," in *International Journal on Control System and Instrumentation*, vol. 03, no. 01, pp. 41–46, 2012.

[9] D. Vlastaras, T. Abbas, D. Leston, and F. Tufvesson, "Universal Medium Range Radar and IEEE 802.11p Modem Solution for Integrated Traffic Safety," in 13th *International Conference on ITS Telecommunications (ITST)*, Tampere, Finland, pp. 193–197, Nov. 2013.

[10] A. Theodorakopoulos, P. Papaioannou, T. Abbas, and F. Tufvesson, "A Geometry Based Stochastic Model for MIMO V2V Channel Simulation in Cross-Junction Scenario," in *Proc. 13th International Conference on ITS Telecommunications (ITST)*, Tampere, Finland, pp. 290–295, Nov. 2013.

[11] T. Abbas, L. Bernadó, A. Thiel, C. F. Mecklenbräuker and F. Tufvesson, "Measurements Based Channel Characterization for Vehicle-to-Vehicle Communications at Merging Lanes on Highway," in *Proc. 5th International Symposium on Wireless Vehicular Communications (WIVEC2013)*, Dresden, Germany, pp. 01–05, June 2013.

[12] J. Nuckelt, T. Abbas, F. Tufvesson, C. F. Mecklenbräuker, L. Bernadó, and T. Kürner, "Comparison of ray tracing and channel-sounder measurements for vehicular communications," in *Proc. IEEE 77th Vehicular Technology Conference (VTC2013-Spring)*, Dresden, Germany, pp. 01–05, June 2013.

[13] R. Chandra, T. Abbas, and A. Johansson, "Directional Analysis of the On-Body Propagation Channels considering Human's Anatomical Variations," in *Proc. 7th International Conference on Body Area Networks (BodyNets2012)*, Oslo, Norway, pp. 120–123, Sept. 2012.

[14] T. Abbas, F. Tufvesson, "System Identification in GSM/EDGE Receivers Using a Multi-Model Approach," in *Proc. Second International Conference*

on Advances in Information and Communication Technologies (ICT2011), Amsterdam, Netherlands, pp. 41–46, Dec. 2012.

[15] J. Karedal, F. Tufvesson, T. Abbas, O. Klemp, A. Paier, L. Bernadó, and A. F. Molisch, "Radio channel measurements at street intersections for vehicle-to-vehicle applications," in *Proc. IEEE* 71st *Vehicular Technology Conference (VTC2010-Spring)*, Taipei, Taiwan, pp. 01–05, May 2010.

[16] S. M. Sulaman, T. Abbas, Krzysztof Wnuk and Martin Höst, "Hazard Analysis of Forward Collision Avoidance System using STPA," in 11th *International Conference on Information Systems for Crisis Response and Management (ISCRAM 2014)*, Penn State University, USA, May. 2014. (Accepted as a short paper)

During my graduate studies, I have also been presenting my research outcomes as temporary documents (TDs) in the European Cooperation in Science and Technology (COST) actions COST2100 and IC1004:

[17] T. Abbas, J. Nuckelt, T. Kürner, C. F. Mecklenbräuker, and F. Tufvesson, "Simulation and Measurement Based Vehicle-to-Vehicle Channel Characterization for Urban Street Intersection," in *COST IC1004* 7th *Management Committee and Scientific Meeting*, TD(13)07059, Ilmenau, Germany, May 2013.

[18] J. Nuckelt, T. Abbas, F. Tufvesson, C. F. Mecklenbräuker, L. Bernado, and T. Kürner, "Comparison of ray tracing and channel-sounder measurements for vehicular communications," in *COST IC1004* 5th *Management Committee and Scientific Meeting*, TD(12)05031, Bristol, UK, Sept. 2012.

[19] T. Abbas, J. Karedal, and F. Tufvesson, "Shadow Fading Model for Vehicle-to-Vehicle Network Simulators," in *COST IC1004* 5th *Management Committee and Scientific Meeting*, TD(12)05020, Bristol, UK, Sept. 2012.

[20] T. Abbas, J. Karedal, and F. Tufvesson, "Initial Investigation to study the Effect of Antenna Placement in Vehicle-to-Vehicle Communications," in *COST IC1004 Technical Meeting*, TD(11)01033, Lund, Sweden, June 2011.

[21] T. Abbas, J. Karedal, F. Tufvesson, A. Paier, L. Bernadó, A. Molisch, "Directional Analysis of Vehicle-to-Vehicle Propagation in Different Traffic Environments," in *COST2100* 12th *Management Committee and Scientific Meeting*, TD(10)12083, Bologna Italy, Nov. 2010.

Acknowledgements

The journey that I set out on in Autumn 2009 ends with the writing of this thesis. It's been long but exciting. I do not feel tired but motivated because I have had the company and generous support of some incredible people, to whom I owe my gratitude. To their kindness,

> *"I can no other answer make but thanks,*
> *And thanks"*
> – Shakespeare.

First and foremost, I would like to express my sincere thanks and heartfelt gratitude to my supervisor, Prof. Fredrik Tufvesson, for his great support, valuable feedback, insightful discussions and encouragement throughout my thesis. His deep knowledge of wireless communications, enthusiasm towards research, ready-availability and organized personality, has been a constant source of inspiration. Working with him has been a wonderful experience. I am also grateful to Dr. Johan Karedal, my co-adviser during first half of my PhD studies, for his support in scientific matters, fruitful discussions and critical feedback. His dedication to the job and keen interest in research served as a true source of motivation. I am also thankful to Prof. Ove Edfors for his role as my co-supervisor, during second half of my PhD, and for helping me with the proofreading of my thesis. I am also indebted to Prof. Andreas F. Molisch for his kind attitude, thoughtful discussions and precious feedback on my results during his short biannual visits to Lund.

I am grateful to all of my research colleagues and co-authors at Lund and abroad for wonderful collaborations: Prof. Christoph F. Mecklenbräuker, Prof. Thomas Zemen, Dr. Laura Bernadó, Dr. Katrin Sjöberg, Dr. Alexander Paier, Rohit Chandra, Dr. Andreas Thiel, Dimitrios Vlastaras, Andreas Theodorakopoulos, and finally, Prof. Thomas Kürner, and Jörg Nuckelt for being my host during a short term scientific mission at TU-Braunschweig, Germany.
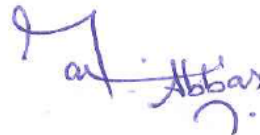
My sincere thanks in particular to my office-mates Rohit Chandra, and Dimitrios Vlastaras, and to many of my gregarious seniors and colleagues at

List of Acronyms and Abbreviations

ACF auto-correlation function

AOA angle-of-arrival

AOD angle-of-departure

CDMA code division multiple access

CIR channel impulse response

DSD Doppler spectral density

EKF extended Kalman filter

EM electromagnetic

EV eigenvalue

ETSI European telecommunication standards institute

FDTD finite-difference time-domain

FEM finite element method

GPRS general packet radio service

GSCM geometry based stochastic channel model

GSM global system for mobile communications

IEEE Institute of Electrical and Electronics Engineers

IoT internet of things

ITS intelligent transportation system

LOS line-of-sight

LSF local scattering function

LTE long-term evolution

LTI linear time invariant

LTV linear time variant

MBCM measurement based channel modeling

MF matched filter

MIMO multiple-input multiple-output

MSE mean square error

MPC multipath component

M2M mobile-to-mobile

NLOS non-line-of-sight

OFDM orthogonal frequency division multiplexing

PAR peak-to-average-ratio

PDP power delay profile

PDF probability density function

RMS root mean square

RT ray-tracing

RX receiver

SAGE space-alternating generalized expectation maximization

SF shadow fading

SISO single-input single-output

SVD singular value decomposition

TDL tap-delay-line

TX transmitter

T2V truck-to-vehicle

US uncorrelated scattering

V2I vehicle-to-infrastructure

V2V vehicle-to-vehicle

WCDMA wide-band code division multiple access

WLAN wireless local area network

WSN wireless sensor network

WSS wireless sensor network

WSSUS wide-sense-stationary uncorrelated-scattering

Contents

Part I

Overview of Vehicular Channels

Chapter 1

Introduction

Wireless communication is the oldest form of communication - jungle drums, smoke and light signals have long been used for quick communication over long distances since the early evolution of mankind. However, the story of wireless communication as we know begins with the discovery of electromagnetic (EM) waves; first predicted mathematically by Scottish mathematical physicist James Clerk Maxwell in 1867 [1], which were experimentally demonstrated later by Heinrich Hertz in 1885 who generated EM waves in his laboratory. A radio receiver built in 1994 by a Russian physicist named Alexander Stepanovich Popov, sometimes spelled Popoff, and a wireless telegraph system in 1896 by Guglielmo Marconi are among the very first wireless communication devices [2]. Since then new wireless communication methods and services have been developed and adopted by the people all around the world. The latest three decades have witnessed an enormous growth in the use of wireless communications. Until recently this growth was mainly associated to the cellular telephony that started back in 1980's, when wireless communication was first time available to the masses. Cellular communication started as analog systems and evolved as 2G (GSM, CDMA), 3G (GPRS, WCDMA), 4G (LTE) and beyond with the main goal to increase throughput and capacity.

The story does not end with the evolution of cellular systems; the advancements in digital electronics has made electronics devices more efficient with reduced price, thus making smart devices and wireless sensors an integrated part of our daily life. Moreover, IEEE standards for wireless local area network (WLAN) such as 802.11, and recent inclusion of technologies like machine-to-machine (M2M) cooperative communications, wireless sensor networks (WSN), internet-of-things (IoTs) together with cloud computing have introduced a new paradigm that will enable future heterogeneous communica-

3

tion networks. Today, more and more wireless communication technologies are being developed that are changing our working habits and have significantly influenced our everyday lives. The applications of these new technologies are spreading rapidly in various fields of life such as social networking, health, environmental protection, economics, mobility, transportation and logistics, and, disaster management and preventions.

Among these of particular interest here are the mobility related applications as the land transportation systems have become crucial components of modern world. On one hand they are beneficial in terms of speedy transportation of goods and people, but on the other hand they are linked to an increasing number of road accidents worldwide. According to the world health organization (WHO), it is estimated that 1.2 million people die each year on the world's roads and 50% of those are vulnerable road users, i.e., 23% motorcyclists, 22% pedestrians and 5% cyclists [3]. In the report it is stated that in 1990 road crashes were the ninth leading cause of disability/death worldwide, and if no further actions are taken to counter this then by 2020, road crashes are predicted to be the third leading cause of disability/death worldwide, which is alarming.

Nowadays, more and more computerized systems and technologies are becoming part of our vehicles, and thus a vehicle in future will be equipped with many different technologies for navigation, location information, safety and inter-vehicle communication. It is anticipated that these systems and technologies can reduce the rate of accidents as well as they can make traffic more efficient.

Intelligent transportation system (ITS); the system which rely on cooperative communication, in general, and networking, in particular, among vehicles thus have the potential to ensure on-road safety, driving comfort and traffic efficiency [4]. Following two main paradigms enable cooperative communications in the connected vehicle domain: First, infrastructure assisted, i.e., vehicle-to-infrastructure (V2I) communications; and second, ad-hoc multi-hop broadcasting, i.e., vehicle-to-vehicle (V2V) communications. However, a hybrid approach where both V2V and V2I can be utilized w.r.t. the ITS applications at hand. Multiple communication technologies and protocols, e.g., IEEE 802.11p, WCDMA, LTE etc., are envisioned to be the base technologies for ITS as shown in Fig. 1.1.

For the safety related applications, V2V communication is a more suitable candidate. It allows vehicles to communicate directly with minimal latency. The primary objective with the message exchange is to improve active on-road safety and situation awareness, e.g., collision avoidance, traffic re-routing, navigation, etc. The reliability of V2V safety applications, which use IEEE 802.11p as the underlying communication technology, highly depend on the quality of
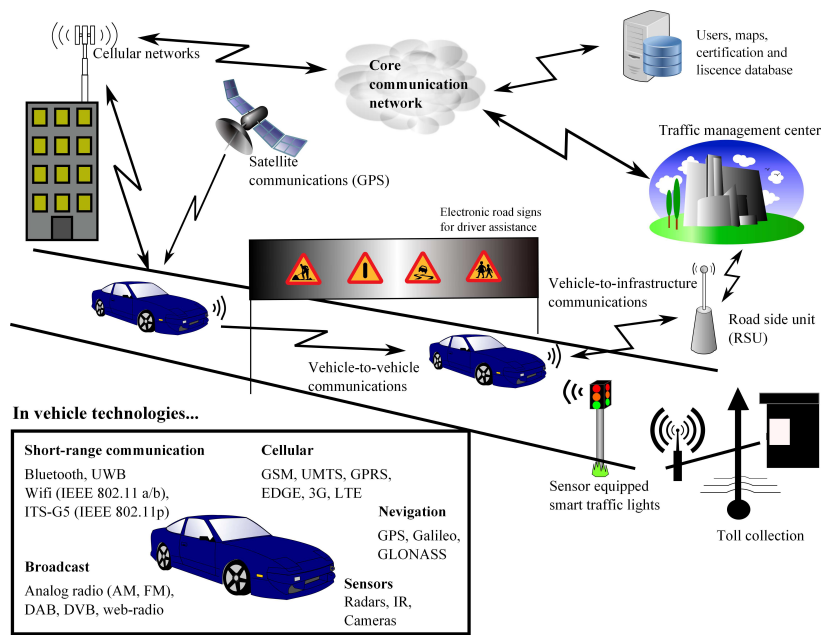
Figure 1.1: Some of the major components of future intelligent transportation system (ITS) and their inter-communications. The inset figure shows in-vehicle technologies for future vehicles [4, 106].

the communication link [6], which rely upon the properties of the propagation channel. It is the channel that determines the ultimate performance limits of any communication system.

It is important to mention that the propagation channel in V2V networks is significantly different from that in cellular networks and thus the results from cellular channel research are not directly applicable to V2V channels. V2V employs an ad-hoc network topology, both transmitter (TX) and receiver (RX) are highly mobile, and TX/RX antennas are situated on approximately the same height and close to the ground level, implying that the V2V channel is more dynamic and non-stationary. Thus, to develop an efficient and reliable system a deep understanding of V2V channel characteristics is required [7].

In this thesis a measurement based characterization and modeling of V2V channels are presented with the main goal to gain a deeper understanding about the channels for an optimized V2V system design. Measurement based analysis is performed in three steps: First, collection of data with channel measurements. Second, channel characterization by analyzing metrics such as

path-loss, fading, time and frequency selectivity, directional properties, and antenna properties to understand key figures of merits. Finally, the third step is modeling the channel such that the certain properties of the channel can be reproduced for system simulation and testing.

The remainder of Part I provides an overview of the research field in such a way that it serves as a refresher for a reader who is familiar with the area of wireless communication systems and a tutorial for other readers. In chapter II we discuss the fundamentals of propagation channel by first describing the channel from a system theoretic point of view. We review characterization and modeling of propagation channels in general and discuss measurement based modeling in particular. Chapter III provides state of the art concerning the vehicle-to-vehicle channels that is relevant to the work presented in this thesis. Chapter IV is about channel measurements where we discuss measurement techniques, used equipment and underlying considerations for the channel measurements. We also give details about channel measurement campaigns we performed over the past few years. Finally, in chapter V we present a summary and highlight contributions of the included papers.

Chapter 2

Propagation Channel fundamentals

Communication systems, wired or wireless, are designed to deliver data packets from the transmitter to the receiver via a physical medium called the channel. In a wireless communication system, the electromagnetic (EM) waves propagate from the transmitter to the receiver over an air-interface, called propagation channel. The description of the propagation channel is influenced by a number of factors such as carrier frequency, bandwidth (narrowband or wideband), number of TX and RX antennas (SISO or MIMO systems), and the propagation environment. It is the properties of the propagation channel that ultimately definte the performance of wireless communication systems, therefore understanding the properties of the propagation channel becomes extremely important for an efficient system design.

In this chapter, we first discuss channel characterization and describe the propagation channel from a system theoretic point of view. We then briefly review statistical channel metrics required to understand the channel properties. We then describe different approaches for channel modeling in order to be able to reproduce channel statistics for system simulations. Finally, in the last section we discuss measurement based channel characterization and modeling which is the main focus of this thesis.

2.1 Channel Characterization

The term channel characterization is used to define the characteristics of the propagation channel in a specific environment by means of simulations as well

as empirical data analysis with a goal to understand the channel behavior and underlying propagation mechanisms. Propagation of EM waves in the channel is governed by four main propagation mechanisms: first, free space propagation due to a line-of-sight path, and other three, reflection, diffraction or scattering due to objects in the surroundings, referred as scatterers. Scatterers give rise to multipath propagation, i.e., multiple attenuated and delayed echoes of the transmitted signal arriving at the receiver from different directions [8]. The superposition of all of these multipath components (MPCs) at a certain instant gives the channel impulse response (CIR) of the channel. In other words, the CIR contains information about each MPC and their interaction with each other, and therefore, the propagation channel can be completely described by a CIR, which under normal conditions can be treated as a linear filter. The CIR can either be obtained by performing channel measurements or it can be derived analytically by solving Maxwell's equations, the later case is usually not feasible. As typical environments are so complex making making it difficult to use Maxwell's equations. The main focus of this thesis is measurement based analysis.

The propagation channel is often classified as two types of linear filters: linear time invariant (LTI) [9], when the channel is static and the impulse response does not change over time, or linear time variant (LTV), when the impulse response is varying with time due to the non-static nature of the channel. Often in reality, at least one, the TX, the RX or scatterers in the channel is moving, thus the propagation channels are LTV, in general.

2.1.1   Channel as a Deterministic Time Variant System

As mentioned above, the time variant CIR is composed by the superposition of MPCs each having a certain time-delay, amplitude and phase that vary over time. Usually, the CIR is estimated using the measurements, but if it is assumed that the exact location of the TX, the RX and all scatterers in the environment is known then we can define it using a deterministic system model. A time varying CIR $h(t, \tau)$ of a channel can be represented as follows [10],

$$h(t, \tau) = \sum_{l=1}^{L} \gamma_l(t) e^{-j\phi_l(t)} \delta(\tau - \tau_l), \tag{2.1}$$

where γ_l denote the complex amplitude, τ_l is delay and $\phi_l(t) = 2\pi f_c \tau_l(t) - \phi_{\nu_l}$, where $\phi_{\nu_l} = \int_t 2\pi f_{\nu_l} dt$ is the phase that depends on the delay and Doppler of the lth MPC at time t, respectively. In time variant systems it is important to distinguish between the delay τ and the absolute time t [8].

Other system functions can also be derived from the time variant impulse response [9]; a Fourier transform of the time variant CIR with respect to τ gives the frequency response $H(t, f)$ and a Fourier transform of $H(t, f)$ with respect to t gives the Doppler variant transfer function also called Doppler spread function $B(\nu, f)$. Finally, an inverse Fourier transform of the Doppler spread function with respect to f, gives the delay Doppler function or the Doppler delay function also known as spreading function $S(\nu, \tau)$. The interrelation between these system functions is summarized in Fig. 2.1.

2.1.2 Channel as Stochastic Time Variant System

To model the propagation channel as a stochastic time-variant system, the deterministic system description alone is not sufficient, but a multidimensional probability density function (pdf) of the CIR is required, which is not feasible in practice. Alternatively, a second order description of the deterministic time-variant system functions, known as an auto-correlation function (ACF), is used. The ACFs are obtained by multiplying the system function with its complex conjugate and then taking the expectation $E\{\cdot\}$ over the ensemble of channel realizations as follows [8, 9],

$$R_h(t, t'; \tau, \tau') = E\{h(t, \tau)h^*(t', \tau')\}, \tag{2.2}$$

$$R_H(t, t'; f, f') = E\{H(t, f)H^*(t', f')\}, \tag{2.3}$$

$$R_B(\nu, \nu'; f, f') = E\{B(\nu, f)B^*(\nu', f')\}, \tag{2.4}$$

$$R_S(\nu, \nu'; \tau, \tau') = E\{S(\nu, \tau)S^*(\nu', \tau')\}. \tag{2.5}$$

These ACFs are interrelated with each other via a two-dimensional Fourier transform, as shown in Fig. 2.1.

2.1.3 WSSUS and non-WSSUS channels

Auto-correlation functions are not easy to estimate and make the channel characterization rather complicated, since each of the ACFs depends on four variables. Therefore, wide sense stationary (WSS) and uncorrelated scattering (US) assumptions are used to simplify the ACFs.

The WSS assumption implies that the second order statistics are independent of absolute time, i.e., the ACF in time depends on the time difference $\Delta t = t - t'$ and not on absolute time t. In other words the contribution from
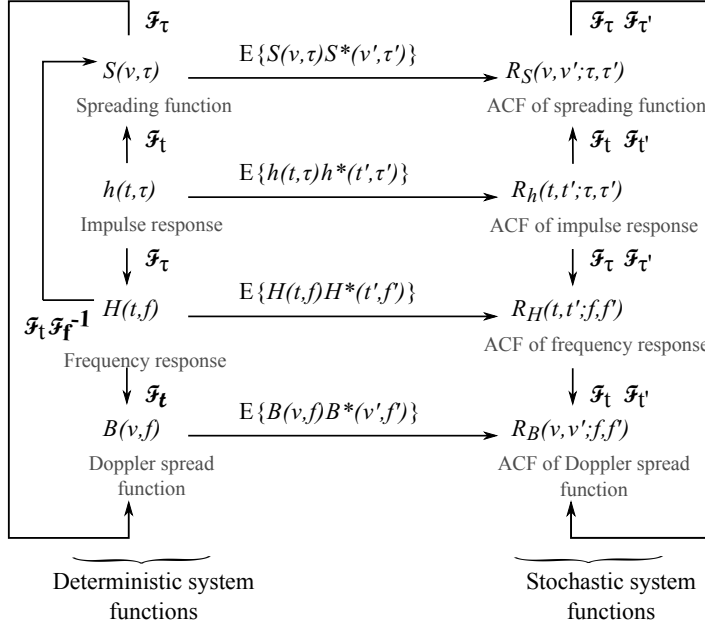
Figure 2.1: Interrelation between channel functions, from [11]; deterministic system functions to the left and stochastic system functions to the right, respectively.The diagram is modified so that it fits well to the contents of this thesis.

different delays are uncorrelated. The simplified ACF of time variant CIR becomes [9],

$$R_h(t, t'; \tau, \tau') = R_h(\Delta t; \tau, \tau'). \tag{2.6}$$

The US assumption implies that the second order statistics are independent of absolute frequency. In other words, contributions at different delays are uncorrelated, i.e., the ACF in frequency depends on the frequency difference $\Delta f = f - f'$ and not on absolute frequency f. The simplified ACF of the time variant frequency response becomes [9],

$$R_H(t, t'; f, f') = R_H(t, t'; \Delta f). \tag{2.7}$$

A channel model that uses both assumptions is called a WSSUS model. Many practical channels such as vehicular channels do not satisfy these assumptions and thus have to be treated as non-WSSUS channels. In general,

the characterization of non-WSSUS channels is more complex. However, one way to look at non-WSSUS channels is to regard them as an extension of the WSSUS case. Characterization of non-WSSUS channels can be performed either by repeating the experiment several times by keeping in mind that the experimental conditions should remain the same, which is unfeasible, and second is by assuming the fading process to be an ergodic process and dividing the observations over small regions given that the WSSUS assumption hold over these small regions [12, 13]. With that assumption a local scattering function (LSF) is adopted to characterize non-WSSUS vehicular channels in [11].

2.1.4 Statistical Channel Metrics

The channel characterization using a sequence of CIRs or ACFs is too cumbersome to work with as they are functions of two or more variables, even after the WSSUS assumption is applied [8]. A preferred way is to provide more compact representations of these functions, which should depend on a single variable or even a parameter, knowing that the compact representation can result in information loss. Consequently, a number of statistical channel matrices have been adopted and can be derived as follows [14];

Power Delay Profile and Doppler Spectral Density

The averaged power delay profile (PDP) describes the expected received power at delay τ and is calculated as the expectation of the squared magnitude of the time-variant channel impulse response $h(t, \tau)$ over the time window t as,

$$P_\tau(\tau) = E\left\{|h(t, \tau)|^2\right\},\tag{2.8}$$

given the channel is WSS over the time window. Typically, averaging over the time window is performed to remove the effects of small-scale fading. Similarly, the expectation of the squared magnitude of the time-variant scattering function over the delay τ gives the Doppler spectral density (DSD) as,

$$P_\nu(\nu) = E\left\{|S(\nu, \tau)|^2\right\},\tag{2.9}$$

given the US assumption holds over the measured bandwidth.

Since vehicular channels are generally non-WSSUS channels, the PDPs of the measurement data are derived by averaging samples recorded within a smaller time window of a certain length based on the speed of the TX and the RX in a given scenario, assuming that the WSSUS assumption holds over the time window. A sliding time window of the same length is used when calculating the DSD, which also defines the Doppler resolution. The time

window length should be chosen as large as possible, because the resolution in the Doppler domain is inversely proportional to the time window length.

Channel gain

The averaged PDP can be further simplified to a single parameter known as channel gain, by integrating it over all delays τ. We thus obtain the channel gain or the time integrated power as [8],

$$G_\tau = \int_{-\infty}^{\infty} P_\tau(\tau) d\tau. \tag{2.10}$$

The channel gain is thus the zeroth order moment of the PDP.

Delay and Doppler Spread

In a multi-path propagation environment the signal spreads both in delay and Doppler domains. A number of delayed and scaled copies of the transmitted signal arrives at the receiver, and the effect of the motion of the TX, RX or scatterers induce frequency and time selective fading that can be characterized by the root mean square (RMS) delay and Doppler spreads, respectively. The instantaneous RMS delay spread is the normalized second-order central moment of the averaged PDP $P_\tau(\tau)$ and is defined as [8],

$$S_\tau = \sqrt{\frac{\int_{-\infty}^{\infty} P_\tau(\tau) \tau^2}{\int_{-\infty}^{\infty} P_\tau(\tau)} - \left(\frac{\int_{-\infty}^{\infty} P_\tau(\tau) \tau}{\int_{-\infty}^{\infty} P_\tau(\tau)} \right)^2}. \tag{2.11}$$

Similarly, the instantaneous RMS Doppler spread is the normalized second-order central moment of the time-variant Doppler spectral density (DSD). The Doppler spread can be computed as

$$S_\nu = \sqrt{\frac{\int_{-\infty}^{\infty} P_\nu(\nu) \nu^2}{\int_{-\infty}^{\infty} P_\nu(\nu)} - \left(\frac{\int_{-\infty}^{\infty} P_\nu(\nu) \nu}{\int_{-\infty}^{\infty} P_\nu(\nu)} \right)^2}. \tag{2.12}$$

The coherence bandwidth B_{coh} is a measure of the frequency selectivity of the channel and is inversely proportional to the RMS delay spread. The B_{coh} is bounded by [15]

$$B_{coh} \lesssim \frac{1}{2\pi S_\tau}. \tag{2.13}$$

The coherence time T_{coh} is a measure of the time selectivity of the channel and is inversely proportional to RMS Doppler spread. The T_{coh} is bounded by [15]

$$T_{coh} \lesssim \frac{1}{2\pi S_{\nu}}. \tag{2.14}$$

2.2   Channel Modeling

Channel characterization is used to define and understand the channel properties where as quantifying these channel properties in such a way that the effects of the channel can be reproduced (in a statistical manner) for network simulations and system testing, is known as channel modeling. There are several approaches to model the channel, and the choice depends on the type of channel under investigation, i.e., time invariant or time varying, narrowband (frequency-flat) or wideband (frequency-selective), SISO or MIMO, deterministic or stochastic and so forth. Almers et al. in [16] provide a generalized classification of channel models based on system assumptions and desired level of complexity. In the following we discuss modeling approaches by classifying them as deterministic and stochastic approaches.

2.2.1   Deterministic

In the deterministic approach, the main goal is to reproduce the actual propagation process in a specific environment by solving Maxwell's equations under certain boundary conditions. In principle, with the help of Maxwell's equations, the channel impulse response can be reproduced when the location of the TX and the RX together with the location, shape, dielectric and conductive properties of all the objects in the surroundings are known [8]. Deterministic models can provide very accurate and meaningful interpretation of the channel for a given location and environment only if an accurate description of the environment is available. To consider the uncertainties in the channel, the deterministic methods sometimes include a statistical component called diffuse scattering [17]. There are several deterministic modeling methods such as the finite-difference time-domain (FDTD) [18] method, the finite-element method (FEM) [19] and so-called ray tracing (RT) [20]. The first two methods are useful when studying near-field problems as they are constrained to structures with limited dimensions. However, the third, RT is the most widely used deterministic approach, which is also of main interest in this thesis, as it gives more appropriate models for far-field propagation environments such as urban areas.

In the RT algorithms, first the geometric (2D/3D) and electromagnetic characteristics of the channel are modeled where buildings and other physical structures are often represented as polygons. Then, to characterize the channel between the TX and the RX, for a specified location of the TX and the RX, the direct path, specular reflections as well as diffuse scattering in terms of non-specular reflections are calculated. Specular reflections are calculated recursively up to a desired order, but depending on the complexity and level of detail of the environment only reflections up to order three or four are practical in terms of computational effort. Faces of buildings or obstacles that can be seen by both the TX and the RX are treated as sources of non-specular reflections of first order, typically modeled by means of Lambertian emitters [21]. Due to the accuracy and adherence to the actual propagation process, RT is sometimes used as a replacement of measurements. The only downside with such methods is that they are computationally expensive, which is often compensated by using a less detailed geometric description of the propagation environment. Reduced information translates to reduced accuracy, and thus a tradeoff between complexity and performance has to be made based on the desired outcome. In this thesis, an accuracy study of deterministic modeling is presented where the RT model is validated against measurement data.

2.2.2 Stochastic

In the stochastic approach the statistics of the channel parameters, e.g., received power statistics at a certain delay, are modeled instead of modeling site-specific realizations of the channel. Usually a probability density function (PDF) of parameters such as pathloss, delay and Doppler spread, and fading are used for that purpose. Stochastic models can be further divided into two categories: geometry-based stochastic models (GSCMs) and non-geometry based stochastic models [16].

In the GSCMs, the location and properties of scatterers are described stochastically according to some probability distributions, and then a simplified ray tracing is performed to model the interaction of propagation waves with the scatterers, which are then combined at the receiver. GSCMs are capable of describing the time-evolution of the channel by the motion of the TX, RX as well as the scatterers, which makes them useful for non-stationary channels such as vehicular channels [22]. Small scale statistics emerging due to superposition of propagation waves coming from different scatterers can be captured by GSCMs, however, the contributions from all the scatterers may not be available at all instants due to mobility of scatters [8, 16, 23].

In the non-geometry based stochastic models the geometry of the environment is not modeled explicitly as in GSCMs, but instead paths from TX to RX

are only described by statistical parameters [16]. One of the most widely used
non-geometry based wideband stochastic channel model is the tapped-delay
line (TDL) model, which is based on the WSSUS assumption [9]. The TDL
model is described by a finite number of delay taps that fade independently,
each tap consists of several MPCs. The TDL models have widely been used
in cellular systems simulations due to low complexity. Other classifications of
non-geometry based stochastics models are; cluster based, which is called ex-
tended Saleh-Vanzuela model [24], and non-cluster based where the MPCs are
treated individually, sometimes referred to as the Zwick model [25].

2.3   Measurement based characterization and modeling

The channel measurement data for time-variant channels is often comprised of
many CIRs, ranging from one to hundreds of thousands of samples, for each
measurement run. Using that many measured CIRs directly for system simu-
lations is not only inconvenient but inefficient. For this reason, a Measurement
Based Channel Modeling (MBCM) approach is adopted, where measurement
data is used to characterize the channel. Certain channel parameters are then
estimated and models are derived from the measurement data that can be used
to reconstruct the statistics of the channel realizations.

MBCM is the main focus of this thesis; in MBCM the channel measurement
data together with parameter estimation techniques are used to estimate the
important channel parameters. The measurement setup, i.e., measurement
equipment, selected scenarios, antenna configuration and bandwidth, as well as
the selected parameter estimation methods are the key factors, which determine
the generality of the measurement results.

The MBCM is closely related to aforementioned, deterministic and stochas-
tic modeling approaches. The channel measurement data contains the charac-
teristics of the propagation environment in the form of CIRs and thus it can be
used as it is for system simulations, also called replay modeling, which is a kind
of deterministic modeling [26]. However, measurement data has an advantage
over conventional deterministic modeling that the measurement data itself do
not always require an explicit description of the environment. In addition to
that, in the MBCM approach the measurement data is used to estimate the en-
vironment specific channel parameters to make stochastic models, e.g., complex
amplitudes, delay, Doppler, angle-of-arrival (AOA), angle-of-departure (AOD)
of MPCs/clusters, which are often independent of the applied measurement
system. The stochastic model or alternatively the estimated parameters are
then used to reproduce CIR for system simulations. A systematic flow dia-

gram of the MBCM is illustrated in Fig. 2.2, as in [27], which is modified to better suit the purpose of this thesis.
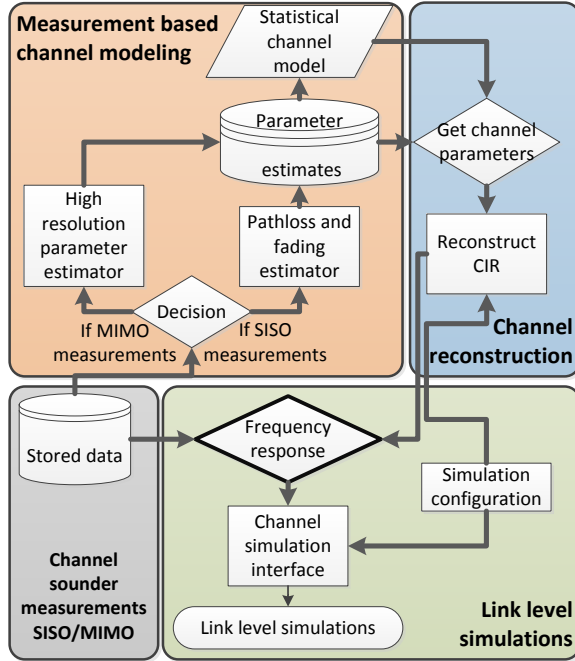
Figure 2.2: A systematic flow diagram of MBCM.

In the following, the MBCM approach and the channel parameter estimation methods are described individually for SISO and MIMO measurements. It is worth mentioning that in the following sections discrete notation is used because we always assume the measured channel response to be sampled and not continuous.

2.3.1   SISO measurements

Signal propagation over the wireless channel is often divided by three statistically independent phenomena named deterministic path loss, small-scale or multipath fading, and large-scale or shadow fading [8]. Important channel metrics used to characterize measured SISO links are PDP, DSD, delay spread and Doppler spread, which have already been discussed in section 2.1.4.

The received signal power $P_{RX}(d)$ at the RX separated from a radiating TX by a distance d can be calculated in dB by using the following expression [7],

$$P_{RX}(d) = P_{TX} - PL(d) - SF - MF \qquad (2.15)$$

where P_{TX} is the transmitted power, $PL(d)$ is the distance dependent pathloss at a distance d, SF is the shadow fading and MF is the multipath fading, respectively. The antenna gain and system losses are not considered, using the assumption that their effects have already been taken away from the measurement data.

Pathloss: Pathloss is the expected (mean) loss at a certain distance compared to the received power at a reference distance. A simple log-distance power law [8] is often used to model the pathloss. The generic form of this log-distance power law path loss model is given by,

$$PL(d) = PL_0 + 10n \log_{10}\left(\frac{d}{d_0}\right), \qquad (2.16)$$

where PL_0 is the path loss at a reference distance d_0 in dB, d is the distance between the TX and the RX, and n is the pathloss exponent, respectively. In general, the pathloss exponent $n = 2$ is used to calculate the free-space path loss. In reality n is an environment dependent parameter commonly provided in modeling papers, which is determined by field measurements. Usually, n is estimated by simple linear regression of $10 \log_{10}(d)$ to the measured power values in dB such that the mean square error (MSE) between the measured and the modeled points is minimized.

In practice for LOS propagation conditions it is observed that a dual-slope model based on two-ray ground model, as stated in [28], can represent measurement data more accurately. We thus characterize a dual-slope model as a piecewise-linear model with the assumption that the power decays with path loss exponent n_1 until the breakpoint distance (d_b) and from there it decays with path loss exponent n_2. The dual-slope model is given by,

$$PL(d) = \begin{cases} PL_0 + 10n_1 \log_{10}\left(\frac{d}{d_0}\right), & \text{if } d_0 \leq d \leq d_b \\ PL_0 + 10n_1 \log_{10}\left(\frac{d_b}{d_0}\right) + & \text{if } d > d_b \\ 10n_2 \log_{10}\left(\frac{d}{d_b}\right). \end{cases} \qquad (2.17)$$

The typical flat earth model consider d_b as the distance at which the first Fresnel zone touches the ground or the first ground reflection has traveled $d_b + \lambda/4$ to reach RX. The d_b can be calculated as, $d_b = \frac{4h_{TX}h_{RX} - \lambda^2/4}{\lambda}$, where λ is the wavelength at carrier frequency f_c, and h_{TX} and h_{RX} are the height of the

TX and RX antennas, respectively. For $d < d_b$, this model is the same as the log-distance power law in (4).

Measurement data often has small or limited amount of data and thus there are a number of associated challenges, which often makes estimation and modeling of the pathloss exponent from measurement data non-trivial. Therefore, special considerations must be taken into account when modeling the pathloss exponent by measurement data. The examples of associated challenges are: 1), the distribution of data samples along a *logarithmic* distance scale is often non-uniform, i.e., the data samples have higher concentration at larger *logarithmic* distances, implying that the standard MSE estimation approach will provide better estimates for large distances rather than smaller distances. One solution can be to use weighted samples according to the logarithmic sampling density for improved prediction [29]. 2), the pathloss exponent can be modeled as a random variable but it is important to understand whether these variations are physically or analytically motivated. Third, it is important to verify the reliability of the estimated pathloss exponent for a given number of measured data samples. Finally, it is important to decide whether to use *linear* or *logarithmic* distance for modeling, because sample distribution is different for both cases and may lead to different estimates for the same data set.

Small-scale fading: The signal from TX can reach RX via several propagation paths or the multi-path components (MPCs), each having different amplitude and phase. The change in the signal amplitude due to constructive or destructive interference of the different MPCs is classified as small-scale fading, that typically occur during movements of nodes over one or more wavelengths. Small scale fading gives fast fluctuation on top of the large-scale signal variations.

There are several distributions that have been proposed to model small-scale fading and the selection of distribution is mainly dependent upon the propagation conditions. Typically, multipath fading is modeled by means of a Ricean random distribution in the presence of a dominant MPC such as a LOS component or a dominant specular component. The probability density function (pdf) for the Ricean envelope r is given by [8],

$$p(r) = \frac{r}{\sigma_{MF}^2} e^{\left\{-\frac{r^2 + A^2}{2\sigma_{MF}^2}\right\}} I_0 \left(\frac{Ar}{\sigma_{MF}^2}\right), \qquad (2.18)$$

where A is the amplitude of the dominant component, σ_{MF} is the standard deviation, and I_0 is the zero-order modified Bessel function of the first kind. The parameters A and σ_{MF} are related to the K factor that is usually used to describe the Ricean distribution, defined as,

$$K = \frac{A^2}{2\sigma_{MF}^2}. \tag{2.19}$$

In NLOS propagation conditions when there is no dominant component, i.e., $K = 0$ as $A = 0$, then (2.18) reduces to Rayleigh PDF as [8],

$$p(r) = \frac{r}{\sigma_{MF}^2} e^{\left\{ -\frac{r^2}{2\sigma_{MF}^2} \right\}}. \tag{2.20}$$

Large-scale fading: Obstacles in the propagation paths of one or more MPCs cause attenuation in the received signal and the effect is called shadowing. Shadowing gives rise to large-scale fading and it occurs not only for the line-of-sight (LOS) component but also for any other major MPC. The most widely accepted approach is to model the large-scale variations with a log-normal distribution with zero mean and standard deviation σ_{SF}, which is a scenario dependent parameter [8, 30].

Once a link goes into a shadow region, it remains shadowed for some time interval implying that the shadowing is a spatially correlated process. The auto-correlation of the Gaussian process can then be modeled by a well-known analytical model proposed by Gudmundson [31], which is a simple negative exponential function,

$$r_x(\Delta d) = e^{-|\Delta d|/d_c}, \tag{2.21}$$

where Δd is an equally spaced distance vector and d_c is a decorrelation distance being a scenario-dependent real valued constant. In the Gudmundson model, d_c is defined as the value of Δd at which the value of the auto-correlation function $r_x(\Delta d)$ is equal to $1/e$.

2.3.2 MIMO measurements

Multiple-input multiple-output (MIMO) systems utilize spatial degrees of freedom to offer improvements in terms of capacity, link reliability, and signal-to-noise ratio (SNR) gain, although these benefits can not always be achieved simultaneously. This section focuses only on the characterization and modeling of MIMO measurements. For further reading on MIMO communications and channel modeling in general, see [8, 32].

Most of the approaches stated above for SISO measurements are applicable for the characterization and modeling of MIMO measurements. One key issue related to MIMO channel models is that they should be able to predict the correlation between different antenna elements since the correlation controls the eigenvalues of the channel matrix, implying that the antenna correlation is

an important metric to be analyzed in order to characterize MIMO channels for possible diversity gain [29]. In the following we discuss antenna correlation, eigenvalue decomposition, and diversity combining techniques as a part of measurement based MIMO channel characterization. We then move on to measurement based MIMO channel models and parameters estimation techniques.

2.3.3   Antenna Diversity

Random fluctuations in the signal power due to multipath propagation impair the wireless channel across space, time and frequency. This is commonly known as channel fading. Diversity techniques are developed to combat fading by combining several independently faded versions of the same transmitted signal at the receiver to improve link reliability by improving the signal-to-noise ratio (SNR). Thus, diversity is an important metric to be analyzed in order to validate the performance of multi-antenna systems.

Among the diversity techniques, here spatial or antenna diversity is of particular interest in which multiple antennas at the TX and/or RX are used to exploit the diversity gain. To evaluate antenna diversity we compare two metrics, the eigenvalue distribution and antenna correlation in the following.

Antenna correlations

The multiple antennas at TX and/or at RX improve the system performance through diversity arrangements but their benefits can only be fully utilized if the correlation between signals at different antenna elements is low [8]. Thus, the antenna correlation for both the TX and the RX array is an important parameter to study. The time-variant antenna correlation $\rho_{ij}^{RX}(t_k)$ between the RX elements i and j is calculated as,

$$\rho_{ij}^{RX}(t_k) = \sum_{n_t=1}^{N_{avg}} \sum_{n_f=1}^{N_f} \frac{\sum_{m=1}^{M_T} H_{i,m} H_{j,m}^*}{\sqrt{\sum_{m=1}^{M_T} |H_{i,m}|^2 \sum_{m=1}^{M_T} |H_{j,m}|^2}}. \qquad (2.22)$$

Similarly, the correlation $\rho_{ij}^{TX}(t_k)$ between the TX elements i and j is calculated as,

$$\rho_{ij}^{TX}(t_k) = \sum_{n_t=1}^{N_{avg}} \sum_{n_f=1}^{N_f} \frac{\sum_{n=1}^{M_R} H_{n,i}^* H_{n,j}}{\sqrt{\sum_{n=1}^{M_R} |H_{n,i}|^2 \sum_{n=1}^{M_R} |H_{n,j}|^2}}, \qquad (2.23)$$

where H is a block matrix for each time instant t_k such that $H \in \mathbb{C}^{N_{avg} \times N_f}$, N_{avg} is the number of snapshots in a time window over which the WSSUS

assumption is valid, N_f is the number of frequency samples within measured bandwidth, and H^* is the conjugate transpose of H.

Eigen-value distribution and array gain

The eigenvalues (EVs) and their distributions capture important properties of the array and the propagation medium [33]. The singular value decomposition (SVD) is a very useful tool to find the singular values of a matrix [34]. An SVD expansion of the normalized channel matrix $H \in \mathbb{C}^{M_R \times M_T}$ can be written as,

$$H = U \cdot S \cdot V^*, \tag{2.24}$$

where U is a $M_R \times M_R$ unitary matrix, S is a diagonal matrix of real non-negative singular values σ_m where $m = 1, 2, ..., \min\{M_R, M_T\}$, and V^* (the conjugate transpose of V) is $M_T \times M_T$ unitary matrix. Singular values of H are the square roots of the eigenvalues of R_H, where $R_H = H \cdot H'$ is the inner product of H and H^*.

2.3.4 MIMO channel models and parameter estimation

Measurement based channel modeling of MIMO systems may involve the estimation of propagation path parameters from the channel sounding measurements by using a proper high-resolution parameter estimation algorithm along with a realistic model. This approach usually models the measured MIMO channel response using three model components: 1) deterministic specular propagation paths, 2) random diffuse or dense multipath components, and 3) measurement noise [27]. Ideally, this approach allows to decompose the influence of the array responses from the MIMO channel measurements to obtain a valid description of the propagation channel. This can only be achieved if the measurement equipment is properly calibrated such that the directional as well as polarimetric array response is available together with the system response of the measurement equipment.

Based on the system model assumption, there exist a number of parameter estimation techniques. For the estimation of static model parameters spectral-, subspace- and maximum likelihood (ML)-based techniques can be used and for the estimation of dynamic model parameters, Kalman filters, and sequential Monte Carlo-based techniques can be used, respectively [27]. The applicability of different estimation techniques is limited in several ways, e.g., spectral, subspace-based techniques are unable to estimate parameters of coherent signals unlike ML-based high-resolution estimators [27]. This is one of the reason why ML-based high-resolution estimators like the Space Alternating Generalized Expectation-maximization algorithm (SAGE) [35], are popular.

In this thesis we mainly focus on the estimation of the deterministic part, i.e., the specular propagation paths, using SAGE. The SAGE is used for parameter extraction in paper I and II. In order to estimate the parameters associated to each of the dominant propagation path using ML-based method such as SAGE, it is assumed that the received signal is a superposition of a finite number, L of specular plane waves or MPCs originating from the scatterers that are in far field of the TX and RX antennas. Further it is assumed that each specular MPCs can be described by geometric parameters such as delay, AOD and AOA, and Doppler frequency. A double directional signal model that is based on L MPCs is used to model a measured transfer function as follows [17],

$$\mathbf{H}(t,f) = \sum_{l=1}^{L} \gamma_l \cdot \mathbf{G}_{TX}(\theta_{TX,l}) \cdot \mathbf{G}_{RX}(\theta_{RX,l}) \cdot e^{j2\pi\nu_l t} \cdot e^{-j2\pi\tau_l f}, \qquad (2.25)$$

where $\mathbf{H}(t,f) \in \mathbb{C}^{M_{TX} \times M_{RX}}$ is a matrix representing a complex time variant frequency response, as a function of time t and frequency f, which can be obtained by Fourier transforming the double directional time varying CIR $h(t,\tau)$ with respect to τ. M_{TX}, M_{RX} are the number of the TX and RX antenna elements, G_{TX} and G_{RX} are $M_{TX} \times 1$ and $M_{RX} \times 1$, complex vectors representing the TX and RX antenna array responses at angles $\Theta_{TX,l}$, $\Theta_{RX,l}$ that contain, elevation as well as azimuth, AOD and AOA, for the lth MPC, respectively.

The SAGE is an extension of the Expectation Maximization (EM) algorithm that uses successive interference cancellation (SIC) for joint estimation of delay, Doppler, elevation and azimuth AOD and AOA from the time variant MIMO measurements [36]. It iteratively evaluates the likelihood function using current parameters' estimates where a subset of the parameters is kept fixed while the likelihood function is maximized with respect to the other subset of the parameters. For the next iteration, these new estimates are then kept fixed to find a new subset of the parameters in similar fashion. The convergence rate is dependent on the choice of the parameter subset, i.e., all the parameters of each individual path or a specific parameter of all MPCs related to a specific measurement data block. SAGE is capable to provide correct estimates in 3-D, elevation as well as azimuth angles, in practice. However, there are a number of limitations associated with SAGE such as high computational complexity and memory requirements, improper SIC and parameter estimation without considering diffuse MPCs.

Another estimation method known as RIMAX was developed to overcome SAGE's limitations [17, 37], and was the first method to consider diffuse scattering together with specular MPCs for parameter estimation. The parameter

estimation in RIMAX for both diffuse and specular MPCs is done alternatively in a sense similar to SAGE. To improve parameter estimates, the algorithm uses a gradient based iterative optimization method, called Levenberg-Marquardt algorithm [38, 39], which is the core of the algorithm.

RIMAX includes the diffuse scattering for parameter estimation but both RIMAX and SAGE are based on a static model where it is assumed that the model parameters remain constant over an observation period and parameters from two different observations are treated independent of each other. In other words, both algorithms try to maximize the likelihood function for parameter estimation based on current observation, period.

In the time-varying channels, and typically some of the specular paths in the channel persist over several time snapshot. Implying that the path parameters can be tracked, which is beneficial in two ways. First, tracking enable to capture dynamic behavior of the channel, and second, reduced computational cost by not performing ML estimation for each individual observation. On the other hand, both the SAGE-based algorithm and RIMAX do not utilize the time-evolution of the parameters for parameter estimation they suffer from high computational complexity issue.

In order to exploit these benefits in terms of cost efficiency and capturing dynamic behavior of the channel, a state-space based sequential estimation technique, e.g., extended Kalman filters (EKF) [40], is adopted for the detection and tracking of multipath parameters where the state of system evolve over time. EKF is not used in this thesis, even though it is a more suitable parameter estimation method for measurement based time-varying vehicular channels. Hence, it is desirable to use EKF in the future instead of SAGE for double directional V2V channel parameter estimation and MIMO modeling.

Following are some related issues, associated to most of these parameter estimation algorithms: First, the source order estimation, i.e. to estimate the number of MPCs L that construct a channel response at the RX is a well known research topic and still an open issue. Second, by using an incomplete data model, e.g., incomplete antenna data models where the antenna response is not characterize both in azimuth and elevation as well as for both vertical and horizontal polarizations, inherently will result in biased estimates and artificially large angular estimates [41]. Therefore, complete data models should be used. Third, is related to the plane wave assumption for signal model that assumes scatterers to be in far field of the TX and RX antennas, which is not accurate in some scenarios such as indoor scenarios where the scatterers can exist in near field. In such scenarios, signal model should consider spherical waves instead.

Chapter 3

Vehicle-to-Vehicle Propagation Channels: State of the art

Vehicular propagation channels, which can be characterized as V2V and V2I channels, are extremely time-varying and are fundamentally different from the well known cellular channels. In V2V communications the propagation environment changes rapidly due to fast mobility of the TX and the RX. Moreover, both the transceiver antennas are often at the same height relatively close to the ground level, which increases scattering around both units. Typically V2V channels are doubly selective, where channel parameters vary significantly both in the time and frequency domain [11, 42]. This implies that the results from cellular channel research can not directly be applied on vehicular channels and for channel modeling redefinition of suitable measurement setups and propagation scenarios are required.

This chapter presents state of the art concerning V2V channel characterization and modeling by including analytical as well as measurement based research on V2V channels in the past. We first discuss V2V channel measurement campaigns, and then move on to channel characterization and modeling.

3.1 V2V Channel Measurements

Channel models, in one way or another, typically rely on real-life measurements of the channel. Measurements are used to understand the channel behavior, to

extract stochastic parameters for the models, and to validate existing models. The channel measurement campaigns should be designed and performed in such a way that a generalized description of the channel can be obtained but this is hard to achieve in reality. The complexity of the measurement setup and equipment increases with the generality of the channel model [14]. Each measurement campaign mentioned, to some extent, has some limitations due to measurement equipment, amount and sampling rates of recorded data and/or choice of scenarios.

A number of real-life channel measurement campaigns have been conducted in the past for cellular as well as for vehicular communication systems, in many different propagation environments and with different measurement setup. The measurement equipment used for vehicular channel measurements is pretty much similar to the one used for cellular channels. However, V2V channel measurements are slightly more trickier than cellular or even V2I measurements, e.g., in V2V channels both the TX and RX are mobile and synchronization during the measurements is a challenge. In the following we have categorized major V2V measurement campaigns performed over the past two decades into three categories;

3.1.1   Carrier frequency and measurement bandwidth

In the beginning and until recently, some of the V2V channel measurements were performed at the 900 MHz band. This bane is a dedicated band for electronic toll collection systems, targeting future M2M or V2V communication systems [43–46]. The Federal Communication Commission (FCC) in the United States, in 1999, realized the importance of dedicated short range communication (DSRC) in vehicular environments and allocated a 75 MHz frequency band at 5.9 GHz. Today, the standardization associations worldwide have allocated the frequency bands for ITS; $5.850 - 5.925$ GHz in North America, $5.875-5.905$ GHz in Europe, and $715-725$ MHz and $5.770-5.850$ GHz in Japan, respectively. For that reason, over the last few years most of V2V measurement campaigns have been conducted at 5 GHz frequency band [28, 42, 47–60], among others, with a few exceptions where the measurements were carried out at 2.4 GHz band [61, 62].

Typically a wideband channel sounder is a suitable device to measure doubly selective channels such as V2V channels [50, 52, 54, 63]. However, some of the measurements were performed using narrow-band measurement systems where a sine wave generator together with vector signal analyzer [28, 49] or spectrum analyzer [26] were used. Parameters like channel gain, fading and and time-selectivity can be measured using narrow band measurement systems but not the frequency-selectivity, thus making them unsuitable for V2V channel

measurements if the complete channel description is required.

3.1.2 Antenna Configuration

Each of the aforementioned measurement campaigns to some extent is different from any other measurement campaign, performed even at the same frequency band. The main difference lies in their particularities such as the types of vehicles used for the TX and the RX, measured scenarios and the antenna configuration. Most of the measurements have almost exclusively been conducted with the same type of antenna configurations: a roof-mounted SISO antenna configuration [43, 46, 47, 53, 61, 64] or a roof-mounted MIMO antenna configuration [50, 52, 54, 63]. However, a small number of exceptions exist. In [51], an antenna other than roof mounted antenna was placed inside the vehicle, next to the windshield. In [48] and [57], the effects of five and three different roof positions, respectively, were tested. In order to explicitly characterize the impact of antenna placement on a vehicle based on real measurements, we performed a measurement campaign with four antennas mounted at four different positions on the TX and the RX car: roof, bumper, inside-windscreen and left-side mirror. The results are included in Paper VI included in the second part of this thesis.

3.1.3 Scenarios

Channel properties of V2V channel are significantly different for different propagation environments. There are big variations in the propagation environments from location-to-location and from country-to-country, but in order to characterize V2V channels a somewhat basic generalization of the propagation environments is required. In the beginning, the classification of scenarios used for V2V channe measurements was derived from the well understood cellular channels, which includes highway, rural, urban and sub-urban scenarios. A number of measurements were performed using this scenario classification [26, 28, 47–49, 53]. Later, there was a need to find a better classification of scenarios that is more relevant for V2V communications. Hence, in [50–52, 63], an alternative scenario definition was used. In these measurements the old scenario definition was modified by introducing new measurements scenarios in order to analyze the impacts of traffic density, convoy and on coming traffic flows. Recently, the automotive industry together with the ETSI ITS standardization organization in Europe and US-DOT in the USA, respectively, have specified a basic set of ITS applications. This motivated the research groups to use more precise definition of the measurement scenarios that are relevant for these ITS applications, especially for safety critical scenarios. In more re-

cent campaigns this new scenario definition is used for channel measurements. In [54–59, 65, 66] V2V communication in situations like, LOS obstruction by buildings and other vehicles, in-tunnel, on bridge, in slopes, and in parking garage have been considered.

3.2 Vehicular Channel Characterization and Modeling

A lot of research efforts have been made in the past to characterize and model V2V propagation channels. V2V channels are highly non-stationary and is one of the key aspects that complicates V2V channel characterization as well as becomes challenging when it comes to modeling. A number of research outcomes have been published in the past few years dealing with non-stationarity issues using the local scattering function (LSF), in wireless channels in general [12], and in V2V channels in particular [11, 67, 68].

In this section, we classify existing work related to V2V channel characterization and modeling as; 1) measurement based, when channel measurement data itself is used for the modeling purpose, 2) non-measurement based, when channel models are developed based on some kind of deterministic or stochastic approach by means of analytical expressions or computer simulations. In the later, measurement data is only used to validate the models.

A wireless link can be categorized into the following three groups:

- Line-of-sight (LOS) is the situation when there is line-of-sight between the TX and the RX. Typically it is required that the first Fresenel zone is free of obstructions.

- Obstructed-LOS (OLOS) is the situation when the LOS between the TX and RX is obstructed partially by another object. In the context of vehicular channels we classify blocking by other vehicles as OLOS.

- Non-LOS (NLOS) is the situation when a larger object, e.g., a building between the TX and RX, completely block the LOS and often many other significant MPCs.

Signal propagation in each of these situations is significantly different from each other as shown in Fig. 3.1. The differences are more pronounced for V2V communications at 5.9 GHz compared to cellular frequencies because at this frequency, the electromagnetic (EM) wave experiences significant losses when passing through buildings and when diffracting around building edges. To further highlight the differences, an example is shown in Fig. 3.2 where the

received power is shown as a function of distance in free-space, LOS, OLOS, and NLOS situation using pathloss model parameters given in [8,69,70], respectively, for V2V channels. The differences in received power motivate to analyze and model the channel individually for each of these situations in order to completely characterize V2V propagation channel. Hence, in the following we discuss measurement and non-measurement based classification in the light of LOS, OLOS and NLOS situations.

(a)

(b)

(c)
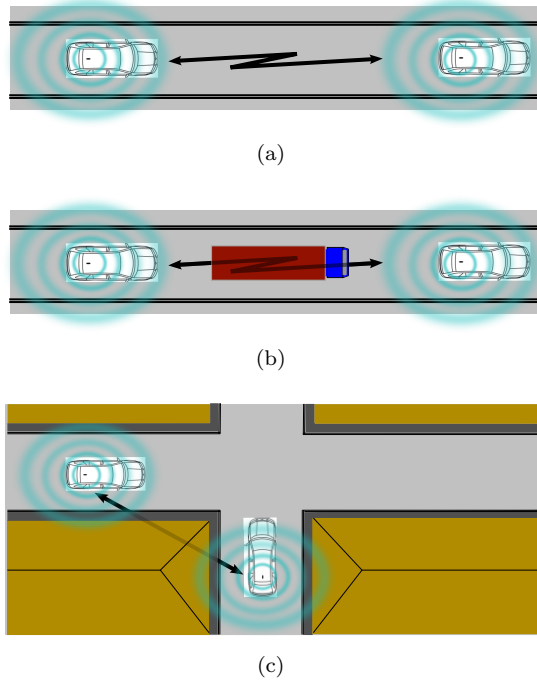
Figure 3.1: Schematic representation of V2V communication links categorized into three groups; (a) LOS (b) OLOS (c) NLOS.

3.2.1   Measurement Based Modeling

Most of the papers based on aforementioned measurement campaigns, have used metrics like, PDP, DSD, RMS delay spread and RMS Doppler spread to describe the channel characteristics using extracted parameters for different scenarios in [26,42,44,50–53,68,71,72]. Most of these studies mainly target typical
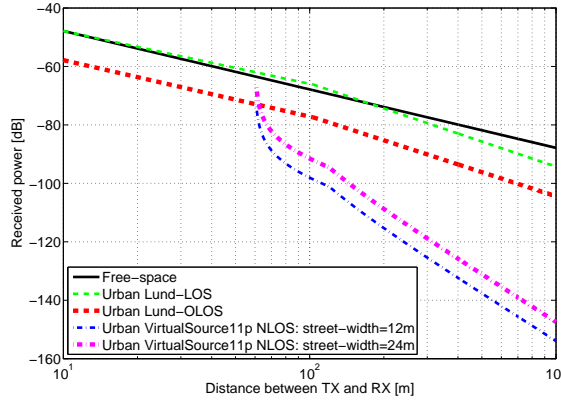
Figure 3.2: Received power as a function of distance using pathloss model parameters given in; [8] for free-space, in [69] for LOS and OLOS, and in [70] for NLOS situations, respectively.

rural, highway and urban scenarios but do not consider some of the important scenarios such as merging lanes on highway and NLOS street intersection scenario. The merging lane scenario is characterized in paper II included in part-II of this thesis as well as in [73]. Moreover, there are no results that describe the double directional properties of V2V channels such as AOA, AOD and angular spread as well as the contribution of different scattering objects in the received signal power. Paper-I in this thesis deal with such issues by analyzing direction properties of V2V channel in different propagation environments.

The pathloss exponents together with respective fading parameters have also been modeled, separately for LOS, OLOS and NLOS links. In LOS situation: the pathloss exponents for a single-slope model were observed to be between; $1.33 - 3.07$ in the highway scenarios [26, 52, 53, 56, 60, 74, 75], $1.79 - 3.18$ in the rural scenarios [53, 56, 71, 75], $1.19 - 2.88$ in the urban scenarios [53, 56, 60, 64, 75], and $1.59 - 3.5$ in the sub-urban scenarios [28, 52, 75]. It is worth mentioning that the value of pathloss exponent less than 2 is observed quite often for V2V channels in LOS, which indicates that power higher than what is received for free-space pathloss is received. In some studies a dual-slope two-ray pathloss model is argued to fit better for V2V pathloss modeling that in turn improves the accuracy of simulation results, as in [28, 49, 53, 76] for urban and highway scenarios, and in [75] for rural scenarios. Most of these studies include small or large scale fading parameters along with the pathloss exponents. However, a few studies have also been reported in the literature in

which only the small-scale fading effects such as multi-dimensional K-Factor of time-varying V2V channels is characterized [77, 78].

In [79] and [55], it was shown that vehicles as obstacles have a significant impact on LOS obstruction in both dense and sparse vehicular networks. This implies that shadowing caused by other vehicles cannot be ignored in V2V channel models. Moreover, the shdowing vehicle type also effects the shadowing distribution [59]. The shadowing impact of vehicles has largely been neglected when modeling the pathloss and the shadow fading model proposed in Paper V in this thesis was the first to model pathloss for V2V communications in OLOS situations in highway and urban environments. Recently, a geometry-based V2V channel model was proposed in [80], which takes into account the effects of vehicles as obstacles. It is important to model vehicles as obstacles, ignoring this can lead to an unrealistic assumptions about the performance of the physical layer, which in turn can effect the behavior of higher layers of V2V systems.

The geometry of street intersections, i.e., street width and alignment, structure of buildings, and antenna height have great impact on the NLOS reception in an urban intersection. A NLOS pathloss model must be able to capture all these effects in order to considered realistic. Initial studies based on VANET simulations have been using the WINNER II channel model [81] as an NLOS pathloss model. However, a few measurements results for V2V channels in NLOS situation are available [46, 56–58, 64, 70, 82], in which the pathloss model is presented for different type of street crossings.

In addition to pathloss and fading models, some other parametric models such as measurement based stochastic channel models for V2V systems are available and are considered to be well suited for time-varying V2V channel. In [22] a geometry-based stochastic channel (GSCM) model is presented for V2V channels. An extension of the GSCM model is presented in [83], which models the diffuse scattering in a pure stochastic way. Finally, there are a few non-geometry based stochastic channel models that describe the channel as a finite-impulse response filter by means using a number of discrete taps, knows as tap-delay line models [61, 62].

3.2.2   Non-Measurement Based Modeling

Beside measurement based modeling, there has been a lot of interest in theoretical as well as simulation based modeling of V2V channels where the channel measurement data was used only for validation purposes. A deterministic approach using ray-tracing (RT) to simulate V2V propagation channels was first introduced by Wiesbeck and coworkers in [20, 26, 84, 85]. Later, many other research groups adopted RT for V2V channel characterization and modeling.

There exist a number RT simulation based channel models for highway and urban environment for LOS situation [85]. Similarly, RT based simulation studies have also been used to model NLOS situations in urban street intersections [86–88]. The effect of different buildings blocking the LOS in urban streets is evaluated in [58]. Another RT simulation based propagation model suitable for OLOS and NLOS situations is proposed in [89], as it can take into account the impact of moving and static obstacles of different sizes.

In addition to modeling the channel characteristics, RT based simulations are also used to analyze the effects of different antenna configurations in [90] and [91] where three and six antenna positions were tested, respectively.

An analytical pathloss model for V2V communications in LOS scenarios on an irregular terrain such as a slope is presented in [92]. A statistical sum of sinusoid simulation model is proposed for mobile-to-mobile Rayleigh fading channels in [93] and for M2M Rician fading channels using classical two-ring modeling assumption in [94] generalized to allow a LOS component. Further, the same model was extended to include single scattering either at the TX or RX side in [95], that was later improved to a 3-D model using two-cylinder model [96] and finally, was verified with measurement data in [96]. Another analytical geometry based scattering model for MIMO propagation channels based on geometrical street model is presented in [97], which is improved to a wideband multiple-cluster MIMO model in [98] and the effect of both static and moving scatterers are included in [99].

Most of these analytical models are targeting LOS propagation environments, however, there exist a few models for NLOS situations in urban street intersections such as [100] and [101], where a statistical channel model for T-junction and four-way street intersection is presented, respectively.

Chapter 4

V2V Channel Measurement Campaigns

In order to understand and model the properties of the propagation environment, channel measurements or channel sounding must be performed. In the past a lot of research efforts have been made to understand and model V2V channels (as discussed in sections 3.1 and 3.2), however, measurement campaigns at that point in time were often defined to investigate a very limited set of scenarios. In order to fill the gap, we have performed a number of V2V channel measurement campaigns in recent years using RUSK-Lund channel sounder.

In this chapter, we first cover the basics of channel sounding techniques and then briefly elaborate on the RUSK-Lund channel sounder. We also discuss main characteristics of each of the measurement campaigns we have performed for the characterization of V2V channels along with the scenario descriptions. The measurement scenarios were selected mainly based on the safety critical V2V applications.

4.1   Channel Sounding Techniques

Channel measurements also known as "channel sounding", is performed to characterize the physical properties of the channel, whereas the channel measurement data is often collected using a device named channel sounder, or simply a sounder. The word "sounder" stems back to early nineteenth century where sounding was primarily used for determining distance, e.g., depth of lakes, rivers and sea, using echo sounding that utilizes sound pulses [102].

In contrast to echo sounding, a radio channel sounder, which is closely related to radar systems, transmits electromagnetic waves to excite (or sound) the channel and records the channel output at the receiver. Over the time, with the advancement of wireless technologies, the complexity of channel sounders has immensely increased. Modern sounders deploy a variety of sounding methods depending on the type of channel of interest, including such as narrowband or wideband, and SISO or MIMO channels. For the MIMO channels, the channel impulse responses between all combinations of the TX and RX antenna branches have to be recorded.

For the MIMO measurements three different types of array architectures are used: 1) *real-array*, in which each antenna element has its own Radio Frequency (RF) chain so that they can transmit or receive simultaneously. Major drawbacks with a real-array architecture are the cost and calibration procedure, 2) *switched array*, in which there is only one RF chain for all TX and RX branches. So only one antenna can transmit and one can receive at a time. The switched-array architecture has a number of advantages over the real-array architecture such as low cost and complexity. Moreover, antenna arrays of any size can be used at both link ends, where the maximum size of the array is a function of coherence bandwidth and the speed of the RF switch [103], and 3) *virtual arrays*, in which there is only one antenna element connected to a single RF chain at each link end. For MIMO measurements the antennas are electronically moved to predefined locations where the channel is sounded sequentially for each location. A major drawback of such an architecture is that it allows very limited temporal variations in the channel. Thus, the switched array architecture is often the most suitable one for MIMO measurements in fast fluctuating, time-variant channels such as vehicular channels.

To determine the statistical properties of the channel, sounding can either be performed in the time domain or in the frequency domain. For the time domain measurements, the time-variant CIR $h(t, \tau)$ at the RX is obtained by exciting the channel with periodic pulses on a PN-sequence at the TX. For the frequency domain measurements, on the other hand, the time-variant channel transfer function $H(t, f)$ is obtained by sounding the channel with chirp-like multi-tone signals.

The channel sounding of the time-invariant and band-limited channels can be done without any problem if the channel is sampled at least at the Nyquist rate. However, for the channel sounding of time-variant channels it has to be ensured that the channel is *doubly underspread*, i.e., that the channel fulfills a two-dimensional Nyquist criterion [12]

$$2\nu_{max}\tau_{max} \ll 1. \tag{4.1}$$

A doubly underspread channel is both dispersion-underspread and correlation-

underspread, and is characterized by having its spreading function and correlation function concentrated about origin of the delay τ and Doppler ν plane. This implies that the product of the maximum delay, τ_{max}, and Doppler, ν_{max}, should be small, such that their product is much smaller than 1. A small τ_{max} and ν_{max} result in a large coherence bandwidth and coherence time, respectively.

The following two inequalities can be used to derive this criterion. First, the sampling rate or snapshot repetition time $t_{rep} = Kt_s$ must be shorter than the coherence time of the channel, i.e., the channel impulse response must not change during the sounding of one snapshot. This implies

$$t_s \leq \frac{1}{2\nu_{max}K}, \tag{4.2}$$

where t_s is the length of sounding sequence and $K = t_{rep}/t_s$ is the repetition period. Second, the length of the sounding signal must always be longer than the excess delay τ_{max} of the channel in order to avoid overlap between consecutive sounding signals. This inequality takes into account the delay dispersion of the channel by

$$t_s \geq \tau_{max}. \tag{4.3}$$

Combination of these two inequalities (4.2) and (4.3), yeilds (4.1) as follows [11]

$$\tau_{max} \leq t_s \leq \frac{1}{2\nu_{max}K} \tag{4.4}$$

In our measurements the values of snapshot repetition time and maximum excess delay are chosen in such a way that the two-dimensional Nyquist criterion in (4.1) holds.

4.2   RUSK-LUND Channel Sounder

The channel sounder used in DRIVEWAY'09, DIVERSITY'11, and WCAE'13 measurement campaigns is the RUSK-LUND channel sounder, manufactured by MEDAV [104]. The sounder uses the switched array principle to perform MIMO measurements, which is done by fast multiplexers that sequentially step through the TX and RX antenna elements. The channel sounder is designed for measurements in the frequency domain, and it is capable to measure in the 300 MHz, 2 GHz, and 5 GHz bands with a bandwidth of up to 240 MHz. For the frequency domain measurements it uses a multi-tone, OFDM-like, signal to ensure a constant power spectral density over the whole bandwidth. The phases of each sub-carrier are selected in order to minimize the peak-to-average-ratio
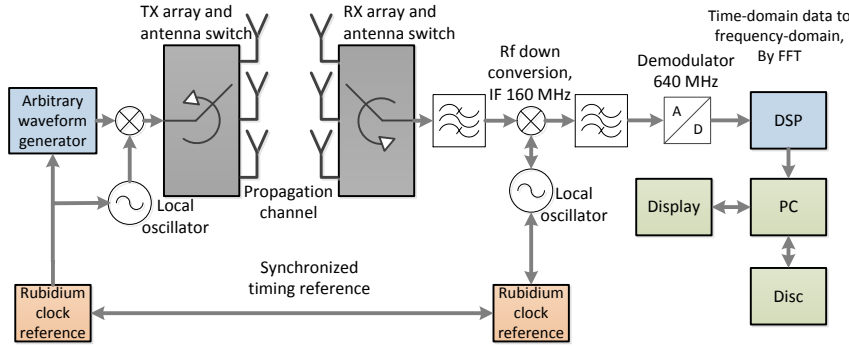
Figure 4.1: Block diagram of the RUSK-Lund channel sounder (courtesy of Medav).

(PAR). The low PAR assures low distortion in the amplifiers and modulator circuits when channel sounding is done simultaneously at different frequencies. A block diagram of this channel sounder is depicted in Fig. 4.1.

The sounder uses switched array principle and hence requires synchronized switching on both the TX and RX switches. This implies that both the TX and RX units of the sounder must be closely synchronized, which is done by using a Rubidium clock reference at the TX and the RX side of the RSUK-LUND sounder.

For a given bandwidth BW, M_{RX} number of antenna elements at the RX, and M_{TX} number of antenna elements at the TX, the sounder records a complete wideband MIMO response or a snapshot in the following fashion as shown in Fig. 4.2.

4.3   Measurement Campaigns

The data used for the evaluation in Papers I-VI was collected during two vehicular measurement campaigns called DRIVEWAY'09 (DiRectional hIgh-speed channel characterization for VEhicular Wireless Access sYstems) in 2009, and DIVERSITY'11 in 2011. The third, WCAE'13 (Wireless Communications in Automotive Environments) in 2013, measurement campaign is carried out recently and the analysis of WCAE'13 data is ongoing.
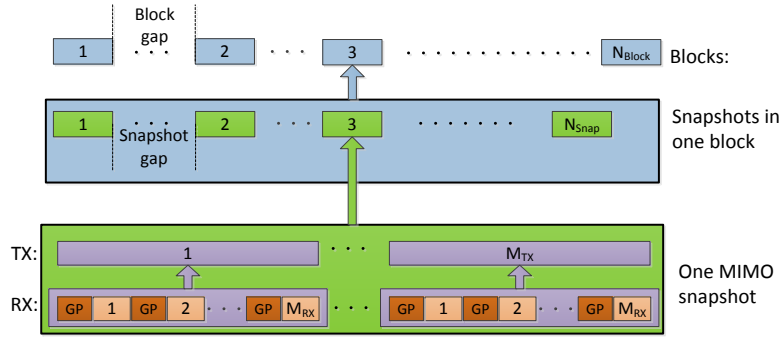
Figure 4.2: Recorded data structure of the RUSK-Lund channel sounder.

4.3.1   DRIVEWAY'09

Vehicular channel measurement campaigns until 2009, were often designed to investigate a set of scenarios typically used for cellular systems. They often included the cases when the TX and RX vehicles are moving either in convoy, in parallel or in opposite directions in urban or rural environments. These scenarios did not cover many of the safety-critical situations and thus it was required to perform new measurements explicitly for such safety-critical scenarios relevant for V2V applications. Having this goal in mind, the DRIVEWAY'09 measurement campaign was performed with realistic measurement setup where the measurement scenarios were chosen based on their importance for safety-related applications [54]. In the following the particularities of the measurement setup are explained in detail.

Measurement Setup

In order to perform a realistic characterization of propagation channel, standard hatchback style cars, 1.73 m high compact multipurpose vehicles (MPVs), were used as TX and RX cars during the measurements. Automotive-grade antenna modules, each consists of a uniform linear array (ULA) with four individual circular patch antenna elements separated by a distance of $\lambda/2$, were designed specifically for the DRIVEWAY'09 measurements at the 5.6 GHz frequency band [105]. The modules were installed on the roof-top, close to rear end of the roof, of each TX and RX car in such a way that the orientation of ULA is perpendicular to the driving direction of the car. Each of the four antenna

Table 4.1: DRIVEWAY'09 measurement parameter settings

Parameter setup	1	2	3	4
Center frequency [GHz], f_c	5.6			
Bandwidth [MHz], BW	240			
Number of frequency samples, N_f	769			
Test signal length [μs], τ_{max}	3.2			
Transmit power [dBm]	27			
Number of TX antenna elements	4			
Number of RX antenna elements	4			
TX/RX antenna height [m]	1.73			
Number of Blocks, N_t	32500			65500
Block gap [μs], t_{BG}	0	205	819	205
Number of snapshots per block	1			
Snapshot gap [μs], t_{SG}	0			
Snapshot repetition time [μs], t_{rep}	102.4	307.2	921.6	307.2
Recording time [s], t_{rec}	3.33	10	30	20

elements in an array was tuned in such a way that it has a somewhat directional radiation pattern. The antenna radiation pattern of element $1, 2, 3$ and 4 have their main lobe pointing to the left-side, backward, forward and to the right-side of the car, respectively. Such an antenna configuration is also beneficial in order to evaluate the double-directional properties of the channel.

The channel sounder sampled the 4×4 MIMO time-varying channel transfer function $H(f,t)$ over a $240\,\text{MHz}$ of measurement bandwidth centered at $5.6\,\text{GHz}$, which is close to the highest allowed center frequency ($5.75\,\text{GHz}$) supported by the RUSK-LUND sounder. It is close enough to the $5.9\,\text{GHz}$ center frequency, dedicated for ITS communications, and thus the differences in the channel properties are expected to be negligible. Four different parameters settings were used, each with different measurement durations, depending on the speed of TX/RX cars. The details of measurement parameters are listed in Table 4.1.

The measurement parameters were carefully chosen such that two dimensional Nyquist criteria in (4.1) is fulfilled. This can further be elaborated with a simple example. The snapshot repetition time for a MIMO system with $M_{TX} = 4$ and $M_{RX} = 4$ antennas, a test signal length of $t_s = 3.2\,\mu$s, and a block gap of $t_{BG} = 205\,\mu$s can be calculated as $t_{rep} = Kt_s = 307.2\,\mu$s, where $K = t_{BG} + 2 \times M_{RX} \times M_{TX} \times t_s$. The maximum Doppler shift that can be resolved associated to $t_{rep} = 307.2\,\mu$s is, $\nu_{max} = 1/2t_{rep} = 1.63\,\text{kHz}$ that corre-

sponds to a maximum relative velocity between TX and RX of $v_{rel} = \nu_{max}\lambda = 87.3\,$m/s (314 km/h). Hence, for $\nu_{max} = 1.63\,$kHz and $t_s = \tau_{max} = 3.2\,\mu$s, $2\tau_{max}\nu_{max} = 5.2 \times 10^{-3} \ll 1$ that satisfies (4.1).

Vehicular environments can suffer maximum Doppler shift upto $\pm 4v\lambda^{-1}$, i.e., 4 times the velocity of cars over the wavelength given that both cars are driving at equal velocity v. Thus, $v_{max} = 1.63\,$kHz allows us to drive maximum at 22 m/s (80 km/h) to be able to observe the maximum Doppler shift in the channel.

4.3.2 DIVERSITY'11

The DRIVEWAY'09 measurement campaign in 2009 was a success in terms of outcome, that helped us to develop a better understanding about the propagation channel for V2V communications. However, one issue that was neither addressed in DRIVEWAY'09 nor in the previous measurement campaigns, with a few exceptions, was the impact of antenna placement at different positions on a vehicle. In [51] an antenna was placed inside the vehicle, next to the windshield other than a roof mounted antenna, whereas in [48] and [57], the effects of five and three different roof positions, respectively, were tested. In, [90] and [91], ray tracing based simulations have been applied to analyze the impact of three and six antenna positions, respectively. That means no (measurement-based) investigations to study the impact of antenna placement at different positions on the car, other than on the roof and windscreen, were available in the literature. Therefore, a new measurement campaign DIVERSITY'11 was planned where four antennas were mounted at four different locations on the TX and RX cars. From one perspective, omni-directional antennas are the most appealing. Then, in the ideal case, the reception of multi-path components from different directions at each position is only due to the antenna placement, not the directivity of the antenna pattern itself. This, however, requires the antenna pattern to be undistorted, i.e., stay tuned, after the antenna has been mounted. An omni-directional antenna may not be a good choice for the bumper mount. Alternatively, a directive antenna is required at this position.

The main goal was to investigate whether there is any antenna combination that is especially suitable for a diversity based system. In the following the particularities of the measurement setup are explained in detail.

Measurement Setup

In order to perform a realistic characterization of the propagation channel, two standard Volvo V70 cars, 1.47 m high station wagons, were used as TX and RX cars during the measurements. The sounder and the batteries needed for power

Table 4.2: V2V-DIVERSITY'11 measurement parameters settings

Parameter setup	ST	LT-1	LT-2	LT-3
Center frequency [GHz], f_c	5.6			
Bandwidth [MHz], BW	200			
Number of frequency samples, N_f	641			
Test signal length [μs], τ_{max}	3.2			
Transmit power [dBm]	27			
Number of TX antenna elements	4			
Number of RX antenna elements	4			
TX/RX antenna height [m]	1.47 approx.			
Number of Blocks, N_t	49152	4915	2048	4915
Block gap [ms], t_{BG}	0.410	89.9		
Number of snapshots per block	1	10	30	10
Snapshot gap [μs], t_{SG}	0	410	410	205
Snapshot repetition time [μs], t_{rep}	512	512	512	307
Recording time [s], t_{rec}	25	460	—	—

supply were stored in the trunk. In this measurement campaign four SkyCross meander SMT-2TO6MB-A antennas were mounted at four different positions on each TX and RX car: roof (R), bumper (B), inside-windscreen (W) and left-side mirror (M). Alternative antenna mounts include the rear bumper as well as the right side mirror, but those antenna positions were not measured in this campaign. Each antenna was omni-directional (in azimuth) vertically polarized, having a frequency range between 2.3 to 5.9 GHz and an antenna gain of around 3 dBi in the used frequency band.

The channel sounder sampled the 4×4 MIMO time-varying channel transfer function $H(f,t)$ over a 200 MHz of measurement bandwidth centered at 5.6 GHz. The measurement time durations were set to 25 s for short term (ST), and 460 s for long term (LT) measurements depending on the speed of TX/RX cars. In the ST measurements it was intended to record fast variations in the channel where as the LT measurements were done to observe variations in the channel over a longer period of time. Four different parameter settings were used. The details of measurement parameters are listed in Table 4.2.

Just like the DRIVEWAY'09, the measurement parameters were again chosen carefully such that two-dimensional Nyquist criteria in (4.1) is fulfilled.

4.3.3   WCAE'13

In the previous measurement campaigns intention was to characterize channel properties for different safety-critical scenarios and/or for different antenna positions on a vehicle, especially when there is LOS between TX and RX or when LOS is blocked by buildings only. However, while driving on different roads, occasionally other vehicles were driving in between the TX and RX obstructing the LOS path. It was observed that the obstruction in the LOS path always introduces an additional loss in the received power, that needs to be quantified as a function of distance. Moreover, there are no dedicated measurement campaigns to characterize the propagation channel for Truck-to-Vehicle (T2V) communications and how different is the channel for different antennas mounted at different positions on a truck. Therefore, a new measurement campaign was performed with two major goals: first, to properly analyze the impact of obstructed LOS as a function of distance, in a controlled fashion using a truck as obstructing vehicle, and second, to measure T2V propagation channel, in various scenarios, respectively. The measurements were performed in November 2013, and the data analysis is in progress.

4.4   Measurement Scenarios

The automotive industry together with ETSI ITS standardization organization in Europe and US-DOT in USA, respectively, have specified a basic set of ITS applications that can effectively reduce the number of road accidents and traffic jams, details can be found in [106] and [107]. Among these of particular interest here are V2V/T2V cooperative road safety and traffic efficiency applications, listed in Table 4.3.

Having these safety applications in mind, a number of scenarios were identified, where vehicular channel measurements were performed. The measurement sites were carefully chosen such that somewhat generalized conclusion about each scenario can be drawn. All sites are located in and around the cities of Lund and Malmö in southern Sweden. We have performed 5-15 measurement runs in each scenario in order to obtain meaningful statistics. In the following the measured scenarios are discussed in detail.

4.4.1   Rural

A rural scenario is characterized as a country road with open surroundings. Therefore, the measurements were performed outside the city of Lund on a road where there were open fields on both sides of the road and a few static scatterers such as houses or road signs at some $300 - 400\,\mathrm{m}$ distance from the

Table 4.3: ITS Applications and use cases for active road safety in [106] and [107]

Applications	Use case
Road hazards	Forward collision warning (FCW)
	Emergency electronics brake light warning (EEBW)
	Blind spot warning (BSW)
	Wrong way driving warning (WWDW)
	Do not pass warning (DNPW)
	Roadwork warning (RWW)
	Traffic condition warning (TCW)
Cooperative-awareness	Cross traffic violation warning (CTVW)
	Intersection collision warning (ICW)
	Left/right turn assistance at intersection (LTA)
	Emergency vehicle warning (EVW)

measurement site. The rural scenario was measured as a reference to analyze the case when there are no or very few scatterers around. Most relevant V2V safety applications for this scenario are Forward collision warning (FCW), Emergency electronics brake light warning (EEBL), and Do not pass warning (DNPW) (see Table 4.3). In such a sparse scenario with very few scatterers, the channel conditions can be challenging, as very little or no power will be received if the LOS between the TX and RX is obstructed by larger vehicles. This scenario is further divided into two sub-scenarios, for the measurements

- Rural - Convoy (Ru-con): When both the TX and RX cars were driving in a convoy at an approximate speed of $17 - 20$ m/s, TX-RX separation was varying during the measurements.

- Rural - Opposite (Ru-opp): When both the TX and RX cars were driving towards each other at an approximate speed of $17 - 20$ m/s.

4.4.2   Highway

A highway scenario in general may include 2-6 lanes in each direction with variable traffic, and the measurements were performed on a $4-$lane highway (E22), $2-$lanes in each driving direction. The measurements were performed on a stretch of the road, over 10 km long, between Lund and Malmö city. The direction of travel on the highway was separated by a (≈ 0.5 m tall) concrete wall whereas the outer boundary of road was guarded by a metallic rail. Most

(a) Ru-con: (N 55°43′46″, E 13°14′33″)   (b) Ru-opp: (N 55°43′46″, E 13°14′33″)
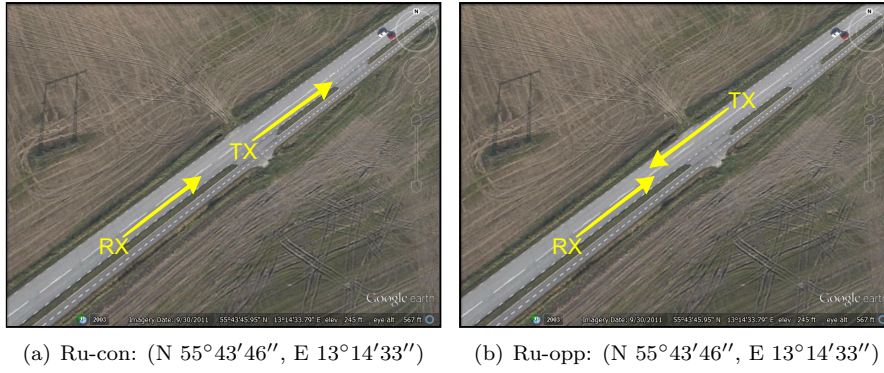
Figure 4.3: Google Earth™ [108] aerial image of a patch of the rural road outside Lund where Ru-con and Ru-opp measurements were performed.

relevant V2V safety applications for this scenario are Forward collision warning (FCW), Emergency electronics brake light warning (EEBW), Roadwork warning (RWW), and Blind spot warning (BSW) (see Table 4.3). This scenario is divided into two sub-scenarios,

- Highway - convoy (Hi-con): When both the TX and RX cars were moving in a convoy at a speed of $22 - 25\,\mathrm{m/s}$. Measurements while overtaking, in obstructed LOS by other vehicles and in traffic congestion were also performed.

- Highway - Merging Lanes (Hi-ml): A scenario at a highway that is characterized by the roads that are used to merge two traffic flows into one, e.g., entrance or exit ramps. An important aspect of this scenario is the possibility of an obstructed LOS path due to the slope and the orientation of the terrain, or the presence of sound barriers, buildings or trees between the intersecting roads. This scenario is similar to the intersection scenario (discussed in the following section), but with slightly more difficult channel conditions in the absence of the LOS due to availability of fewer scatterers and higher vehicle speeds.

(a) Hi-con: (N 55°43′46″, E 13°14′33″)   (b) Hi-ml: (N 55°43′46″, E 13°14′33″)
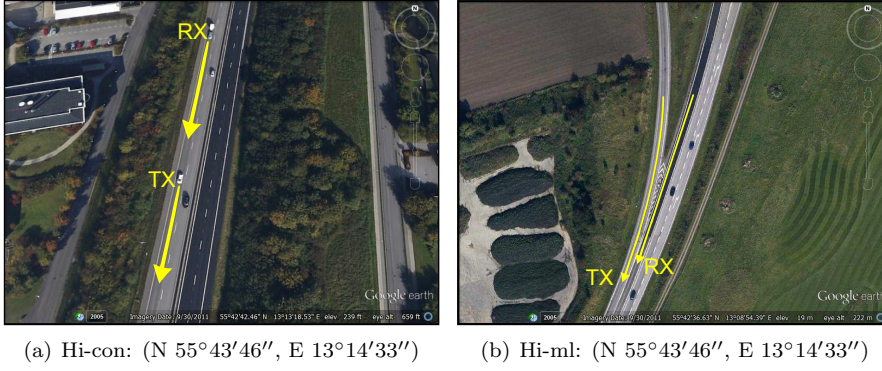
Figure 4.4: Google Earth™ [108] aerial image of a patch of the highway E20 between Lund and Malmö.

4.4.3 Urban

Urban scenario is characterized by streets/roads in densely populated areas with single- to multi-story buildings lined on both sides of the streets. Therefore, the measurements were performed in Lund and Malmö where the streets are $12 - 40$ m wide, either single or multi-lane, lined with $2 - 4$ storied buildings. The vehicles were driven over $2 - 6$ km long loops and on a 3 km long stretch at varying speeds ranging from 0 to 14 m/s. Most relevant V2V safety applications for this scenario are Forward collision warning (FCW), Emergency electronics brake light warning (EEBW), Roadwork warning (RWW), Wrong way driving warning (WWDW) and Do not pass warning (DNPW) (see Table 4.3). This scenario is divided into two sub-scenarios,

- Urban - convoy (Ur-con): When both the TX and RX cars were moving in a convoy at varying speeds ranging $0 - 14$ m/s. During the measurements, the cars where driving through varying surroundings and traffic conditions, i.e., from no traffic to traffic-jam and while standing at redlights.

- Urban - opposite (Ur-opp): When both the TX and RX cars were approaching each other while driving at speeds between $12 - 14$ m/s in different streets.

(a) Ur-con: (N 55°35′41″, E 13°0′31″)   (b) Ur-opp: (N 55°42′37″, E 13°11′15″)
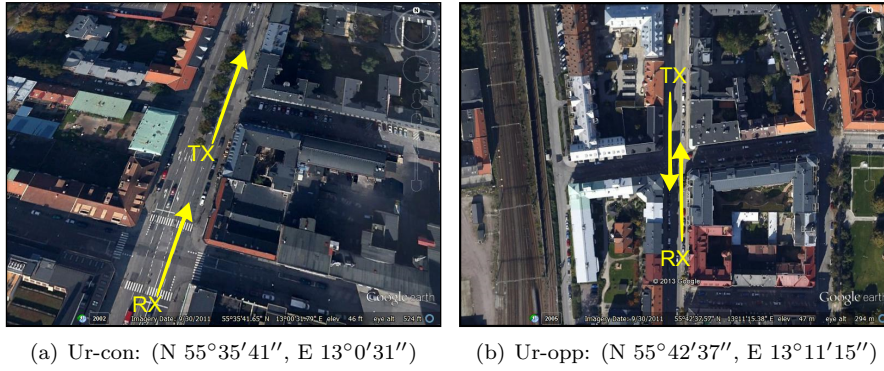
Figure 4.5: Google Earth™ [108] aerial image of the urban streets intersections in Lund and Malmö where Ur-con and Ur-opp measurements were performed.

4.4.4   Intersection

An intersection scenario is described as when more than one rural, urban, or suburban streets/roads of varying widths intersect at a certain point. In this scenario, the visual LOS between cars approaching the intersection is often blocked by buildings of certain height situated at the corner of the intersection. In such a NLOS scenario the V2V link reliability depends on the availability of scattering objects nearby, e.g., buildings, trees, light poles, street signs, and parked cars. These objects are expected to provide many additional multi-path components which is beneficial for signal reception in NLOS situation. Most relevant V2V safety applications for this scenario are Forward collision warning (FCW), Emergency electronics brake light warning (EEBW), Roadwork warning (RWW), Wrong way driving warning (WWDW) and Do not pass warning (DNPW) (see Table 4.3). This scenario is divided into four sub-scenarios,

- Intersection - urban multiple lane (Int-uml): Four-way intersection with wider streets having two or more lanes in each driving direction. In addition to that each intersection has multi-story buildings situated at each corner of the intersection, either to block the LOS or act as a scatter.

- Intersection - urban single lane (Int-usl): Four-way intersection with narrow streets having single lane in each driving direction. In addition to that each intersection has multi-story buildings situated at each corner of the intersection, either blocking the LOS or acting as a scatter.

(a) Int-uml: (N 55°35′56″, E 13°0′30″)

(b) Int-usl: (N 55°42′37″, E 13°11′15″)

(c) Int-swt: (N 55°41′42″, E 13°11′19″)

(d) Int-swot: (N 55°42′26″, E 13°9′39″)
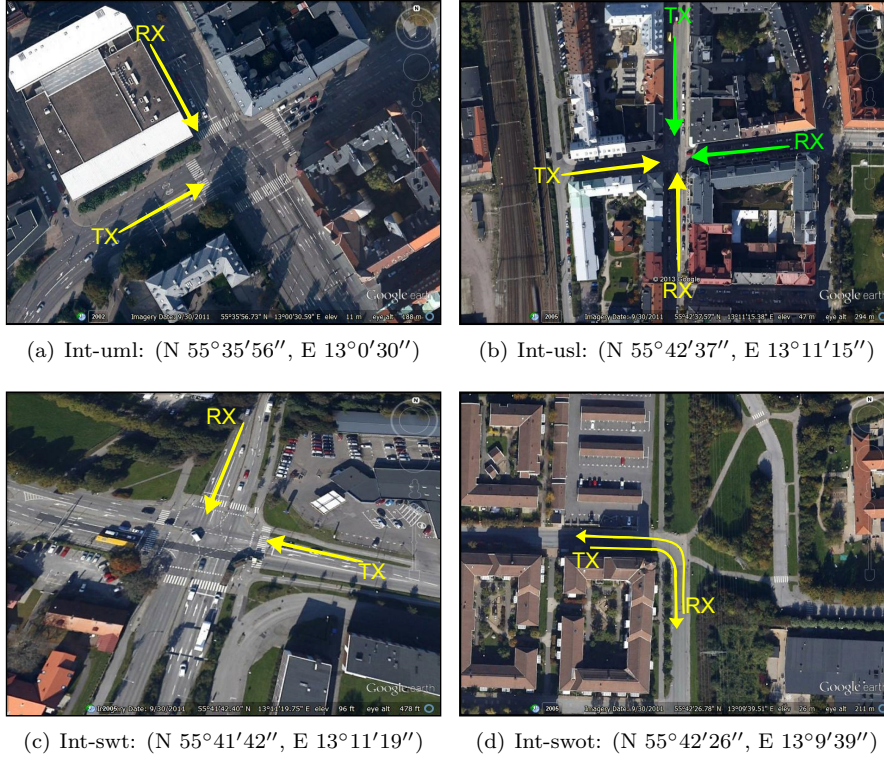
Figure 4.6: Google Earth$^{\text{TM}}$ [108] aerial image of the four types of street intersections in Lund and Malmö. In each intersection the TX and RX vehicles were approaching the intersection center while driving along the yellow lines. All the images have same map scale.

- Intersection - suburban with traffic (Int-swt): Four-way intersection with little to no building next to the intersection, but with a busy traffic situation.

- Intersection - suburban without traffic (Int-swot): T-shaped intersection in which buildings are situated at the intersection corner blocking LOS of the TX and RX vehicles that are approaching the intersection. There is no building or traffic on the other side of the of the intersection, but an open surrounding with some vegetation.

4.4.5   Tunnel

- Tunnel - convoy (Tu-con): This scenario is characterized by a tunnel with two or more lane roads and traffic in one direction only. Tunnels sometime allocate one driving direction for each tunnel thus main safety applications targeting this scenario include overtaking and hazard notifications inside tunnels. The channel is considered to have rich scattering inside tunnels due to MPC from the walls, roof, ground and metallic structures inside the tunnel. Therefore, the measurements were performed in the tunnel between Denmark and Sweden, as shown in Fig. 4.7(a), when both the TX and RX cars were driving in a convoy inside the tunnel.

4.4.6   On Bridge

- Bridge - convoy (Br-con): This scenario is characterized by a bridge with two or more lane roads, typically with open surroundings except some metallic bars guarding roadside, and traffic in one direction only. Therefore, the measurements were performed on a bridge between Denmark and Sweden when both the TX and RX cars are driving in a convoy, as show in Fig. 4.7(b).

(a) Tu-con   (b) Br-con

Figure 4.7: Google Maps^{TM} [109] images of the tunnel and öresund bridge, between Denmark and Sweden where Tu-con and Br-con measurements were performed.

In terms of analysis it is important to consider that in each of these scenarios a V2V radio link can have either of the three possible channel situations.

Table 4.4: Measured safety-critical scenarios:(i) means LOS, (ii) means OLOS, (iii) means NLOS, (+) means measurements performed and (-) means no measurements

Campaigns	DRIVEWAY'09			DIVERSITY'11			WCAE'13		
Scenarios	i	ii	iii	i	ii	iii	i	ii	iii
Ru-con	+	-	-	+	-	-	+	+	-
Ru-opp	+	-	-	+	-	-	+	+	-
Hi-con	+	+	-	+	+	-	+	+	-
Hi-ml	+	-	+	-	-	-	-	-	-
Ur-con	+	+	+	+	+	+	+	+	+
Ur-opp	+	-	+	+	+	+	+	+	+
Int-uml	+	-	+	+	-	+	+	+	+
Int-usl	+	-	+	+	-	+	+	+	+
Int-swt	+	-	+	+	-	+	-	-	-
Int-swot	+	-	+	+	-	+	-	-	-
Tu-con	+	+	-	-	-	-	-	-	-
Br-con	+	+	-	-	-	-	-	-	-

Table 4.4 summarizes all the aforementioned measured scenarios w.r.t. to each measurement campaign.

4.5   Route Documentation

To keep track of the positions of the TX and RX vehicles, GPS coordinates were also logged during each measurement run. In addition to GPS data, videos of each measurement were also recorded through the windscreen of each of the TX and RX cars. GPS coordinates together with video information are used in the post processing of the data to find the reasons whenever an unexpected but significant difference between the links is observed due to variations in traffic density, number of pedestrians, houses and road side environment. GPS antennas were attached to the sounder, in such a way that the GPS data is already synchronized to the sounder clock. However, video documentation was manually synchronized with the measurement data.

Chapter 5

Summary and Contributions

This chapter summarizes main contributions of the thesis to the research field. In the first section, the six papers, which constitutes the core of this thesis, are summarized and my contributions in the individual papers are highlighted. The papers are not listed in a chronological order, but in an order based on their content. In the second section, general conclusions regarding the research area are provided together with some ideas on future work. We believe that the thesis contributes to the better understanding of vehicular channels and takes it one step further by filling some gaps of knowledge in the area of vehicular channel characterization.

5.1 Research contributions

5.1.1 Paper I: Directional Analysis of Vehicle-to-Vehicle Propagation Channels

Analysis of directional properties is important for the assessment of MIMO systems, e.g., for evaluating the possible diversity gain, as well as to improve the understanding of important propagation effects. Moreover, there is a lack of available results on directional properties of V2V channels in the literature. In this paper we present a double directional analysis of DRIVE-WAY'09 V2V MIMO channel measurements conducted in three different traffic scenarios: street-intersection, traffic-congestion and obstructed-LOS. Using SAGE, a high-resolution algorithm for parameter estimation, we estimate chan-

nel parameters like angle-of-arrival, angle-of-departure, propagation delay and Doppler shift and identify underlying propagation mechanisms by manually combining these estimates with maps of the measurement sites. To our best knowledge this is the first double directional analysis of V2V channels performed and also the first paper quantifying the power contribution of different common objects in the environment for V2V channels.

The results show that first-order reflections from a small number of interacting objects can account for a large part of the received signal in the absence of line-of-sight (LOS). This effect is especially pronounced in the two traffic scenarios where the road is not lined with buildings. We also found that the direction spread is low (and conversely that the antenna correlation is high) in such scenarios, which suggests that beam-forming rather than diversity-based methods should be used if multiple antenna elements are available. The situation is reversed, however, in the third scenario, a narrow urban intersection, where a larger number of higher-order reflections is found to result in a higher direction spread, which encourages potential use of diversity-based methods in such environments.

I am the main contributor to this paper and I was involved in all parts of the scientific work such as data analysis and writing of the paper except the channel measurements which were done before I started as a PhD student. The first implementation of parameter estimation algorithm SAGE was available, however it was not fully functional to begin with. I worked on SAGE to make it functional and also extended it for Doppler estimation.

5.1.2 Paper II: Radio Channel Properties for Vehicular Communication: Merging Lanes versus Urban Intersections

Vehicles that are approaching a street intersection or merging on a highway often have NLOS from the vehicles in the other street or road because the visual LOS is blocked by nearby buildings or objects. In such situations the scattering of radio waves, i.e., reflection, diffraction, and refraction, implicitly enable NLOS reception. Moreover, merging lanes occur often in highway or rural environments, there is a limited number of large objects in the surrounding that can contribute to increase the scattering. Similarly, some street intersections, often called open intersections which have one big building that block the LOS and only few scattering objects in the surrounding. Thus, NLOS reception in merging lane and open intersection scenarios could probably be very bad, and that needs to be characterized explicitly.

In this paper, results for V2V channel characterization based on DRIVE-WAY'09 channel measurements conducted for merging lanes on a highway, and

four-way street intersection scenarios are presented. This paper is the first to present a detailed measurement based analysis of the merging lane scenario. The importance of different propagation mechanisms in NLOS situations and the impact of the antenna radiation pattern on the total received power in LOS situations is highlighted for these scenarios. For the analysis and comparison we use channel metrics like power delay proles as well as channel gains. We also analyze important propagation mechanisms to see the impact of line-of-sight (LOS) and the antenna radiation pattern on the total received power. It is found that the absence of LOS and strong scattering objects, in the area close to the point where the ramp merges with a highway, may result in poor to no received signal power and hence two times reduced communication range, when the LOS is blocked.

It is found that the street intersection scenario is similar to the merging lane scenario with slightly better propagation conditions due to availability of scatterers. This implies that the merging lane scenario is more critical in terms of communication reliability. Moreover, the antenna radiation pattern plays an important role especially in the situation when there are few scatterers and if the antenna has a poor gain in the direction of the TX, then the received power level can drop significantly. Thus designing an antenna that has an omni-directional gain, or using multiple antennas that radiate towards different directions becomes more important for such safety critical scenarios.

I am the main contributor to this paper and I was involved in all parts of the scientific work such as data analysis and writing of the paper except the channel measurements which were done before I started as a PhD student.

5.1.3   Paper III: Simulation and Measurement Based Vehicle-to-Vehicle Channel Characterization: Accuracy and Constraint Analysis

In this paper, a deterministic channel model for vehicle-to-vehicle (V2V) communication, developed by TU Braunschweig, is compared against the channel measurements data collected during the DRIVEWAY'09 channel measurement campaign. Channel metrics such as channel gain, delay and Doppler spreads, angular spread, eigenvalue decomposition and antenna correlations are derived from the measurement data as well as from the channel simulation data obtained from the ray-tracing simulations for two different measurements in an urban four-way intersection scenario. In the literature there are only a few papers dealing with a detailed comparison between ray-tracing and channel measurement results, to our best knowledge none in the field of V2V channels.

Most of the power contributions arising from specular and non-specular reflections are also captured by the ray-tracing simulation regardless of some

known implementation-based limitations of the ray-tracing model. Measurement and simulation results show a very good agreement in the presence of line-of-sight (LOS), because most of the power in the LOS is contributed by the LOS component. This is not the case when the LOS is absent, as the ray-tracer is unable to capture some of the diffuse and higher-order reflected paths. The directional properties of the channel also look very similar for the measurement and simulated data, however a more detailed directional analysis will be performed to investigate common clusters and reflection points.

I am the main contributor to this paper and I was involved in all parts of the scientific work such as data analysis and writing of the paper except the channel measurements which were done before I started as a PhD student.

5.1.4   Paper IV: Validation of a Non-Line-of-Sight Path-Loss Model for V2V Communications at Street Intersections

There exists a number of V2V measurement and ray-tracing simulation based studies to characterize the radio channel in urban street intersections [57, 65, 69, 72, 86, 88]. In these studies it was found that the geometry of the street intersections, i.e., street width and alignment, structure of buildings, and antenna height have great impact on the NLOS reception in an urban intersection at 5.9 GHz frequency. Moreover, it is found that V2V ray-tracing simulation models often underestimate channel parameters like, e.g., delay spread and Doppler spread, for certain streets due to limited geographical information. Thus, a NLOS model is needed for urban intersections that is generalized and incorporates specific geometric aspects in a closed-form expression.

In the literature there exists a NLOS pathloss model named *Virtual-Source11p*, which is claimed to be flexible and of low complexity. In this paper we take this model as a reference NLOS model and validate the accuracy of the model with the help of independent channel measurement data collected during DRIVEWAY'09 measurement campaign.

From the analysis it is found that the model fits well, with a few exceptions, to the measurements. Those are in turn made in different intersections having variable geometries and scattering environments. It is found that the model can be made more general if an intersection dependent parameter, that depends on the property and number of available scatterers in that particular intersection, is included in the model. The main contribution of this paper is that an existing model is validated with independent measurement data (recorded in different cities and a different country), and with good agreement. The proposed model seems to be a good candidate for the received power levels in urban street intersections.

I am the main contributor to this paper and I was involved in all parts of the scientific work such as data analysis and writing of the paper except the channel measurements which were done before I started as a PhD student.

5.1.5   Paper V: Measurement Based Shadow Fading Model for Vehicle-to-Vehicle Network Simulations

The vehicle-to-vehicle (V2V) propagation channel has significant implications on the design and performance of novel communication protocols for vehicular *ad hoc* networks (VANETs). Extensive research efforts have been made to develop V2V channel models to be implemented in advanced VANET system simulators for performance evaluation. The impact of shadowing caused by other vehicles has, however, largely been neglected in most of the models, as well as in the system simulations. It is important to model vehicles as obstacles, ignoring this can lead to an unrealistic assumptions about the performance of the physical layer, which in turn can effect the behavior of higher layers of V2V systems.

In this paper we present a shadow fading model targeting system simulations based on based on DIVERSITY'11 channel measurements performed in urban and highway scenarios. The measurement data is separated into three categories, line-of-sight (LOS), obstructed line-of-sight (OLOS) by vehicles, and non line-of-sight (NLOS) by buildings, with the help of video information, recorded during the measurements. It is observed that vehicles obstructing the LOS induce an additional attenuation of about $10\,\mathrm{dB}$ in the received signal power. An approach to incorporate the LOS/OLOS model into existing VANET simulators is also provided. Finally, system level VANET simulation results are presented, which show the difference between the LOS/OLOS model and a channel model based on Nakagami-m fading.

This paper was one of the first (when published at arxiv.org) to quantify the impact of obstructing vehicles in real traffic conditions and to highlight the influence on the communication range of those.

I am the main contributor to this paper and I was involved in all parts of the scientific work: channel measurements, data analysis and writing of the paper.

5.1.6   Paper VI: Measurement-Based Analysis: The Effect of Complementary Antennas and Diversity on Vehicle-to-Vehicle Communication

In V2V systems the antennas are prone to shadowing and the antenna gain is dissimilar even for same antenna elements if mounted at different positions on

the car. In the past, a majority of V2V measurement campaigns have exclusively been performed with the same type of antenna mounting: a roof-mounted antenna (array). However, a small number of exceptions exists in which antennas were mounted on alternate locations, e.g., different position on the roof or inside the vehicle (next to windscreen). Therefore, experimental studies employing real-time-measurement are essential to understand how antennas mounted at different positions on a car affect the behavior and performance of the radio link.

This paper investigates the impact of antenna placement based on DIVERSITY'11 channel measurements performed with four omni-directional antennas mounted on some of the most favorable antenna positions on a car such as roof, bumper, windscreen and left-side mirror of the transmitter and receiver cars. We use diversity combining methods such as selection combining (SC) and maximum ratio combining (MRC) to evaluate the performance differences for all possible SIMO, MISO and MIMO link combinations. We then short list and analyze the most interesting cases, that are 2x2 MIMO diversity with SC and MRC, and 1x2 SIMO diversity with SC only. This investigation suggests that a pair of antennas with complementary properties, e.g., a roof mounted antenna together with a bumper antenna is a good solution for obtaining the best reception performance, in most of the propagation environments. The use of these antenna positions requires, however, long cables which introduce an additional attenuation unless some countermeasures are taken.

To the best of our knowledge this is the first paper that explicitly characterize the impact of antenna placement, other then roof mounting, on a vehicle using channel measurement data. The main contribution of this paper is that the two antenna positions with complementary properties out of four measured positions are proposed that can provide full diversity gain.

I am the main contributor to this paper and I was involved in all parts of the scientific work: channel measurements, data analysis and writing of the paper.

5.2   General Conclusions and Future Work

The wireless propagation channel in general is a complicated process and it has significant influence on the received signal and resulting performance. There are a large number of parameters that define the properties of a channel. To define and understand the channel properties with the help of channel measurements is known as channel characterization where as quantifying these channel properties in such a way that the effects of the channel can be reproduced (in a statistical manner) for network simulations and system testing, is known as

channel modeling. Such a measurement based characterization and modeling for time-varying V2V channels have been the topic of this thesis. In this section, I would like to take the opportunity to share some general conclusions about the field that I have drawn over the last few years and how my works relates to the topic.

The channel measurements are essential, not only to characterize and model the channel properties but to validate theoretical and simulation based channel models. Gathering channel data is a time-consuming task which requires a lot of preparations and planning, thorough considerations in terms of scenario selection, and state of the art measurement equipment so that a generalized description of the channel can be obtained. An attractive alternative to measurements is the use of ray-tracing simulations for channel characterization given that the detailed geometric description of the site of interest is available. The ray-tracing approach has a clear advantage over measurements, as it requires much less efforts and is less time-consuming as compared to channel measurements but you can never be guaranteed that it reflects the true behavior of real channels. The computational complexity can be an underlying issue for ray-tracing based characterization especially for V2V scenarios due to high mobility of the TX and RX vehicles. Modeling of all the scattering objects when the environment is changing rapidly can be a non-trivial task. However, this issue can be solved by restricting the analysis to small geographical areas and by finding a good trade-off between complexity and performance, the issue is addressed in paper III.

There has been a lot of research in the area of V2V channel characterization and many models have been developed over the last few years. Field trials to test system performance in real-life are on going too. Still little or no attention was paid to some of the very important aspects, discussed in the following:

First, most of the studies were targeting LOS situations only, the shadowing effects caused by neighboring vehicles, and NLOS reception when the LOS is blocked by buildings were paid little to no attention. These situations do not only degrade the received signal power significantly at $5.9\,\mathrm{GHz}$ frequency, but they occur mostly in the safety critical scenarios such as overtaking other vehicles, changing lanes, merging on a highway, and crossing street intersections in urban environments. These facts motivate thorough characterization of V2V channels in obstructed-LOS and NLOS situations. This includes modeling of pathloss, fading statistics, spatial correlation, time, frequency, and angular dispersion, and finally geometry based stochastic channel model. A subset of these aspects have been addresses in the literature as well as in papers I-V.

Second, most of the channel measurement campaigns have been conducted with two vehicles, one TX and one RX vehicle. For large scale simulations of V2V communication systems, where several vehicles may transmit and receive

simultaneously, the correlation between different links is also of interest to obtain reliable results. This link correlation, however, has not yet been studied.

Third, it is typically desirable to have antenna beam radiating equal power in all directions for V2V communications. A single directional antenna can suffer from serious power losses in the situations when the LOS or otherwise dominating multipath component is blocked and there exits very few scattering objects in the environment. For that reason, arrays with multiple antennas radiating in different directions are preferred. Moreover, the location of the antenna on a vehicle is found to have a large impact on the performance of V2V systems. It is observed that the antenna mounted at the rear end of the roof can experience over $3\,\mathrm{dB}$ up to $10\,\mathrm{dB}$ loss in comparison to an alternative antenna position on a vehicle, such as, e.g., the front bumper. The loss for the roof antenna is mainly due to the beam tilt caused by vehicle roof in the driving direction. In addition to that a lot of attention has always been paid to the design of the vehicle itself in the auto-motive industry. Antenna mounted at a location that is hidden in the vehicle chase is preferred in a design perspective. In the literature there are very few measurement and simulation based studies investigating alternative antenna positions, and using multiple antenna to exploit spatial diversity. Paper VI investigates the effect of complementary antennas on V2V communications. However, many antenna related issues have not been investigated and still require further research while keeping aforementioned aspects in mind.

Last but not least, one of the most intriguing issue concerning V2V channel research I felt is that there has not been many efforts to independently validate each others work. Many models have been developed and many measurement based studies for V2V channel characterizing have been published, but comparison of different modeling approaches and validation of different models are still missing. This will certainly help us to find a way to converge and to find suitable yet simplified models for V2V propagation channels.

References

[1] J. C. Maxwell, "A dynamical theory of the electromagnetic field," *Philosophical Transactions of the Royal Society of London*, vol. 155, pp. 459–512, 1865. [Online]. Available: http://rstl.royalsocietypublishing.org/content/155/459.short

[2] R. W. Simons, "Guglielmo Marconi and early systems of wireless communications," *GEC J. Tech*, vol. 11, pp. 37–56, 1996.

[3] M. Peden, R. Scurfield, D. Sleet, D. Mohan, A. A. Hyder, E. Jarawan, and C. Mathers, "World report on road traffic injury prevention," Geneva: World Health Organization, Tech. Rep., 2004.

[4] R. Uzcategui and G. Acosta-Marum, "Wave: A tutorial," *Communications Magazine, IEEE*, vol. 47, no. 5, pp. 126–133, 2009.

[5] ETSI-TR-102638, "Intelligent transport sytems (ITS), vehicular communications, basic set of applications, definitions," *V1.1.1*, June 2009.

[6] *IEEE Std. 802.11p-2010, Part 11: Wireless LAN Medium Access Control (MAC) and Physical Layer (PHY) specifications: Amendment 7: Wireless Access in Vehicular Environment*, IEEE Std., July 2010.

[7] J. Gozalvez, M. Sepulcre, and R. Bauza, "Impact of the radio channel modelling on the performance of VANET communication protocols," *Telecommunication Systems*, pp. 1–19, Dec. 2010.

[8] A. Molisch, *Wireless Communications.* Chichester, West Sussex, UK: IEEE Press-Wiley, 2005.

[9] P. Bello, "Characterization of randomly time-variant linear channels," *Communications Systems, IEEE Transactions on*, vol. 11, no. 4, pp. 360–393, 1963.

[10] G. Matz and F. Hlawatsch, *Wireless Communications over Rapidly Time-Varying Channels, Gerald Matz and Franz Hlawatsch.* Eds. Academic Press, 2011, ch. Fundamentals of Time-Varying Communication Channels, pp. 1–63.

[11] L. Bernadó, "Non-stationarity in vehicular wireless channels," Ph.D. dissertation, Technische Universität Wien, Vienna, Austria, 2012.

[12] G. Matz, "On non-wssus wireless fading channels," *Wireless Communications, IEEE Transactions on*, vol. 4, no. 5, pp. 2465–2478, 2005.

[13] L. Bernado, T. Zemen, F. Tufvesson, A. Molisch, and C. Mecklenbrauker, "The (in-) validity of the wssus assumption in vehicular radio channels," in *Personal Indoor and Mobile Radio Communications (PIMRC), 2012 IEEE 23rd International Symposium on*, 2012, pp. 1757–1762.

[14] A. F. Molisch, F. Tufvesson, J. Karedal, and C. F. Mecklenbräuker, "A survey on vehicle-to-vehicle propagation channels," in *IEEE Wireless Commun. Mag.*, vol. 16, no. 6, 2009, pp. 12–22.

[15] A. Molisch and M. Steinbauer, "Condensed parameters for characterizing wideband mobile radio channels," *International Journal of Wireless Information Networks*, vol. 6, no. 3, pp. 133–154, 1999.

[16] P. Almers, E. Bonek, A. Burr, N. Czink, M. Debbah, V. Degli-esposti, H. Hofstetter, P. Kysti, D. Laurenson, G. Matz, A. F. Molisch, C. Oestges, and H. Özcelik, "Survey of channel and radio propagation models for wireless mimo systems," *EURASIP Journal on Wireless Communications and Networking*, vol. 2007, p. 19, 2007.

[17] A. Richter, "Estimation of radio channel parameters: Models and algorithms," Ph.D. dissertation, Ph.D. dissertation,Technischen Universitt Ilmenau, Germany, May 2005. [Online]. Available: http://www.db-thueringen.de/

[18] S. C. H. Allen Taflove, *Computational Electrodynamics: The Finite-Difference Time-Domain Method*, 2nd ed. Norwood, MA, USA: Artech House, June 2000.

[19] J. N. Reddy, *An Introduction to the Finite Element Method.* New York, NY: McGraw-Hill, 1985.

[20] W. Wiesbeck and S. Knorzer, "Characteristics of the mobile channel for high velocities," in *Electromagnetics in Advanced Applications, 2007. ICEAA 2007. International Conference on*, 2007, pp. 116–120.

[21] J. Nuckelt, M. Schack, and T. Kürner, "Deterministic and stochastic channel models implemented in a physical layer simulator for Car-to-X communications," *Advances in Radio Science*, vol. 9, pp. 165–171, Sept. 2011.

[22] J. Karedal, F. Tufvesson, N. Czink, A. Paier, C. Dumard, T. Zemen, C. Mecklenbräuker, and A. F. Molisch, "A geometry-based stochastic MIMO model for vehicle-to-vehicle communications," *IEEE Transactions on Wireless Communications*, vol. 8, no. 7, pp. 3646–3657, 2009.

[23] A. F. Molisch, A. Kuchar, J. Laurila, K. Hugl, and R. Schmalenberger, "Geometry-based directional model for mobile radio channelsprinciples and implementation," *European Transactions on Telecommunications*, vol. 14, no. 4, pp. 351–359, 2003. [Online]. Available: http://dx.doi.org/10.1002/ett.928

[24] J. Wallace and M. Jensen, "Modeling the indoor MIMO wireless channel," *Antennas and Propagation, IEEE Transactions on*, vol. 50, no. 5, pp. 591–599, 2002.

[25] T. Zwick, C. Fischer, D. Didascalou, and W. Wiesbeck, "A stochastic spatial channel model based on wave-propagation modeling," *Selected Areas in Communications, IEEE Journal on*, vol. 18, no. 1, pp. 6–15, 2000.

[26] J. Maurer, T. Fugen, and W. Wiesbeck, "Narrow-band measurement and analysis of the inter-vehicle transmission channel at 5.2 GHz," in *Vehicular Technology Conference, 2002. VTC Spring 2002. IEEE 55th*, vol. 3, 2002, pp. 1274–1278 vol.3.

[27] J. Salmi, "Contributions to measurement-based dynamic MIMO channel modeling and propagation parameter estimation," Ph.D. dissertation, Ph.D. dissertation at Helsinki University of Technology, Helsinki, Finland, August 2009. [Online]. Available: http://lib.tkk.fi/Diss/2009/isbn9789522480194/

[28] L. Cheng, B. Henty, D. Stancil, F. Bai, and P. Mudalige, "Mobile vehicle-to-vehicle narrow-band channel measurement and characterization of the 5.9 GHz dedicated short range communication (DSRC) frequency band," *Selected Areas in Communications, IEEE Journal on*, vol. 25, no. 8, pp. 1501 –1516, Oct. 2007.

[29] J. Karedal, "Measurement-based modeling of wireless propagation channels - MIMO and UWB," Ph.D. dissertation, Department of Electrical and information technology, Lund University, Sweden, Feb. 2009.

[30] G. Stüber, *Principles of Mobile Communication*, second ed. ed. Dordrecht: Norwell, MA: Kluwer Academic Publishers, 2000.

[31] M. Gudmundson, "Correlation model for shadow fading in mobile radio systems," *Electronics Letters*, vol. 27, no. 23, pp. 2145 –2146, nov. 1991.

[32] C. Nelson and H. Simon, *MIMO Channel Models: Thoery and Pratice*. John Wiley & Sons, 2010.

[33] R. Vaughan and J. B. Andersen, *Channels, Propagation and Antennas for Mobile Communications (IEE Electromagnetic Waves Series, 50)*. Institution of Engineering and Technology, Feb. 2003.

[34] J. Andersen, "Array gain and capacity for known random channels with multiple element arrays at both ends," *Selected Areas in Communications, IEEE Journal on*, vol. 18, no. 11, pp. 2172–2178, 2000.

[35] J. Fessler and A. Hero, "Space-alternating generalized expectation-maximization algorithm," *Signal Processing, IEEE Transactions on*, vol. 42, no. 10, pp. 2664–2677, 1994.

[36] B. H. Fleury, M. Tschudin, R. Heddergott, D. Dahlhaus, and K. I. Pedersen, "Channel parameter estimation in mobile radio environments using the SAGE algorithm," *IEEE J. Select. Areas Commun.*, vol. 17, no. 3, pp. 434–450, Mar. 1999.

[37] A. Richter, J. Salmi, and V. Koivunen, "An algorithm for estimation and tracking of distributed diffuse scattering in mobile radio channels," in *Signal Processing Advances in Wireless Communications, 2006. SPAWC '06. IEEE 7th Workshop on*, 2006, pp. 1–5.

[38] K. Levenberg, "A method for the solution of certain non-linear problems in least squares," *Quarterly Journal of Applied Mathmatics*, vol. II, no. 2, pp. 164–168, 1944.

[39] D. W. Marquardt, "An algorithm for least-squares estimation of nonlinear parameters," *SIAM Journal on Applied Mathematics*, vol. 11, no. 2, pp. 431–441, 1963. [Online]. Available: http://dx.doi.org/10.1137/0111030

[40] J. Salmi, A. Richter, and V. Koivunen, "Detection and tracking of MIMO propagation path parameters using state-space approach," *Signal Processing, IEEE Transactions on*, vol. 57, no. 4, pp. 1538–1550, 2009.

[41] M. Landmann, W. Kotterman, and R. Thoma, "On the influence of in-complete data models on estimated angular distributions in channel characterisation," in *Antennas and Propagation, 2007. EuCAP 2007. The Second European Conference on*, 2007, pp. 1–8.

[42] P. Alexander, D. Haley, and A. Grant, "Cooperative intelligent transport systems: 5.9-GHz field trials," *Proceedings of the IEEE*, vol. 99, no. 7, pp. 1213–1235, 2011.

[43] I. Davis, J.S. and J. Linnartz, "Vehicle to vehicle rf propagation measurements," in *Signals, Systems and Computers, 1994. 1994 Conference Record of the Twenty-Eighth Asilomar Conference on*, vol. 1, 1994, pp. 470–474 vol.1.

[44] F. Pallares, F. Juan, and L. Juan-Llacer, "Analysis of path loss and delay spread at 900 MHz and 2.1 GHz while entering tunnels," *Vehicular Technology, IEEE Transactions on*, vol. 50, no. 3, pp. 767–776, 2001.

[45] D. Dudley, M. Lienard, S. Mahmoud, and P. Degauque, "Wireless propagation in tunnels," *Antennas and Propagation Magazine, IEEE*, vol. 49, no. 2, pp. 11–26, 2007.

[46] J. Turkka and M. Renfors, "Path loss measurements for a non-line-of-sight mobile-to-mobile environment," in *8th International Conference on ITS Telecommunications (ITST-2008), Hilton Phuket, Thailand*, oct. 2008, pp. 274 –278.

[47] D. Matolak, I. Sen, W. Xiong, and N. Yaskoff, "5 GHz wireless channel characterization for vehicle to vehicle communications," in *Military Communications Conference, 2005. MILCOM 2005. IEEE*, 2005, pp. 3016–3022 Vol. 5.

[48] S. Kaul, K. Ramachandran, P. Shankar, S. Oh, M. Gruteser, I. Seskar, and T. Nadeem, "Effect of antenna placement and diversity on vehicular network communications," in *4th Annual IEEE Communications Society Conference on Sensor, Mesh and Ad Hoc Communications and Networks, SECON '07*, Jun. 2007, pp. 112 –121.

[49] L. Cheng, B. Henty, D. D. Stancil, F. Bai, and P. Mudalige, "A fully mobile, gps enabled, vehicle-to-vehicle measurement platform for characterization of the 5.9 GHz dsrc channel," in *Antennas and Propagation Society International Symposium, 2007 IEEE*, 2007, pp. 2005–2008.

[50] A. Paier, J. Karedal, N. Czink, C. Dumard, T. Zemen, F. Tufvesson, A. F. Molisch, and C. F. Mecklenbräuker, "Characterization of vehicle-to-vehicle radio channels from measurements at 5.2 GHz," *Wireless Personal Commun.*, vol. 50, pp. 19–29, 2009.

[51] I. Sen and D. W. Matolak, "Vehicle-vehicle channel models for the 5 GHz band," *IEEE Trans. Intell. Transp. Syst.*, vol. 9, no. 2, pp. 235–245, Jun. 2008.

[52] O. Renaudin, V. Kolmonen, P. Vainikainen, and C. Oestges, "Wideband MIMO car-to-car radio channel measurements at 5.3 GHz," in *Vehicular Technology Conference, 2008. VTC 2008-Fall. IEEE 68th*, 2008, pp. 1–5.

[53] J. Kunisch and J. Pamp, "Wideband car-to-car radio channel measurements and model at 5.9 GHz," in *Vehicular Technology Conference, 2008. VTC 2008-Fall. IEEE 68th*, 2008, pp. 1–5.

[54] A. Paier, L. Bernado, J. Karedal, O. Klemp, and A. Kwoczek, "Overview of vehicle-to-vehicle radio channel measurements for collision avoidance applications," in *Vehicular Technology Conference (VTC 2010-Spring), IEEE 71st, Taipei, Taiwan*, May 2010, pp. 1–5.

[55] R. Meireles, M. Boban, P. Steenkiste, O. Tonguz, and J. Barros, "Experimental study on the impact of vehicular obstructions in VANETs," in *2010 IEEE Vehicular Networking Conference (VNC), New Jersey, USA*, dec. 2010, pp. 338 –345.

[56] P. Paschalidis, A. Kortke, K. Mahler, M. Wisotzki, W. Keusgen, and M. Peter, "Pathloss and Multipath Power Decay of the Wideband Car-to-Car Channel at 5.7 GHz," in *IEEE 73th Vehicular Technology Conference (VTC2011-Spring)*, Budapest, Hungry, May 2011.

[57] T. Mangel, M. Michl, O. Klemp, and H. Hartenstein, "Real-world measurements of non-line-of-sight reception quality for 5.9 GHz IEEE 802.11p at intersections," *Communication Technologies for Vehicles, Springer Berlin Heidelberg*, vol. 6596, pp. 189–202, 2011.

[58] C. Sommer, D. Eckhoff, R. German, and F. Dressler, "A computationally inexpensive empirical model of IEEE 802.11p radio shadowing in urban environments," in *Wireless On-Demand Network Systems and Services (WONS), 2011 Eighth International Conference on*, 2011, pp. 84–90.

[59] M. Segata, B. Bloessl, S. Joerer, C. Sommer, R. L. Cigno, and F. Dressler, "Vehicle Shadowing Distribution Depends on Vehicle Type: Results of

an Experimental Study," in *5th IEEE Vehicular Networking Conference (VNC 2013)*. Boston, MA: IEEE, December 2013, pp. 242–245.

[60] H. Fernãndez, L. Rubio, J. Reig, V. Rodrigo-Pearrocha, and A. Valero, "Path loss modeling for vehicular system performance and communication protocols evaluation," *Mobile Networks and Applications*, pp. 1–11, 2013. [Online]. Available: http://dx.doi.org/10.1007/s11036-013-0463-x

[61] G. Acosta and M.-A. Ingram, "Model development for the wideband expressway vehicle-to-vehicle 2.4 ghz channel," in *Wireless Communications and Networking Conference, 2006. WCNC 2006. IEEE*, vol. 3, 2006, pp. 1283–1288.

[62] G. Acosta-Marum and M. Ingram, "Six time- and frequency- selective empirical channel models for vehicular wireless LANs," *IEEE Veh. Technol. Mag.*, vol. 2, no. 4, pp. 4–11, 2007.

[63] P. Paschalidis, M. Wisotzki, A. Kortke, W. Keusgen, and M. Peter, "A wideband channel sounder for car-to-car radio channel measurements at 5.7 GHz and results for an urban scenario," in *Vehicular Technology Conference, 2008. VTC 2008-Fall. IEEE 68th*, 2008, pp. 1–5.

[64] J. Otto, F. Bustamante, and R. Berry, "Down the block and around the corner the impact of radio propagation on inter-vehicle wireless communication," in *ICDCS '09. 29th IEEE International Conference on Distributed Computing Systems*, June 2009, pp. 605 –614.

[65] T. Abbas, J. Kredal, and F. Tufvesson, "Measurement-Based Analysis: The Effect of Complementary Antennas and Diversity on Vehicle-to-Vehicle Communication," *IEEE Antennas and Wireless Propagation Letters*, vol. 12, no. 1, pp. 309–312, 2013. [Online]. Available: http://lup.lub.lu.se/record/3516482/file/3555826.pdf

[66] A. Borhani and M. Patzold, "Modelling of non-stationary mobile radio channels using two-dimensional brownian motion processes," in *Advanced Technologies for Communications (ATC), 2013 International Conference on*, 2013, pp. 241–246.

[67] A. Paier, T. Zemen, L. Bernadó, and G. Matz, "Non-wssus vehicular channel charachterization in highway and urban scenario at 5.2GHz using the local scattering function," in *WSA*, Feb. 2008.

[68] L. Bernadó, T. Zemen, F. Tufvesson, A. F. Molisch, and C. F. Mecklenbräuker, "Delay and doppler spreads of non-stationary vehicular channels for safety relevant scenarios," *CoRR*, vol. abs/1305.3376, 2013.

[69] T. Abbas, F. Tufvesson, and J. Karedal, "Measurement based shadow fading model for vehicle-to-vehicle network simulations," *ArXiv e-prints*, Mar. 2012.

[70] T. Mangel, O. Klemp, and H. Hartenstein, "5.9 GHz inter-vehicle communication at intersections: a validated non-line-of-sight path-loss and fading model," *EURASIP Journal on Wireless Communications and Networking*, vol. 2011, no. 1, p. 182, 2011.

[71] I. Tan, W. Tang, K. Laberteaux, and A. Bahai, "Measurement and analysis of wireless channel impairments in dsrc vehicular communications," in *Communications, 2008. ICC '08. IEEE International Conference on*, 2008, pp. 4882–4888.

[72] J. Karedal, F. Tufvesson, T. Abbas, O. Klemp, A. Paier, L. Bernadó, and A. F. Molisch, "Radio channel measurements at street intersections for vehicle-to-vehicle safety applications," in *IEEE VTC 71st Vehicular Technology Conference (VTC 2010-spring), Taipei, Taiwan*, May 2010, pp. 1–5.

[73] T. Abbas, L. Bernado, A. Thiel, C. F. Mecklenbruker, and F. Tufvesson, "Measurements Based Channel Characterization for Vehicle-to-Vehicle Communications at Merging Lanes on Highway," in *5th International Symposium on Wireless Vehicular Communications: WIVEC2013*. IEEE, June 2013, pp. 1–5.

[74] A. Paier, J. Karedal, N. Czink, H. Hofstetter, C. Dumard, T. Zemen, F. Tufvesson, A. Molisch, and C. Mecklenbrauker, "Car-to-car radio channel measurements at 5 GHz: Pathloss, power-delay profile, and delay-doppler spectrum," in *Wireless Communication Systems, 2007. ISWCS 2007. 4th International Symposium on*, 2007, pp. 224–228.

[75] J. Karedal, N. Czink, A. Paier, F. Tufvesson, and A. Molisch, "Path loss modeling for vehicle-to-vehicle communications," *IEEE Transactions on Vehicular Technology*, vol. 60, no. 1, pp. 323–328, 2011.

[76] C. Sommer, S. Joerer, and F. Dressler, "On the applicability of two-ray path loss models for vehicular network simulation," in *Vehicular Networking Conference (VNC), 2012 IEEE*, 2012, pp. 64–69.

[77] L. Bernado, T. Zemen, J. Karedal, A. Paier, A. Thiel, O. Klemp, N. Czink, F. Tufvesson, A. Molisch, and C. Mecklenbräker, "Multi-dimensional k-factor analysis for v2v radio channels in open sub-urban street crossings," in *Personal Indoor and Mobile Radio Communications (PIMRC), 2010 IEEE 21st International Symposium on*, 2010, pp. 58–63.

[78] L. Bernadó, T. Zemen, F. Tufvesson, A. F. Molisch, and C. F. Mecklenbräuker, "Time-, frequency-, and space-varying k-factor of non-stationary vehicular channels for safety relevant scenarios," *CoRR*, vol. abs/1306.3914, 2013.

[79] M. Boban, T. Vinhoza, M. Ferreira, J. Barros, and O. Tonguz, "Impact of vehicles as obstacles in vehicular ad hoc networks," *Selected Areas in Communications, IEEE Journal on*, vol. 29, no. 1, pp. 15 –28, Jan. 2011.

[80] M. Boban, J. Barros, and O. K. Tonguz, "Geometry-based vehicle-to-vehicle channel modeling for large-scale simulation," *CoRR*, vol. abs/1305.0124, 2013.

[81] P. Kyösti, J. Meinilä, L. Hentilä, X. Zhao, T. Jämsä, C. Schneider, M. Narandzić, M. Milojević, A. Hong, J. Ylitalo, V.-M. Holappa, M. Alatossava, R. Bultitude, Y. de Jong, and T. Rautiainen, "WINNER II Channel Models," EC FP6, Tech. Rep., Sep. 2007.

[82] E. Giordano, R. Frank, G. Pau, and M. Gerla, "Corner: a realistic urban propagation model for vanet," in *Seventh International Conference on Wireless On-demand Network Systems and Services (WONS-2010)*, feb. 2010, pp. 57 –60.

[83] O. Renaudin, V.-M. Kolmonen, P. Vainikainen, and C. Oestges, "Wide-band measurement-based modeling of inter-vehicle channels in the 5-GHz band," *Vehicular Technology, IEEE Transactions on*, vol. 62, no. 8, pp. 3531–3540, 2013.

[84] J. Maurer, T. Schafer, and W. Wiesbeck, "A realistic description of the environment for inter-vehicle wave propagation modelling," in *Vehicular Technology Conference, 2001. VTC 2001 Fall. IEEE VTS 54th*, vol. 3, 2001, pp. 1437–1441 vol.3.

[85] J. Maurer, T. Fugen, T. Schafer, and W. Wiesbeck, "A new inter-vehicle communications (ivc) channel model," in *Vehicular Technology Conference, 2004. VTC2004-Fall. 2004 IEEE 60th*, vol. 1, 2004, pp. 9–13 Vol. 1.

[86] M. Schack, J. Nuckelt, R. Geise, L. Thiele, and T. Kürner, "Comparison of path loss measurements and predictions at urban crossroads for C2C communications," in *5th European Conference on Antennas and Propagation (EuCAP), Rome, Italy*, April 2011.

[87] S. Hosseini Tabatabaei, M. Fleury, N. Qadri, and M. Ghanbari, "Improving propagation modeling in urban environments for vehicular ad hoc networks," *Intelligent Transportation Systems, IEEE Transactions on*, vol. 12, no. 3, pp. 705–716, 2011.

[88] J. Nuckelt, T. Abbas, F. Tufvesson, C. F. Mecklenbräuker, L. Bernado, and T. Kürner, "Comparison of ray tracing and channel-sounder measurements for vehicular communications," in *2013 IEEE 77th Vehicular Technology Conference: VTC2013-Spring, Dresden, Germany*, June 2013, pp. 1–5.

[89] T. G. K. Z. L. J. S. M. Khokhar, Rashid Hafeez; Zia, "Realistic and efficient radio propagation model for v2x communications," *KSII Transactions on Internet & Information Systems*, vol. 7, no. 8, pp. 1933–1954, August 2013.

[90] M. Schack, D. Kornek, E. Slottke, and T. Kürner, "Analysis of channel parameters for different antenna configurations in vehicular environments," in *IEEE 72nd Vehicular Technology Conference (VTC 2010-Fall)*, Sept. 2010, pp. 1 –5.

[91] L. Reichardt, T. Fugen, and T. Zwick, "Influence of antennas placement on car to car communications channel," in *3rd European Conference on Antennas and Propagation, EuCAP 2009*, March 2009, pp. 630 –634.

[92] P. Liu, D. Matolak, B. Ai, and R. Sun, "Path loss modeling for vehicle-to-vehicle communication on a slope," *Vehicular Technology, IEEE Transactions on*, vol. PP, no. 99, pp. 1–1, 2013.

[93] A. Zajic and G. Stuber, "A new simulation model for mobile-to-mobile rayleigh fading channels," in *Wireless Communications and Networking Conference, 2006. WCNC 2006. IEEE*, vol. 3, 2006, pp. 1266–1270.

[94] L.-C. Wang, W.-C. Liu, and Y.-H. Cheng, "Statistical analysis of a mobile-to-mobile rician fading channel model," *Vehicular Technology, IEEE Transactions on*, vol. 58, no. 1, pp. 32–38, 2009.

[95] A. G. Zajić and G. L. Stüber, "Space-time correlated mobile-to-mobile channels: Modelling and simulation," *IEEE Trans. Veh. Technol.*, vol. 57, no. 2, pp. 715–726, Mar. 2008.

[96] A. Zajic, G. Stuber, T. Pratt, and S. Nguyen, "Wideband MIMO mobile-to-mobile channels: Geometry-based statistical modeling with experimental verification," *Vehicular Technology, IEEE Transactions on*, vol. 58, no. 2, pp. 517–534, 2009.

[97] A. Chelli and M. Patzold, "A MIMO mobile-to-mobile channel model derived from a geometric street scattering model," in *Wireless Communication Systems, 2007. ISWCS 2007. 4th International Symposium on*, 2007, pp. 792–797.

[98] ——, "A wideband multiple-cluster MIMO mobile-to-mobile channel model based on the geometrical street model," in *Personal, Indoor and Mobile Radio Communications, 2008. PIMRC 2008. IEEE 19th International Symposium on*, 2008, pp. 1–6.

[99] ——, "The impact of fixed and moving scatterers on the statistics of MIMO vehicle-to-vehicle channels," in *Vehicular Technology Conference, 2009. VTC Spring 2009. IEEE 69th*, 2009, pp. 1–6.

[100] H. Zhiyi, C. Wei, Z. Wei, M. Patzold, and A. Chelli, "Modelling of MIMO vehicle-to-vehicle fading channels in t-junction scattering environments," in *Antennas and Propagation, 2009. EuCAP 2009. 3rd European Conference on*, 2009, pp. 652–656.

[101] A. Theodorakopoulos, P. Papaioannou, T. Abbas, and F. Tufvesson, "A geometry based stochastic model for MIMO V2V channel simulation in cross-junction scenario," in *ITS Telecommunications (ITST), 2013 13th International Conference on, Tampere, Finland*, 2013, pp. 290–295.

[102] S. Salous, *Radio Channel Models, in Radio Propagation Measurement and Channel Modelling.* John Wiley & Sons, Ltd, Chichester, UK, 2013.

[103] N. Costa and S. Haykin, *Channel Sounding.* John Wiley & Sons, Inc., 2010, pp. 111–158. [Online]. Available: http://dx.doi.org/10.1002/9780470590676.ch5

[104] Medav GmbH. [Online]. Available: http://www.medav.de/?L=2

[105] A. Thiel, O. Klemp, A. Paier, L. Bernadó, J. Karedal, and A. Kwoczek, "In-situ vehicular antenna integration and design aspects for vehicle-to-vehicle communications," in *Antennas and Propagation (EuCAP), 2010 Proceedings of the Fourth European Conference on, Barcelona, Spain*, Apr. 2010, pp. 1–5.

[106] "ETSI TR 102 638 -intelligent transport systems (ITS); vehicular communications; basic set of applications; definitions," Tech. Rep. V1.1.1, June 2009.

[107] "Intelligent transportation systems: Vehicle-to-vehicle technologies expected to offer safety benefits, but a variety of deployment challenges exist," GAO-14-13, Tech. Rep., November 2013. [Online]. Available: http://www.gao.gov/products/GAO-14-13

[108] Google earth v7.1.1.1888 (2013). [Online]. Available: http://www.google.com/earth/index.html [Accessed: 2013/08/15]

[109] Google maps. google, 01 jan. 2014. web. 01 jan 2014.(2013). [Online]. Available: http://www.google.com/earth/index.html [Accessed: 2013/08/15]

Part II

Included Papers

Paper I

Directional Analysis of Vehicle-to-Vehicle Propagation Channels

This paper presents a double directional analysis of vehicle-to-vehicle channel measurements conducted in three different traffic scenarios. Using a high-resolution algorithm, we derive channel parameters like Angle-of-Arrival (AOA), Angle-of-Departure (AOD), propagation delay and Doppler shift and identify underlying propagation mechanisms by combining these estimates with maps of the measurement sites. The results show that first-order reflections from a small number of interacting objects can account for a large part of the received signal in the absence of line-of-sight (LOS). This effect is especially pronounced in the two traffic scenarios where the road is not lined with buildings. We also found that the direction spread is low (and conversely that the antenna correlation is high) in such scenarios, which suggests that beam forming rather than diversity-based methods should be used if multiple antenna elements are available. The situation is reversed, however, in the third scenario, a narrow urban intersection, where a larger number of higher-order reflections is found to result in a higher direction spread.

1 Introduction

Vehicle-to-vehicle (V2V) communication systems have attracted a lot of interest in recent years due to their anticipated usefulness for traffic safety enhancement. Particularly, it is envisioned that future vehicles, equipped with radio transceivers, can share information about traffic dynamics with each other in order to facilitate driving and avoid accidents. Since the efficiency and the accuracy of such systems ultimately depends on the properties of the propagation channel, a lot of research effort has been spent on V2V propagation channels, usually with the intent of developing realistic simulation models (see e.g., [1–3]).

Although a number of propagation channel measurement campaigns have been performed in recent years (see e.g., [4–7]), there are still many important aspects that have been little explored. First, the antenna impact is not well understood. Almost exclusively, the measurements conducted so far have been done with "regular" antenna arrays placed at an elevated position (above the vehicle roof). Neither the impact of design constraints nor antenna placement has been given much attention. Secondly, most measurement campaigns have been conducted under "general" traffic conditions, with cars driving either in convoy or in the opposite directions on the same road, e.g., on highways [4,5] (a recent is found in [8], where signal obstruction due to vehicles is analyzed). In addition to such general traffic situations there are a number of *application-specific* scenarios where special propagation conditions apply, e.g., collision avoidance scenarios in street intersections or traffic congestion scenarios. These conditions are not well captured by the former standard measurement scenarios, and hence separate characterization of such scenarios is required.

Furthermore there is a lack of available results on directional properties of V2V channels in the literature; to the authors' best knowledge there is only the paper by Pedersen et al., [9], which presents the angular spectra for convoy measurements. Analysis of directional properties is important for the assessment of multi-antenna capabilities, e.g., for evaluating the possible diversity gain, as well as to improve understanding of important propagation effects.

The current paper addresses these gaps of knowledge by presenting the results of extensive multiple-input multiple-output (MIMO) V2V channel measurements performed in Lund, Sweden. We present results of directional analysis for three *application-specific* scenarios and use these results to identify the underlying propagation mechanisms and analyze their impact on the total received power. We also evaluate the directional spread of the propagation channels in the different scenarios, and derive antenna correlation coefficients. The scenarios we study are: (*i*) an intersection scenario, (*ii*) a congestion scenario, and (*iii*) a controlled line-of-sight (LOS) obstruction between the vehicles

moving on a highway. This paper partly extends the results of [10], where we presented power-delay profiles and root mean square (RMS) delay spreads (but no directional results) for different types of intersections.

The paper is organized as follows: In Section II the measurement setup is described in detail and the properties of three different scenarios are explained. The parameter extraction process is described in Section III, whereas the results, including the identified propagation mechanisms, are presented in Section IV. Finally, the summary and conclusions are presented in Section V.

2   Channel Measurements

2.1   Measurement Setup

V2V channel measurement data were recorded using the RUSK Lund channel sounder that performs switched-array MIMO measurements. The measurements were conducted over a 240 MHz bandwidth centered around 5.6 GHz, the highest allowed center frequency of the sounder. The measurements were performed using standard hatch-back style cars with roof mounted four-element antenna arrays, specifically designed for V2V communication [11]. The antenna height was 1.73 m. For each branch of this 4×4 MIMO configuration, the channel sounder sampled the complex time varying channel transfer function $H(f,t)$ every $\Delta t = 307.2\,\mu$s during 10 or 20 s. To keep track of the positions of the transmitter (TX) and and receiver (RX) vehicles during the measurements, each vehicle logged the GPS coordinates and had videos, taken through the windshield. These data were also combined with the measurement data, in order to identify important scatterers in the post-processing.

2.2   Measurement Scenarios

The measurement data we study were collected in different traffic scenarios.

In the first scenario (intersection) the TX and RX, were approaching a four way intersection in an urban environment at a speed of $30 - 40$ km/h ($8 - 11$ m/s); see Fig. 1(a). There were houses on both sides of the streets, which obstructed the LOS until the cars met in the intersection (in practice, the TX car stopped at a yield sign while the RX car drove by). The streets were narrow; the street width was $14 - 18$ m. Moreover, there were several street lights and road signs in this scenario, and many parked cars along the streets, but few moving vehicles.

In the second scenario (congestion) the TX car had just entered a congested area on a two-lane highway (due to a road works further ahead forcing the two lanes to merge). The TX car was stuck in the right lane whereas the RX car

was approaching from behind in the left lane at a speed of about 70 km/h (20 m/s); see Fig. 1(b). There were road signs, light poles, various objects and a multitude of other vehicles in this scenario; beside the large number of cars standing still in the TX/RX direction, there was also (moving) traffic in the opposite direction, including some trucks. There was a metallic fence on the outer (right) boundary of the road and the directions of travel were separated by a low concrete wall (approximately 0.5 m).

In the third scenario (obstructed-LOS) the TX and RX cars were moving in the same direction on the right lane on a two-lane highway at a speed of 110 km/h (30 m/s); see Fig. 1(c). There were trucks in front of as well as behind the TX/RX convoy, and the LOS path was obstructed by a tall van between TX and RX. The LOS path appeared when the van decided to change lanes. There were many vehicles (moving) in the opposite direction and there were a couple of road signs and overhead electrical power transmission lines with poles on the roadside. Finally, the directions of travel were separated by a low metallic fence.

3 Parameter Extraction

We assume that the 4×4 channel matrix $\mathbf{H}$ can be described by a sum of L plane waves or multipath components (MPCs) where each wave l is characterized by a complex amplitude γ_l, propagation delay τ_l, and a Doppler shift ν_l. We then model the channel transfer function at each temporal instant (snapshot) t_s and frequency point f_k by [12]

$$\mathbf{H}[t_s, f_k] = \sum_{l=1}^{L} e^{j2\pi\nu_l t_s} \left[\begin{array}{cc} g_{TX}^H(\Theta_{TX,l}) & g_{TX}^V(\Theta_{TX,l}) \end{array} \right]$$

(1)

$$\cdot \left[\begin{array}{cc} \gamma_l^{HH} & \gamma_l^{HV} \\ \gamma_l^{VH} & \gamma_l^{VV} \end{array} \right] \left[\begin{array}{c} g_{RX}^H(\Theta_{RX,l})^T \\ g_{RX}^V(\Theta_{RX,l})^T \end{array} \right] \exp{-j2\pi\tau_l f_k},$$

where $\mathbf{H} \in \mathbb{C}^{4 \times 4}$; g_{TX}^H, g_{TX}^V and g_{RX}^H, g_{RX}^V are 4×1 complex vectors representing TX and RX antenna responses, respectively. Furthermore, $\Theta_{TX,l} = (\theta_{TX,l}, \phi_{TX,l})$, $\Theta_{RX,l} = (\theta_{RX,l}, \phi_{RX,l})$ are angle-of-departure in elevation and azimuth, and angle-of-arrival in elevation and azimuth, respectively. Superscript H and V indicate horizontal and vertical polarization, respectively.

The parameters of (1) for 50 MPCs are estimated using the space-alternating generalized expectation-maximization (SAGE) algorithm [13]. In order to reduce the computational complexity, we use measurement data with a bandwidth of 20 MHz, out of the full 240 MHz, centered around 5.6 GHz, and
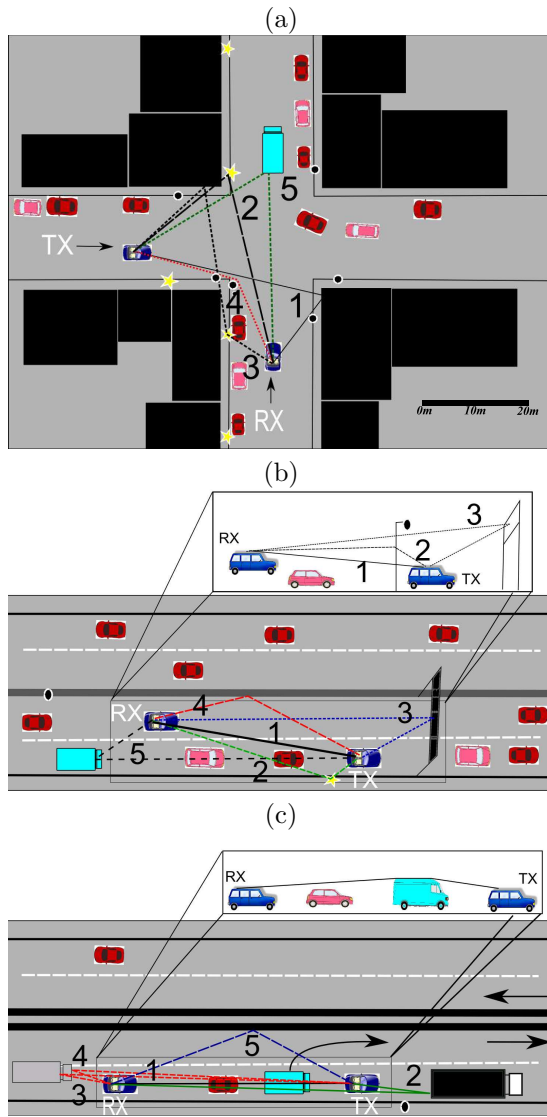
Figure 1: Identified propagation mechanism behind the five strongest MPCs at a particular instant t, for the (a) intersection ($t = 6\,\text{s}$); (b) congestion ($t = 13\,\text{s}$) and (c) obstructed LOS ($t = 1\,\text{s}$) scenarios. Stars, dots, blocks and dark strip represent streetlights, roadsigns, houses and concrete wall/metallic fence that separates the direction of travel on the highway, respectively.
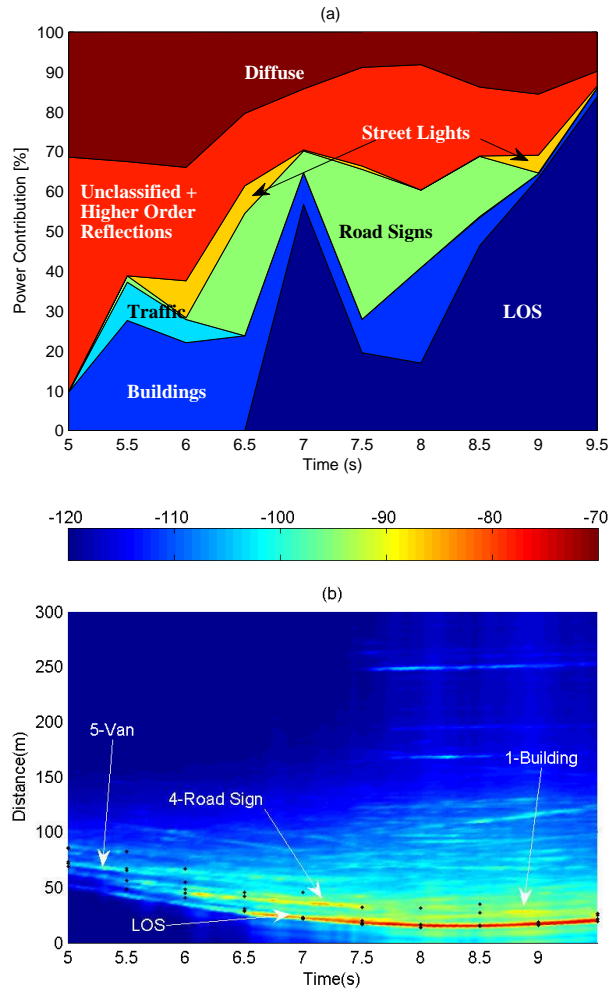
Figure 2: Results for the intersection scenario: (a) shows the relative power contribution from different propagation mechanisms, only LOS and first-order reflections are categorized explicitly; (b) shows some identified propagation mechanisms in the time-delay domain (power-delay profile), dots indicate the SAGE delay estimates for the five strongest MPCs.

a temporal window of length 19.4 ms (64 snapshots). This temporal window corresponds to a Doppler resolution of 52 Hz and is selected based on the estimated *stationarity time* of the channel (see [14] for details), which is 97.6 ms, 374.4 ms, and 1337.9 ms for the intersection, congestion and obstructed-LOS scenarios, respectively. Due to the computational efforts of estimating parameters using SAGE, we limit the analysis to a temporally sparse subset of the measurements data; every 0.5 s in the intersection, every 1 s in the other two. The 50 extracted MPCs account for $68 - 90\%$, $83 - 98\%$ and $68 - 94\%$ of the available power in the intersection, congestion and obstructed-LOS scenarios, respectively. For this power percentage evaluation, the mean squared amplitude of the inverse Fourier transform of, the measured and the reconstructed, channel transfer functions were noise thresholded, i.e., anything below noise floor with an additional 3 dB margin was considered as noise and thus set to zero. We label the fraction of power which is not extracted by SAGE as *diffuse* power, though strictly speaking this part also contains measurement noise. Moreover, the extracted part may also contain diffuse contributions to some extent (for those time instants where the selected source order is too high); this will be discussed further in the paper. The percentage of extracted power is generally lower for instants where non-LOS conditions apply.

4   Results

For each scenario and each time instant we plot the estimated propagation paths on the corresponding site maps and then perform a measurement based ray-tracing from the TX and RX, in order to identify the underlying propagation mechanisms, e.g., if an object is found at (or more specifically "sufficiently close" to) the intersection of the lines drawn in the direction of the AOA from the RX and the direction of the AOD from the TX for a certain MPC, and the geometric length from TX to RX via this intersection matches the delay estimate for the MPC, we consider a single-bounce reflection from that object to be the underlying mechanism behind it. In this process, the coordinates of the TX and RX are determined by combining recorded GPS and video data, whereas the coordinates of moving scatterers are determined using video data only. Obviously, only the coordinates of moving scatterers within the visibility range of the TX and RX can be determined, and the accuracy of their coordinates depends on their position relative to the TX and/or RX. Although a small discrepancy between the coordinates of an actual object and the location indicated by the estimated parameters is inevitable due to errors in the positions of the TX and RX cars, we are able to identify the likely propagation process in the vast majority of the cases. We are further aided in the iden-
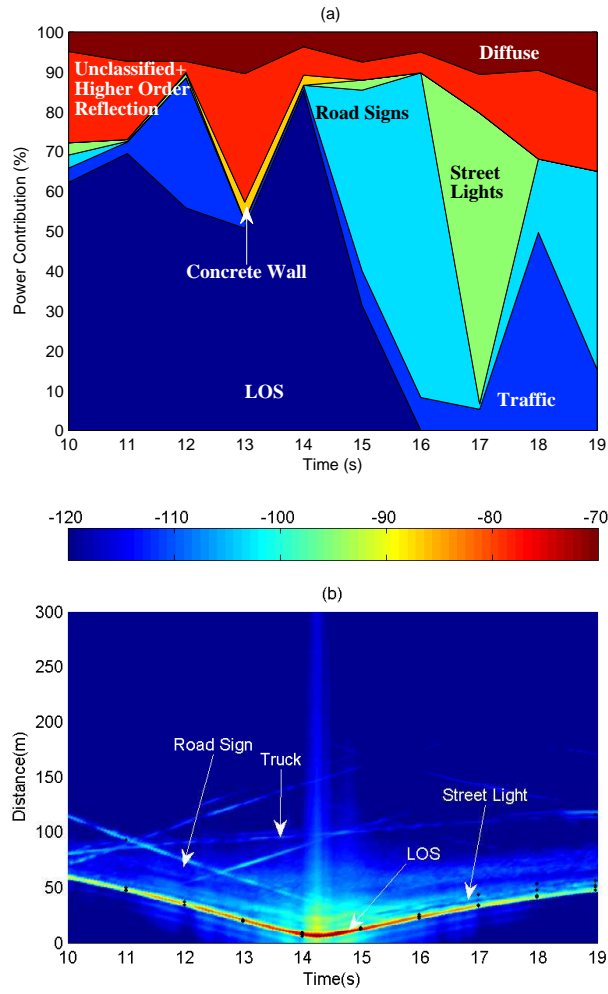
Figure 3: Results for the congestion scenario: a) shows the relative power contribution from different propagation mechanisms, only LOS and first-order reflections are categorized explicitly; (b) shows some identified propagation mechanisms in the time-delay domain (power-delay profile), dots indicate the SAGE delay estimates for the five strongest MPCs.

tification process by the Average Power Delay Profiles (APDPs), which are defined, for each time instant, as the averaged (over the 4×4 MIMO branches) squared magnitude of inverse Fourier transform of the channel transfer function at that instant. Many important MPCs show up as "lines" in the APDP, and the APDP can therefore be used to assess the temporal evolution of the propagation delay of those MPCs. APDPs for the three scenarios are shown in Fig. 2, 3, and 4, respectively. It is important to mention that the SAGE for some reasons cannot subtract the LOS completely and model the residue as specular paths. These paths cannot be tied to any of the described propagation mechanism and thus regarded as unclassified.

Sample plots of the identified MPCs at a certain time instant are shown in Fig. 1. As an example of the identification process, consider MPC#5 in the intersection scenario in Fig. 1(a). This MPC is arriving at the RX from a direction where the only physical object is another vehicle (a van). In some cases, such as MPC#3, the interacting objects cannot be identified for certain, but we can say with high probability that a single-bounce process is *not* the underlying mechanism. Similarly in the congestion scenario (Fig. 1(b)), where there is a multitude of traffic around the TX/RX we can still identify important propagation mechanism, e.g., MPC#2 which is a street light, using the fact that it is only object in the estimated direction and that the measured geometric distance also matches the estimated delay. As a final example, consider MPC#3 and MPC#4 in the obstructed LOS scenario (Fig. 1(c)). We conclude that they both stem from same object, a truck behind the RX, since they have very similar AOAs and AODs. There is, however, a small difference in the propagation distance which indicates the possibility that one signal is reflected from the bonnet whereas the other stems from the body of the truck.

Once the identification process is complete, we classify the propagation mechanisms into two different categories: the LOS path, single-bounce interactions (with buildings, traffic, road signs, street lights, and parked cars, and the concrete wall/metallic fence that separates the directions of travel on the highway) are used in all scenarios. In the obstructed-LOS scenario we split the traffic category into three sub-categories: trucks in front and behind the TX/RX, a van between the TX/RX and other traffic. Lastly, we use a category labeled "unclassified plus higher order reflections account" for both higher-order reflections and for the MPCs that cannot be tied to a specific propagation mechanism. This category will also contain a small amount of diffuse power extracted by SAGE.

Before we study how the received signal is composed, we add antenna influence to the extracted path weights. This way, the weights can be related to the energy that is *not* extracted by SAGE (see Section III). We thus have:
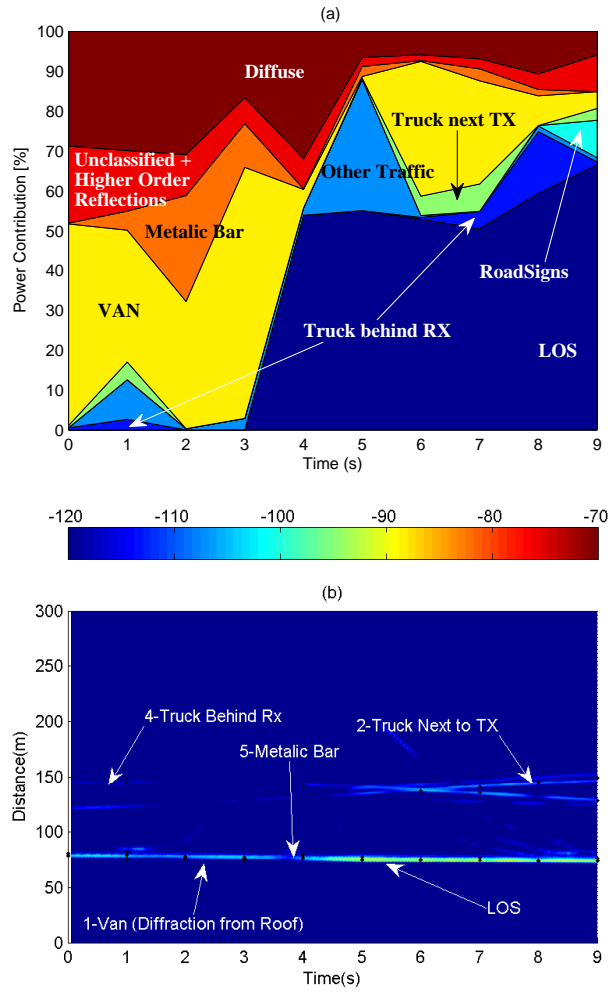
Figure 4: Results for the general LOS-obstruction scenario: a) shows the relative power contribution from different propagation mechanisms, only LOS and first-order reflections are categorized explicitly; (b) shows some identified propagation mechanisms in the time-delay domain (power-delay profile), dots indicate the SAGE delay estimates for the five strongest MPCs.

$$\alpha_l = \left| \sum_k g_{TX}^H \diamond \begin{bmatrix} g_{RX}^H g_{RX}^V \end{bmatrix} \begin{bmatrix} \gamma_l^{HH} \\ \gamma_l^{HV} \end{bmatrix} + g_{TX}^V \diamond \begin{bmatrix} g_{RX}^H g_{RX}^V \end{bmatrix} \begin{bmatrix} \gamma_l^{VH} \\ \gamma_l^{VV} \end{bmatrix} \right|^2, \quad (2)$$

where, $\gamma_l^{HH}, \gamma_l^{VV}$ and $\gamma_l^{VH}, \gamma_l^{HV}$ represent the the co-polarized and cross-polarized estimated complex path gains of extracted MPCs, respectively whereas the variable k and the operator $\diamond$ refer to the number of channels and the Khatri-Rao product respectively. Finally, the contribution from each propagation mechanism in total received power is calculated as,

$$P_j = \frac{\sum_{l \in S_j} \alpha_l}{\sum_l^L \alpha_l}, \quad (3)$$

where P_j is the power contribution corresponding to the jth MPC category S_j. The results (see (a) of Fig. 2, 3,and 4) show that first-order interactions often dominate in the absence of LOS; they account for up to 70%, 90% and 65% of the total received power in the intersection, congestion and obstructed-LOS scenarios, respectively. Furthermore, we find that very few MPCs stem from other traffic in the intersection and congestion scenarios. This is mainly due to the antenna arrangements we use. The mounting of the antenna close to the car roof only allows for a limited gain below the azimuth plane. Therefore, other regular (sedan-type) cars are not "seen" by the antennas.[1] Taller vehicles, on the other hand, are often found to constitute good scatterers.This is evident in the obstructed-LOS where the trucks and van surrounding the TX/RX account for the majority of the received signal.

The *azimuth direction spread* [15] is an important measure that indicates what level of spatial diversity can be anticipated. A direction spread of unity indicates that the signal arrives at the receiver uniformly spread over all directions, whereas a direction spread of zero implies that the signal arrives from a single direction. For all three scenarios, we derive the azimuth RMS direction spread at the receiver as,

$$\sigma_{\mathbf{ang}} = \sqrt{\sum |e^{j\phi_{R,l}} - \mu_{\mathbf{ang}}|^2 P_{\mathbf{ang}}(\phi_{R,l})}, \quad (4)$$

where

$$\mu_{\mathbf{ang}} = \sum_{l=1}^{L} e^{j\phi_{R,l}} P_{\mathbf{ang}}(\phi_{R,l}), \quad (5)$$

---

[1]This is particularly interesting given that the antennas were designed especially for V2V communications, with the aim of having an omni-directional antenna pattern that is maximal in the azimuth plane (given the particular position at the car roof). Readers are referred to [11] for further details.
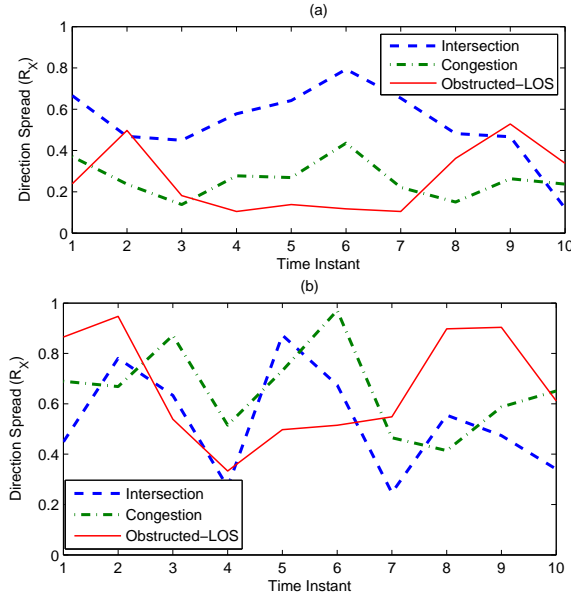
Figure 5: RMS direction spread at RX: (a) with antenna influence; (b) without antenna influence.

and $P_{\mathbf{ang}}(\phi_{R,l})$ is the normalized azimuth angular power spectrum. The direction spread is calculated with and without antenna influence and the results are shown in Fig. 5. Taking antenna influence into account, we find that the direction spread is higher in the intersection scenario because of the congested surrounding. This is in contrast to the other two scenarios where the signal is mainly composed of a small number of MPCs within a small angular range, and hence the average direction spread is low. However, the direction spread is high when removing antenna influence which encourages potential use of multi-antenna arrangements to exploit the diversity gain (see Fig. 5).

Finally, we derive the correlation coefficients between the different branches of our measured MIMO system. The correlation coefficients for both TX and RX branches are presented for all scenarios in Fig. 6. The correlation between the branches is low when there are multiple contributions from certain angles and/or there is a non-LOS condition. It is evident from Fig. 6, the correlation is low for a larger duration of time in the intersection scenario as compared to the other scenarios. This is also consistent with Fig. 5, where the intersection scenario is found to have the highest direction spread.
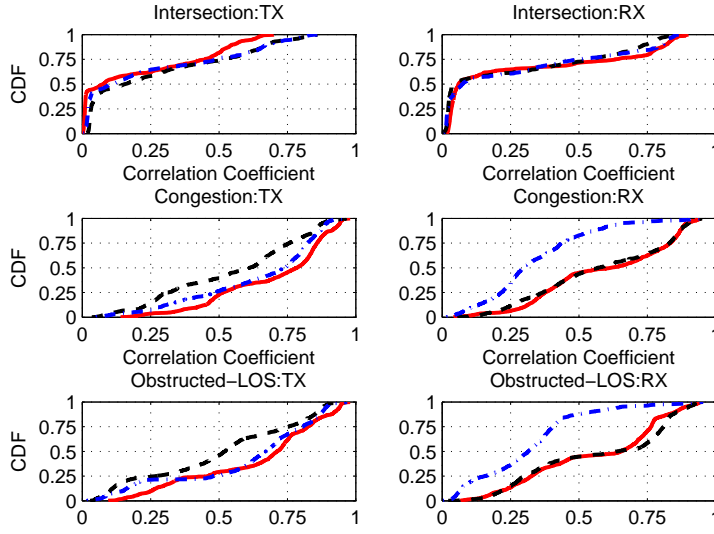
Figure 6: Cumulative distribution function (CDF) of correlation coefficients of TX and RX antenna elements for particular separation distance d; line styles (-), (- -) and (-.) represent correlation between elements 2-1 ($d = 0.5\lambda$), 3-1 ($d = \lambda$) and 4-1 ($d = 1.5\lambda$) respectively whereas λ indicates wavelength.

5   Summary and Conclusions

We have presented directional analysis of Vehicle-to-Vehicle propagation channels in three different propagation environments. We found that single-bounce reflections with static objects e.g., buildings, roadsigns, and streetlights, often are the dominating propagation mechanisms in the absence of line-of-sight whereas the reflections from other vehicles contribute little unless these vehicles are tall enough. We also observe that the directional spread of the propagation channel is high, which encourages potential use of diversity-based methods.

References

[1] M. Pätzold, B. O. Hogstad, and N. Youssef, "Modeling, analysis, and simulation of MIMO mobile-to-mobile fading channels," *IEEE Trans. Wireless*

Commun., vol. 7, no. 2, pp. 510–520, Feb. 2008.

[2] A. G. Zajić and G. L. Stüber, "Space-time correlated mobile-to-mobile channels: Modelling and simulation," *IEEE Trans. Veh. Technol.*, vol. 57, no. 2, pp. 715–726, Mar. 2008.

[3] A. F. Molisch, F. Tufvesson, J. Karedal, and C. F. Mecklenbräuker, "A survey on vehicle-to-vehicle propagation channels," in *IEEE Wireless Commun. Mag.*, vol. 16, no. 6, 2009, pp. 12–22.

[4] G. Acosta-Marum and M. Ingram, "Six time- and frequency- selective empirical channel models for vehicular wireless LANs," *IEEE Veh. Technol. Mag.*, vol. 2, no. 4, pp. 4–11, 2007.

[5] I. Sen and D. W. Matolak, "Vehicle-vehicle channel models for the 5 GHz band," *IEEE Trans. Intell. Transp. Syst.*, vol. 9, no. 2, pp. 235-245, Jun. 2008.

[6] A. Paier, J. Káredal, N. Czink, C. Dumard, T. Zemen, F. Tufvesson, A. F. Molisch, and C. F. Mecklenbräuke, "Characterization of vehicle-to-vehicle radio channels from measurements at 5.2 GHz," *Wireless Personal Commun.*, vol. 50, pp. 19–29, 2009.

[7] O. Renaudin, V. M. Kolmonen, P. Vainikainen, and C. Oestges, "Non-stationary narrowband MIMO inter-vehicle channel characterization in the 5 GHz band," *IEEE Trans. Veh. Technol.*, vol. 59, no. 4, pp. 2007–2015, May 2010.

[8] M. Boban, T. Vinhoza, M. Ferreira, J. Barros, and O. Tonguz, "Impact of vehicles as obstacles in vehicular ad hoc networks," *Selected Areas in Communications, IEEE Journal on*, vol. 29, no. 1, pp. 15 –28, 2011.

[9] T. Brown, P. Eggers, K. Olesen, and G. Pedersen, "Artificial wideband multi user channels for rural high speed vehicle to vehicle links," *Selected Areas in Communications, IEEE Journal on*, vol. 29, no. 1, pp. 29 –36, 2011.

[10] J. Karedal, F. Tufvesson, T. Abbas, O. Klemp, A. Paier, L. Bernadó, and A. F. Molisch, "Radio channel measurements at street intersections for vehicle-to-vehicle safety applications," in *IEEE VTC '71*, May 2010.

[11] A. Thiel, O. Klemp, A. Paier, L. Bernadó, J. Karedal, and A. Kwoczek, "In-situ vehicular antenna integration and design aspects for vehicle-to-vehicle communications," in *EUCAP*, Apr 2010.

[12] A. F. Molisch, *Wireless Communications* 2nd *edition*, IEEE Press - Wiley, 2010.

[13] B. H. Fleury, M. Tschudin, R. Heddergott, D. Dahlhaus, and K. I. Pedersen, "Channel parameter estimation in mobile radio environments using the SAGE algorithm," *IEEE J. Select. Areas Commun.*, vol. 17, no. 3, pp. 434–450, Mar. 1999.

[14] A. Paier, T. Zemen, L. Bernadó, and G. Matz, "Non-wssus vehicular channel charachterization in highway and urban scenario at 5.2GHz using the local scattering function," in *WSA*, Feb. 2008.

[15] B. H. Fleury, "First- and second-order characterization of direction dispersion and space selectivity in the radio channel," *IEEE Trans. Inform. Theory*, vol. 46, no. 6, pp. 2027–2044, Sep. 2000.

Paper II

Radio Channel Properties for Vehicular Communication:
Merging Lanes Versus Urban Intersections

Vehicle-to-vehicle (V2V) communication is a challenging but fast-growing technology. It has the potential to enhance road safety by helping the driver to avoid collisions during basic maneuvers such as crossing street intersections, changing lanes, merging on a highway, and driving safely in blind turns. The significance of V2V safety applications increases further where the visual line-of-sight (LOS) is unavailable because of buildings, roadside sound berms, or small hills at an intersection point of two or more roads intersecting at a certain angle, e.g., merging lanes, the entrance or exit ramps on a highway, or four-way street intersections. The reliability of V2V safety applications, which use IEEE 802.11p [1] as the underlying communication technology, highly depends on the quality of the communication link, which relies on the properties of the propagation channel. Therefore, understanding the properties of the propagation channel becomes extremely important. In this paper we characterize and compare the channel properties for vehicular communication in merging lanes versus urban intersection.

Vehicle-to-vehicle (V2V) communication is a challenging but fast growing technology. It has a potential to enhance the road safety by supporting the driver to avoid collisions in the basic maneuvers such as crossing street intersections, changing lanes, merging on a highway, and driving safely in blind turns. The significance of V2V safety applications increases further where the visual line-of-sight (LOS) is unavailable due to buildings, roadside sound berms or small hills at an intersection point of two or more roads intersecting at a certain angle, e.g. merging lanes, the entrance or exit ramps on a highway, or four-way street intersections. The reliability of V2V safety applications, which use IEEE 802.11p as the underlying communication technology [1], highly depend on the quality of the communication link, which rely upon the properties of the propagation channel. Therefore, understanding the properties of the propagation channel becomes extremely important.

A number of research outcomes have been published covering many aspects of V2V propagation channels [2]. In this paper results for V2V channel characterization based on measurements conducted for merging lanes on a highway, and four-way street interception scenarios are presented. The importance of different propagation mechanisms in non-line-of-sight (NLOS) situations and the impact of antenna radiation pattern on the total received power in LOS situations is highlighted for these scenarios. These metrics are of particular interest for V2V safety critical applications such as collision avoidance application.

Some theoretical, simulation and measurement based studies have been conducted in the past dealing with the merging lane scenarios [3–7], in which the merging/changing lane control algorithms, systems and channel properties are discussed, and simulation results are provided to show how to avoid possible collisions. Similarly, channel characterization and path-loss models for the situation when two cars are approaching an intersection with a risk of collision have been presented in [8, 9].

Vehicles that are approaching a street intersection or merging on a highway often have NLOS from the vehicles in the other street or road because the visual LOS is blocked by nearby buildings or objects. In such situations scattering of radio waves, i.e., reflection, diffraction, and refraction, implicitly enable NLOS reception. Moreover, merging lanes occur often in highway or rural environments, this is why there are few big objects in the surrounding that can contribute to increase the scattering. Similarly, some street intersections, often called open intersections which have one big building that block the LOS and only few scattering objects in the surrounding. Thus, NLOS reception in merging lane and open intersection scenarios could probably be very bad.

In contrary to NLOS, LOS reception can go really bad if the antenna pattern has a dip in the direction-of-departure (DOD) or direction-of-arrival (DOA) of

the LOS path. In open environments the probability of losing the packets due to bad reception is even higher because there are no other significant scatterers to carry the signal power. Thus an antenna pattern should be designed such that it has good coverage in all directions or multiple antennas should be considered. Multiple antennas mounted at different locations on the car can help to exploit diversity and combat shadow fading [10].

In many simulation studies the antennas are assumed to be isotropic, radiating equal power in all directions, and the communication range is assumed to be a circle around the TX, which is a perfect condition for reception but its not the case in reality. The communication range depends on a number of factors involving the antenna radiation pattern, location of the antenna on the car, the traffic density, obstacles such as buildings and vehicles, and the transmitted power. The antenna pattern is one of the major limiting factors and to perform a realistic simulation studies it is necessary to use somewhat realistic antenna patterns.

To emphasize this, measurements data is collected and analyzed for both scenarios, and results for this antenna-channel interaction are presented. To identify the important propagation mechanisms, a directional analysis is performed using a high resolution space-alternating expectation maximization algorithm (SAGE) [11] for selected time-snapshots. Particular focus is put on the LOS component as it carries most of the received power. The DOA/DOD estimates are presented to show how the antenna pattern can affect the received signal strength, when the LOS component is received at an angle where the antenna has a lower gain.

1   V2V Measurement Setup

V2V channel measurements were conducted using the RUSK Lund channel sounder that performs multiple-input multiple-output (MIMO) measurements based on the switched-array principle [12]. For the measurements, two standard hatch-back style cars were used and the four-element antenna arrays were mounted on the roof. The height of each antenna array was $1.73\,\mathrm{m}$ from the ground. The channel sounder sampled the 4×4 MIMO time-varying channel transfer function $H(f, t)$ over a $240\,\mathrm{MHz}$ of measurement bandwidth centered at $5.6\,\mathrm{GHz}$. The temporal sampling and the measurement duration were set to $307.2\,\mu\mathrm{s}$ and $20\,\mathrm{s}$, respectively, with a test signal length of $3.2\,\mu\mathrm{s}$. The 4×4 MIMO antenna arrays were used to exploit diversity as the different TX-RX pairs give rise to different directional links. These arrays were designed specifically for V2V communication [13]. Each element of the arrays has a directional antenna gain such that the antenna pattern of element $1, 2, 3$ and 4 have their

Figure 1: Google Earth™ [14] aerial image shows the investigated merging lane scenario outside the city of Lund. The TX enters the highway while RX is approaching the merging point on the highway. (N $55°42'36''$, E $13°8'53''$)

main gain pointing to the left-side, backward, forward and to the right-side of the car, respectively. In the subsequent analysis we consider all four elements of the TX array such that the transmitter has somewhat omni-directional gain and then the power received at the element-1 is compared against the element-2 of the RX array.

To keep track of the positions of the transmitter (TX) and receiver (RX) cars, during the measurements, each vehicle logged the GPS coordinates and videos were recorded through the windshield. This data was combined with the measurement data, in order to identify the important scatterers in the post-processing.

1.1   Scenario Description

Merging lanes

The merging lane scenario at a highway is characterized by the roads that are used to merge two traffic flows into one, e.g., entrance or exit ramps. An important aspect of this scenario is the possibility of an obstructed LOS path due to the slope and the orientation of the terrain, or the presence of sound barriers, buildings or trees between the intersecting roads. This scenario is similar to the urban street crossings scenario [8], but with slightly more difficult channel
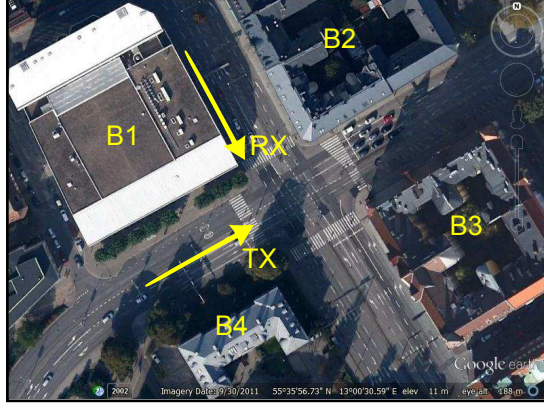
Figure 2: Google Earth[TM] [14] aerial image shows the investigated four-way intersection scenario in Malmö where both the TX and RX are approaching the intersection. Four buildings at each corner B1, B2, B3 and B4 are marked clockwise starting from the top left corner, respectively. (N $55°35'56''$, E $13°0'30''$)

conditions in the absence of the LOS due to open surroundings, availability of fewer scatterers and higher vehicle speeds. In order to draw conclusions on the importance of scatterers in the absence of LOS, two types of measurements were conducted for the merging lanes scenario: 1) Vehicles merging at an entrance ramp, when the RX car was driving on the highway and the TX car was entering on the highway; 2) Vehicles splitting at an exit ramp, where the RX car was exiting from the highway and the TX car continued driving on the highway. In this paper we focus mainly on entrance ramps (see Fig. 1), since this is the most important case in terms of collision avoidance and the experiences learned from these results can be applied on exit ramps.

Several measurements were made and during each measurement the RX car was moving on the highway and the TX car was entering on the highway from the entrance ramp. Both the cars were moving at the speed of $20 - 28 \, \mathrm{m/s}$ ($70 - 100 \, \mathrm{km/h}$). Two measurements are chosen for the analysis;

Scenario-1: when the TX enters the highway and remains behind the RX, which is already driving on the highway, and there are other vehicles driving by.

Scenario-2: when the TX enters the highway and remains in front of the RX, which is already driving on the highway, and there are no vehicles around.

Four-way Intersection

In order to highlight the importance of scattering objects in NLOS situations the measurement results for a four-way intersection have also been included. A four-way intersection scenario is characterized by that four urban-streets of varying widths meet at a certain point, such that the visual LOS between cars on the intersecting streets is blocked by building of certain height situated at the corner of the intersection. There are buildings, trees, light poles, and street signs at random location. These objects are expected to provide many additional multi-path components which is beneficial especially in the NLOS situation.

Several measurements were conducted in different types of four way intersections [8] in the city of Lund and Malmö in Sweden. A single measurement is however chosen for the analysis;

Scenario-3: when the TX and RX cars are approaching a wide-urban intersection from the streets almost perpendicular to each other. All four streets have different widths varying between $20 - 43$ m with different traffic conditions that makes the scenario very dynamic. Four multi-story buildings are situated at each corner of the intersection marked as B1, B2, B3 and B4, respectively (see Fig. 2).

2   Data Evaluation and Results Analysis

To analyze the radio channel properties the data evaluation is performed as follows;

2.1   Averaged Power Delay Profile

To analyze the impact of time-variations on the received signal power, especially in the absence of LOS, the time-varying instantaneous power-delay-profile (PDP) is derived for each time sample. The effect of small-scale fading is removed by averaging the PDPs of N_{avg} time samples. The averaged-PDP (APDP) is calculated as,

$$P_h(t_k, \tau) = \frac{1}{N_{avg}} \sum_{n=0}^{N_{avg}-1} |h(t_k + n\Delta t, \tau)|^2, \tag{1}$$

for $t_k = \{0, N_{avg}\Delta t, ..., \lfloor N_t/N_{avg} - 1 \rfloor N_{avg}\Delta t\}$, where $h(t_k + n\Delta t, \tau)$ is the complex time varying channel impulse response derived by an inverse Fourier transform of a channel transfer function $H(f, t)$ for a single-input single-output (SISO) antenna configuration. Moreover, the $N_{avg} = 64$ is calculated as
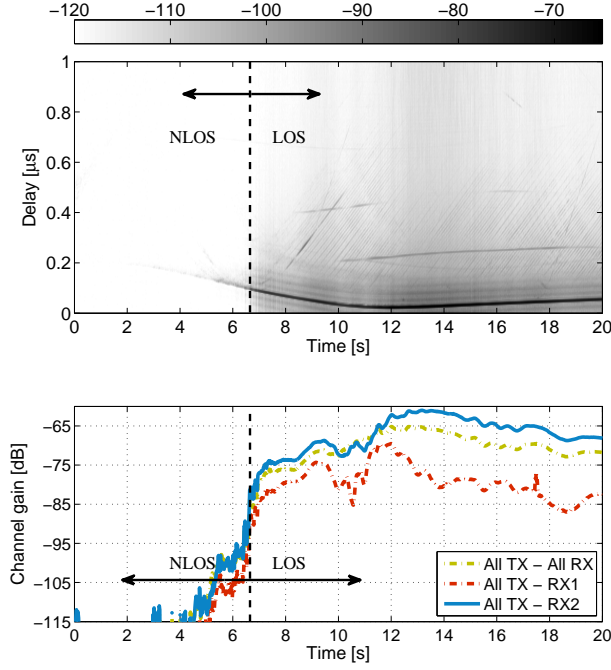
Figure 3: Scenario-1: Averaged power delay profile (top) and channel gain of the strongest and weakest links among the 4×4 MIMO links (bottom).

$N_{avg} = \lceil \frac{s}{v\Delta t} \rceil$, where $\Delta t = 307.2\mu$ s is the time spacing between snap shots, $s =$ corresponds to the movement of the TX and RX of 10 wavelengths and v is the velocity of the TX and RX, $28\,\text{m/s}$, approximately.

We also derive the time varying channel gain, as $G(t) = \sum_\tau P_\tau(t, \tau)$, where we apply a noise threshold setting all components within $3\,\text{dB}$ of the noise floor to zero.

The time-varying APDP and the corresponding channel gain are shown in Fig. 3 (Scenario-1), in Fig. 4 (Scenario-2) and in Fig. 5 (Scenario-3). From the APDP it is found that the channel is very poor in terms of scattering in scenario-1 and 2. It can be observed in both of the measurements that in the absence of LOS there are very few scattering objects that can provide additional propagation paths. Whereas in scenario-3 the situation is different,
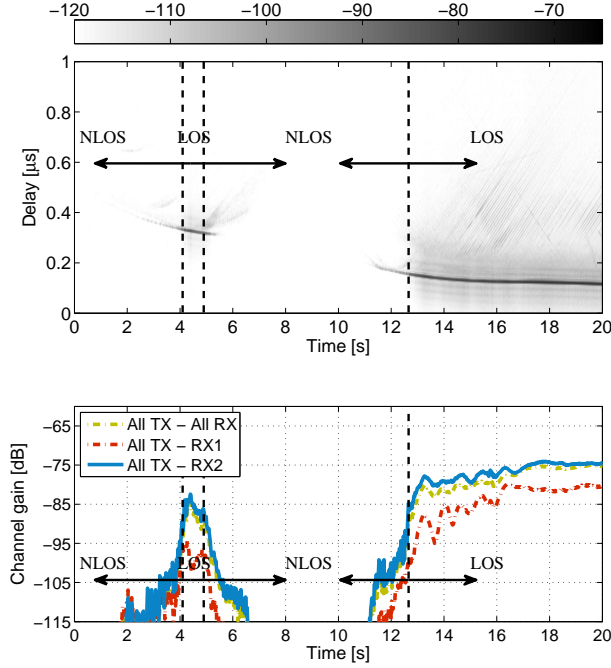
Figure 4: Scenario-2: Averaged power delay profile (top) and channel gain of the strongest and weakest links among the 4×4 MIMO links (bottom).

there exist a few significant multi-path components even in the absence of LOS originating from nearby buildings and multitude of cars waiting at traffic lights. In scenario-1 and 2 some additional power is received from the MPCs reflected from the vehicles moving next to the TX/RX, but their contribution seem to appear only when the LOS is available (see Fig. 3). It is observed that the channel gain is higher in Fig. 3 than in Fig. 4 and 5 due to the smaller distance between TX and RX.

Differences due to the antenna gain can be best appreciated in the plots of the channel gain in Fig. 3, 4 and 5 (bottom) where we show that the different TX-RX antenna pairs result in different channel gains due to different directional properties, e.g., the difference in the gain of the RX element-1 and element-2 in the forward and backward direction. The overall difference in the
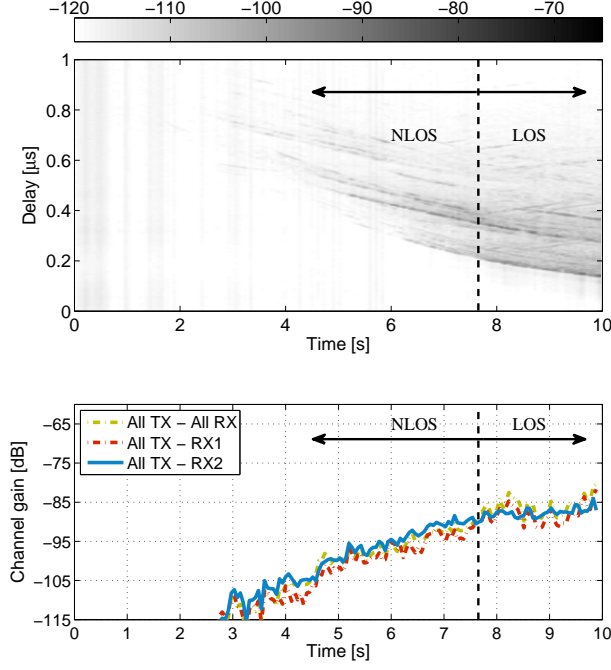
Figure 5: Scenario-3: Averaged power delay profile (top) and channel gain of the strongest and weakest links among the 4×4 MIMO links (bottom).

channel gain for the two links is higher in scenario-1 than in scenario-2 and 3 because in scenario-1 the RX is driving next to the TX, unlike in scenario-2, and the antenna gain of the RX is higher in the backward direction as compared to the forward direction. For both Scenario-1 and 2, the channel gain for all TX-RX1 is $5 - 15$ dB lower than the all TX-RX2 link because the main gain of RX element-1 is pointing in the direction opposite to the direction of the TX. Furthermore in scenario-3 the difference in the channel gain is not so big as the four-way intersection has a rich scattering environment and there exist few MPCs wide spread in space that carry significant power in addition to the LOS component. Therefore the antenna gain do not really influence the channel gain in scenario-3. It is observed that the number of scatterers do improve the channel gain but when there exist no scattering objects then the

LOS is the only major power carrying component.

2.2   Impact on collision avoidance applications

One of the main features of collision avoidance applications is the early warning of the possible threats to be issued few seconds in advance. Such applications require reliable communication up to a certain distance that depends on the received signal power especially in the NLOS situation. To further emphasize this and to highlight the importance of scatterers, the channel gain as a function of distance-to-collision (d_{dc}), i.e., distance from the TX to the collision point and to the RX, is shown in Fig. 6 for scenarios-1, 2 and 3. The d_{dc} can directly be related to warning time t_w, by $t_w = \frac{d_{dc}}{v_{TX}+v_{RX}}$, where v_{TX} and v_{RX} are average velocities of the TX and RX, respectively. From Fig. 6 it can be seen that the scenario 3, four-way intersection, has good signal strength at a larger d_{dc} compared to the case in scenario-1 and 2. The major difference in the channel gain in scenario-3 is due to the LOS component that is available even up to $d_{dc} = 90\,\mathrm{m}$ because of wider streets, and the buildings B2 and B3 (see Fig. 2) that provide strong reflections in the NLOS. However, scenario-2 has a few samples with high channel gain even at a distance of about $150\,\mathrm{m}$ due to occasional availability of LOS, mentioned in APDP plot between $4 - 5\,\mathrm{s}$ in Fig. 4 (top).

In the merging lane scenarios-1 and 2, LOS appears at a very short distance to the collision d_{dc} and no objects are available in the surrounding that can contribute to improve the signal strength in the NLOS. The intersection scenario-3 on the other hand has wider geometry and buildings at the corners that act as reflection points that improve the signal strength and enable reception at larger d_{dc}. For the collision avoidance applications larger d_{dc} translates to an increased t_w, i.e., additional time to asses the hazardous situation and issue collision avoidance warnings well in time. Both the LOS as well as the scattering objects do play a critical role to enable reliable communication for such applications. Another factor that can influence the performance of the safety applications is the antenna gain as discussed in the following.

2.3   Directional Analysis

The propagation mechanism driving these differences in the channel gain and antenna-channel interaction can be well understood by performing a directional analysis of the measurement data. A directional analysis, similar to [15], is performed using SAGE [11]. It is assumed that the 4×4 channel matrix H can be described by a sum of L plane waves or multi-path components (MPCs) where each wave l is characterized by a complex amplitude γ_l, propagation
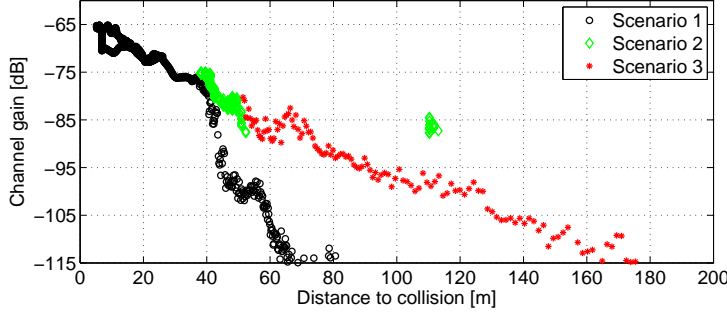
Figure 6: Channel gain as a function of distance to collision from the TX to collision-point and to the RX averaged over all MIMO links for Scenarios 1, 2 and 3, respectively.

delay τ_l, Doppler shift ν_l, DOD and DOA, respectively, for both the azimuth and the elevation angles. The parameters for 100 MPCs are estimated from the measured channel matrices and the DOA against the DOD for the estimated MPCs are presented in Fig. 7 for selected snapshots. The snapshots in scenario-1; at time instant and 17.56 s, in scenario-2; at time instant 13.51 s, and in scenario-3; at time instant 8.33 s, are chosen as example for the analysis. MPCs with a power 20 dB less than the LOS component are not shown in the figures. The propagation delay τ_l of each MPC is normalized by the propagation delay of the LOS component τ_{LOS} such that the LOS has $\tau_{LOS} = 0$ s delay. The delay τ_l is shown as the propagation distance $S_l = c \times (\tau_l - \tau_{LOS})$ in the color bar in Fig. 7.

In the merging lane scenarios, scenario-1 and 2, there are very few interacting objects, often widely separated in space, which results in very few reflected propagation paths in addition to the LOS component. Due to the sparsity of interacting objects, the propagation distances of these MPCs are large and the signal strength is usually very low. MPCs with power $10 - 20$ dB lower than the LOS component can be seen in Fig. 7, (a) and (b). These MPCs, with $1 - 3$ m longer propagation distance relative to LOS propagation distance, are the paths originating from the single bounce reflection with road signs and the metallic guard rail between the ramp and the highway, and the ground reflections. Most of these MPCs are available only when there is LOS. Therefore, the received power is negligible in the absence of LOS (as shown in Fig. 3 and 4) and the LOS component constitutes most of the received power when there is a LOS between the TX and the RX (see Fig. 7).
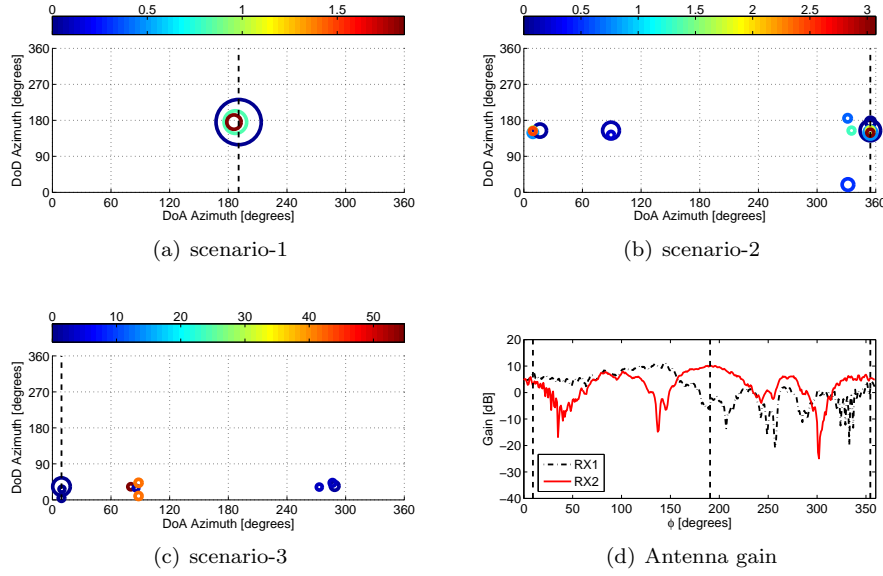
(a) scenario-1

(b) scenario-2

(c) scenario-3

(d) Antenna gain

Figure 7: The azimuth direction-of-arrival (DOA) and azimuth
direction-of-departure (DOD) estimates for the snapshots at time in-
stants 17.56 s (scenario-1), 13.51 s (scenario-2), and 8.33 s (scenario-3),
and the azimuth antenna gain of RX element-1 and element-2 (Antenna
gain) are shown. The color bar is representing the relative distance (m)
w.r.t. the LOS component such that the LOS component is at 0 m. The
size of the circles depicts the power carried by each MPC.

In the four-way intersection, scenario-3, relatively higher number of MPCs
are available that can be tracked even in the absence of LOS and at a larger
propagation distance. These MPCs, with $1-60$ m longer propagation distance
relative to LOS propagation distance, are the paths originating from the cars,
a bus waiting at the traffic light, and from the buildings B1 and B2, see Fig. 2.
Although there exist strong MPCs, the LOS component still dominates as it
constitutes most of the power.

To analyze the variations in the received power due to the variation in
the antenna gain it is important to analyze the power variations in the LOS
component. The vertical dotted lines are drawn to visualize the DOA of the
LOS component, the largest circle, for each snapshot to compare the differences

in the antenna gain for RX element-1 and element-2 at that particular angle. As a first observation it is found that the received power can drop up to 20 dB depending upon the DOA and the differences in the antenna gain of the RX elements-1 and 2 at that angle. Comparing these results with the channel gain results in Fig. 3 (Scenario-1), in Fig. 4 (Scenario-2) and in Fig. 5 (Scenario-3), we find a direct correlation between the channel gain and the antenna radiation pattern. This implies that, even if there is a LOS between the TX and RX, the power level can drop significantly when there is a dip in the antenna pattern. This can have severe impact on the communication range and thus it needs to be considered when designing an antenna for automotive safety applications.
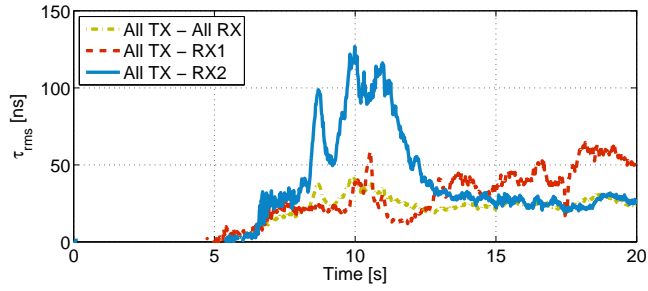
2.4   Delay Spreads

The root mean square (rms) delay and Doppler spreads are also important parameters in the system design. They describe how the power is spread by the channel in time and in frequency, and they are good indicators of the frequency selectivity (rms delay spread) and the time selectivity (rms Doppler spread) of the channel. Moreover, they can be related to the coherence bandwidth and coherence time as described in [16].

In this paper we consider only the time-varying rms delay spread as in [17], and we apply a threshold on the data such that we can avoid erroneous results due to spurious components. The rms Doppler spread results can be found in [7], but are not included here due to space limitation. All components below the noise floor plus 3 dB (*noise thresholding*) are set to zero.

The time-varying rms delay spread for the three scenarios (scenario-1, 2 and 3) are shown in Fig. 8. We plot the results for three different configurations, as similarly done in the previous section: in green dotted line we show the rms spreads when considering all TX antennas and all RX antennas; in red dashed line we show the results obtained when considering all TX antennas and only RX element-1; and in blue solid line we consider all TX antennas and only RX element-2.

First we observe that the rms spreads are not equal for the three links in scenario-1, clearly observable in the rms delay spread plot (Fig. 8 (a)). The link between all TX antennas and RX element-2 is the most frequency selective one, since some MPCs that are only visible to RX element-2 contribute to a large rms delay spread. The RX element-2 is focusing towards the TX (the RX driving in front of the TX), therefore, the surrounding scatterers are illuminated the most, thus resulting in strong MPCs at the RX element-2. On the other hand, when considering all RX antennas, the power of the LOS and all other MPCs is averaged over all RX antennas. Often all scatterers do not contribute to the power received at each RX antenna, therefore the averaged power of the

(a) scenario-1
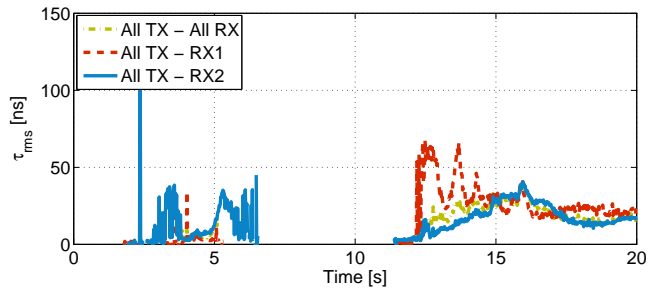
(b) scenario-2
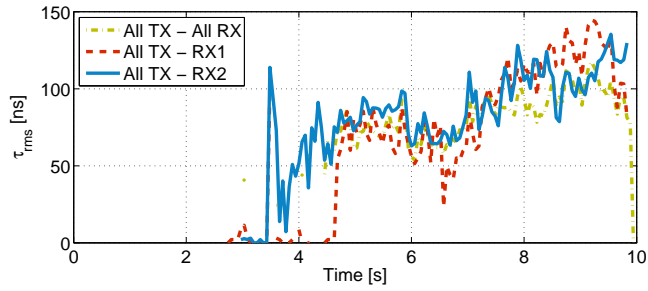
(c) scenario-3

Figure 8: Time-varying rms delay spread for scenario 1, 2 and 3.

scatterers over all RX antennas can be lower than their power in each link. Moreover, the power of the LOS component is much larger than the power of the later MPCs, so the rms delay spread is small.

We depict the time-varying rms delay spread for the second scenario (scenario-2) in Fig. 8 (b). Here we observe a similar behavior, but since now the TX is driving in front of the RX, the RX element-2 is not focusing on the TX anymore, and the number of illuminated objects is smaller than it is for the other links. Therefore, the link all TX - RX element-2 shows the smallest rms delay spread compared to the other links.

Finally in Fig. 8 (c), the rms delay spread for the third scenario is presented. A first observation is that scenario-3 is overall more frequency selective than the other two scenarios as the delay spread is large for almost all links. The main reason behind this is relatively rich scattering environment which is also observed in the APDP and DOA/DOD plots for scenario-3. For the same reason no big difference lies in the delay spread of the three links.

3   Summary and Conclusions

This paper presents results from a vehicle-to-vehicle measurement campaign for the safety applications targeting collision avoidance applications in merging lanes and intersection scenarios. Looking at the results for the merging lane scenario, we found that the channel gain is highly dependent on the line-of-sight (LOS) in such a sparse scattering environment. Due to lack of significant scatterers, such as road side objects and vehicles, the received power decays abruptly in the NLOS which demonstrates the importance of the LOS. On the other hand, in the four-way intersection scenario there exist some buildings at the street corners, cars and road signs that contribute to the signal strength even in the NLOS. Therefore, to summarize the discussion we can say that the street intersection scenario is similar to the merging lane scenario with slightly better propagation conditions due to availability of scatterers. This implies that the merging lane scenario is more safety critical. Moreover, the antenna radiation pattern plays an important role especially in the situation when there are few scatterers and if the antenna has a poor gain in the direction of the TX, then the received power level can drop significantly. Thus designing an antenna that has an omni-directional gain, or using multiple antennas that radiate towards different directions becomes more important for such safety critical scenarios.

References

[1] *IEEE Std. 802.11p-2010, Part 11: Wireless LAN Medium Access Control (MAC) and Physical Layer (PHY) specifications: Amendment 7: Wireless Access in Vehicular Environment*, IEEE Std., July 2010.

[2] A. F. Molisch, F. Tufvesson, J. Karedal, and C. F. Mecklenbräuker, "A survey on vehicle-to-vehicle propagation channels," in *IEEE Wireless Commun. Mag.*, vol. 16, no. 6, 2009, pp. 12–22.

[3] T. Sakaguchi, A. Uno, and S. Tsugawa, "Inter-vehicle communications for merging control," in *Vehicle Electronics Conference (IVEC '99) Proceedings of the IEEE International*, 1999, pp. 365 –370 vol.1.

[4] A. Uno, T. Sakaguchi, and S. Tsugawa, "A merging control algorithm based on inter-vehicle communication," in *Intelligent Transportation Systems. Proceedings of the IEEE/IEEJ/JSAI International Conference on*, 1999, pp. 783 –787.

[5] Q. Xu and R. Sengupta, "Simulation, analysis, and comparison of ACC and CACC in highway merging control," in *Intelligent Vehicles Symposium, 2003. Proceedings. IEEE*, june 2003, pp. 237 – 242.

[6] Y. Liu, U. Ozguner, and T. Acarman, "Performance evaluation of inter-vehicle communication in highway systems and in urban areas," in *Intelligent Transport Systems, IEE Proceedings*, vol. 153, no. 1, march 2006, pp. 63 – 75.

[7] T. Abbas, L. Bernado, A. Thiel, C. F. Mecklenbruker, and F. Tufvesson, "Measurements based channel characterization for vehicle-to-vehicle communications at merging lanes on highway," in *5th International Symposium on Wireless Vehicular Communications: WIVEC2013*. IEEE, June 2013, pp. 1–5.

[8] J. Karedal, F. Tufvesson, T. Abbas, O. Klemp, A. Paier, L. Bernadó, and A. F. Molisch, "Radio channel measurements at street intersections for vehicle-to-vehicle safety applications," in *IEEE VTC 71st Vehicular Technology Conference (VTC 2010-spring)*, May 2010, pp. 1–5.

[9] T. Mangel, O. Klemp, and H. Hartenstein, "5.9 GHz inter-vehicle communication at intersections: a validated non-line-of-sight path-loss and fading model," *EURASIP Journal on Wireless Communications and Networking*, vol. 2011, no. 1, p. 182, 2011.

[10] T. Abbas, J. Kredal, and F. Tufvesson, "Measurement-based analysis: The effect of complementary antennas and diversity on vehicle-to-vehicle communication," *IEEE Antennas and Wireless Propagation Letters*, vol. 12, no. 1, pp. 309–312, 2013. [Online]. Available: http://lup.lub.lu.se/record/3516482/file/3555826.pdf

[11] B. H. Fleury, M. Tschudin, R. Heddergott, D. Dahlhaus, and K. I. Pedersen, "Channel parameter estimation in mobile radio environments using the SAGE algorithm," *IEEE J. Select. Areas Commun.*, vol. 17, no. 3, pp. 434–450, Mar. 1999.

[12] R. Thoma, D. Hampicke, A. Richter, G. Sommerkorn, A. Schneider, U. Trautwein, and W. Wirnitzer, "Identification of time-variant directional mobile radio channels," *Instrumentation and Measurement, IEEE Transactions on*, vol. 49, no. 2, pp. 357 –364, apr 2000.

[13] A. Thiel, O. Klemp, A. Paier, L. Bernadó, J. Karedal, and A. Kwoczek, "In-situ vehicular antenna integration and design aspects for vehicle-to-vehicle communications," in *EUCAP*, Apr. 2010, pp. 1–5.

[14] Google earth v7.1.1.1888 (2013). [Online]. Available: http://www.google.com/earth/index.html [Accessed: 2013/08/15]

[15] T. Abbas, J. Karedal, F. Tufvesson, A. Paier, L. Bernado, and A. Molisch, "Directional analysis of vehicle-to-vehicle propagation channels," in *2011 IEEE 73rd Vehicular Technology Conference (VTC Spring)*, May 2011, pp. 1–5.

[16] A. Molisch and M. Steinbauer, "Condensed parameters for characterizing wideband mobile radio channels," *International Journal of Wireless Information Networks*, vol. 6, no. 3, pp. 133–154, 1999.

[17] L. Bernadó, T. Zemen, A. Paier, G. Matz, J. Karedal, N. Czink, F. Tufvesson, M. Hagenauer, A. F. Molisch, and C. F. Mecklenbräuker, "Non-WSSUS vehicular channel characterization at 5.2 GHz - Spectral divergence and time-variant coherence parameters," in *Assembly of the International Union of Radio Science (URSI)*, August 2008, pp. 9–15.

Paper III

Simulation and Measurement Based Vehicle-to-Vehicle Channel Characterization: Accuracy and Constraint Analysis

In this paper, a deterministic channel model for vehicle-to-vehicle (V2V) communication, is compared against a channel measurements data collected during V2V channel measurement campaign using a channel sounder at 5.6 GHz in the city of Lund, Sweden. Channel metrics such as channel gain, delay and Doppler spreads, eigenvalue decomposition and antenna correlations are derived from the ray-tracing simulations as well as from the measurement data obtained from two different measurements in an urban four-way intersection scenario. The channel metrics are compared separately for line-of-sight (LOS) and non-LOS (NLOS) situation. Most of the power contributions arising from specular and non-specular reflections are captured by the ray-tracing simulation regardless of some known implementation-based limitations of the ray-tracing model. As for the ray-tracing simulations, specular reflections up to second order and non-specular reflections of first order are considered only to analyze, how well channel properties can be described while keeping the minimal computational cost. Measurement and simulation results show a very good agreement in the presence of LOS, because most of the power in the LOS is contributed by the LOS component. This is not the case in NLOS, when the LOS is absent, as the ray-tracer is unable to capture some of the higher-order specular and non-specular reflected paths, which are non considered in simulations.

1   Introduction

Vehicle-to-Vehicle (V2V) communication has recently attracted considerable attention from both academia and industry as it facilitates cooperative driving among vehicles for improved safety, collision avoidance, and better traffic efficiency. The radio channel poses one of the main challenges of V2V communication systems design because the V2V channel is highly dynamic. Fast variations in the traffic density, varying vehicle speeds and changing roadside environment, with a height of transmitter (TX) and receiver (RX) antennas relatively close to the ground level makes the V2V channel significantly different from the well studied channels of other technologies such as cellular networks. Thus, a deep understanding of the underlying propagation channels is required. There is a need for adequate and reliable, deterministic as well as stochastic, channel models allowing a realistic and sophisticated V2V system analysis [1,2].

In order to characterize V2V channel properties, a number of channel measurements and ray-tracing simulation-based studies have been presented in recent years, e.g., [1,3–6]. The measurement based investigations require a lot of effort and are costly in contrast to the deterministic model based ray-tracing simulations which allow to investigate any desired scenario with less effort and reduced complexity. However, the results obtained from the ray tracing simulations strongly depend on the implemented mathematical models as well as on the accuracy of the data used to describe the environment, thus it is necessary to validate the simulations. Most of the measurement and simulation studies in the past have almost exclusively been performed independently except in a few cases [7–9]. This study is an extension of the work presented in [9], in which the simulation results obtained using a ray-optical model were compared against the results obtained from the DRIVEWAY channel measurements performed in the city of Lund using the RUSK Lund channel sounder [4]. The ray-tracing simulator is developed by the researchers at TU Braunschweig especially for vehicular communications at the 5.9 GHz band [5]. The simulations were done for the same urban intersections as where the measurements were performed. In [9] the analysis was limited to a single-input single-output (SISO) antenna configuration and a comparison was made only in terms of power delay profile (PDP) and path loss metrics.

The importance of an urban street intersection scenario is that the line-of-sight (LOS) path is often obstructed by surrounding buildings which strongly limits the wave propagation and affects the link reliability in a crucial manner. In such a scenario the communication is highly dependent on the availability of reflected multipath components (MPCs) which in turn depends on the location of the scatterers, street width, distance to the intersection, and side distance of the transmitting node to surrounding buildings. Some path loss

Figure 1: Google Earth™ [10] aerial image of the investigated urban crossroads scenario in the city of Lund with two vehicles moving towards the intersection at a speed of approximately $10\,\text{m/s}$ (N55° 42′ 37″, E13° 11′ 15″).

models have been derived to characterize such scenarios [6, 11] and validated using channel measurement data [12]. Both models assume an intersection with perpendicular side roads and cannot directly be applied to intersections with an irregular geometry. Hence, urban intersections constitute an interesting scenario to investigate where a flexible semi-deterministic channel model for V2V communications is still required.

The main contribution of this work is that it extends the work presented in [9], and compare the results for a 4×4 multiple-input multiple-output (MIMO) configuration, by providing a detailed comparison of V2V channel parameters obtained from ray-tracing simulations and measurements in a four-way-urban street intersection. The comparison is made by evaluating channel metrics such as PDP, channel gain, delay and Doppler spreads, eigenvalue distribution and MIMO diversity for two different TX and RX configurations in the same scenario. The measurement data is analyzed separately for both LOS and NLOS situations, where mean and standard deviation of the error is provided individually for each of the channel metrics. With the help of these channel metrics the accuracy of the ray-tracing tool is analyzed and possible flaws or limitations of the underlying channel models are identified.

The remainder of the paper is organized as follows: Section 2 describes the measured urban intersection scenario as well as the different configurations of

(a)   (b)

Figure 2: (a) and (b) sshow the perspective from the receiving vehicle
$RX - M1$ and $TX - M1$.

the TX and RX vehicles used during the measurements. Section 3 describes
the RUSK-Lund channel sounder and the measurement setup. In section 4 the
ray-optical channel model used for the simulations is described. The channel
measurement data and the simulation data are compared and analyzed in sec-
tion 5. Finally, in section 6 the discussion is summarized and conclusions are
presented.

2   Urban Intersection Scenario

For the comparison of simulation results against measurement data, we have
chosen an urban four-way intersection (N55° 42′ 37″, E13° 11′ 15″, see Fig. 1)
in the city of Lund, Sweden.

The scenario is exactly the same as the narrow urban scenario described
in [13]. Two measurements have been selected for the analysis: $M1$) when the
TX and RX cars are driving from the streets $TX - M1$ and $RX - M1$, and $M2$)
when the TX and RX cars are driving from the streets $TX - M2$ and $RX - M2$,
respectively, towards the intersection at a speed of approximately 10 m/s. The
line-of-sight (LOS) component is obstructed by four-story buildings arranged
along each leg of the intersection. On the walls of the buildings there were
doors and windows and balconies with metallic frames. The canyon of the
street is quiet narrow and ranges from $14 - 17$ m. The four side roads are not
perfectly perpendicular. During the measurements there were parked vehicles
along both sides of the streets. Furthermore, there were some traffic signs and

lamp posts in the close environment of the intersection. The photos shown in Fig. 2(a) and Fig. 2(b) show a view from the RX vehicle of the the street $RX - M1$ and the TX vehicle of the street $TX - M1$, respectively. It is worth mentioning that in $M1$ a bus is driving in front of the RX and turns left from $RX - M1$ street to $TX - M1$ street in Western direction at the beginning of the scenario.

3   Channel Measurement Setup

The RUSK Lund channel sounder, which performs MIMO measurements based on the switched array principle, was used to record the complex time-varying channel transfer function $H(f,t) \in \mathbb{C}^{M_R \times M_T}$, where M_T and M_R denote the number of transmit and receive antennas, respectively. The corresponding channel impulse response (CIR), $h(\tau, t)$, is derived from $H(f,t)$ by applying a Hann window to suppress side lobes and then an inverse Fourier transform. For each measurement the sounder sampled the channel for $10\,\text{s}$ using a time increment of $\Delta t = 307.2\,\mu s$ over a bandwidth of $240\,\text{MHz}$ at $5.6\,\text{GHz}$ carrier frequency. Two regular hatchback cars with a height of $1.73\,\text{m}$ and each equipped with a four-element antenna array were used to perform V2V measurements. Each antenna element in the array had a somewhat directional beam pattern pointing; 1) left, 2) back, 3) front, and 4) right, respectively These antenna arrays, integrated into the existing radomes ('shark fins') on the car roof, were specifically designed for V2V communications [14]. The interested reader is referred to [4], where a detailed description of the measurement setup can be found.

4   3D Ray-optical Channel Model

The underlying simulation-based channel model that is used in this paper belongs to the class of deterministic channel modeling approaches using 3D ray-optical algorithms [5,15]. In order to characterize the channel between the TX and RX, the direct path, specular reflections as well as diffuse scattering in terms of non-specular reflections are taken into account. Specular reflections are calculated recursively up to a desired order, but depending on the complexity and level of detail of the environment only reflections up to order three or four are practical due to the computational effort. Faces of buildings or obstacles that can be seen by both the TX and the RX are treated as sources of non-specular reflections of first order, modeled by means of Lambertian emitters. Furthermore, the ray tracing model is able to include the full-polarimetric antenna patterns of TX and RX, respectively.

The output of the ray-optical model is the time-variant CIR $h(\tau, t) \in \mathbb{C}^{M_R \times M_T}$, which completely characterizes the frequency-selective channel for each TX/RX link. We can express the CIR as

$$h\left(\tau, t\right) = \sum_{k=1}^{N(t)} a_k\left(t\right) \cdot e^{j(2\pi f \tau_k(t) + \varphi_k(t))} \cdot \delta(\tau - \tau_k(t)) \qquad (1)$$

$$= \sum_{k=1}^{N(t)} \tilde{a}_k\left(t\right) \cdot \delta(\tau - \tau_k(t)), \qquad (2)$$

where $\tilde{a}_k\left(t\right) = a_k\left(t\right) \cdot e^{j(2\pi f \tau_k(t) + \varphi_k(t))}$ and the k-th multipath component is described by an amplitude $\tilde{a}_k\left(t\right)$, a delay $\tau_k(t)$ and an additional phase shift $\varphi_k(t)$ at time t. $N(t)$ denotes the time-variant number of multipath components. Based on the predicted CIR further metrics like the PDP, the channel gain or the RMS delay spread can be derived and compared with measurement-based data.
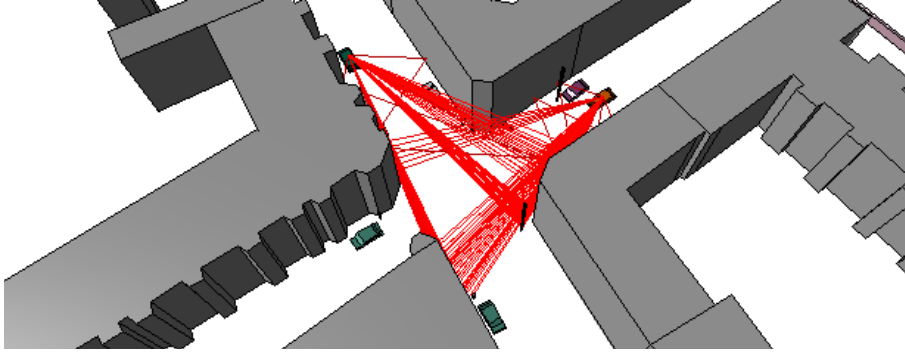

Figure 3: Simulation of the underlying urban intersection scenario by means of ray tracing. The data of the environment includes buildings, traffic signs, lamp posts as well as parked cars along the roadside.

In order to characterize the wireless V2V channel using ray-tracing techniques, the investigated scenario has to be described, including all buildings and obstacles that mainly interact with the transmitted signal and, therefore, affect the wave propagation. We obtain building data from the OpenStreetMap database [16], which of the considered scenario provides reasonably detailed description of the buildings. Since the height of the buildings around the considered intersection is not available in the database, we define a fixed height

of 15 m for all buildings. The specific height is not critical in this peer-to-peer scenario as most propagation processes take place at street level. By analyzing videos captured during the measurements and on-site inspections of the intersection, we identify relevant obstacles like traffic signs, lamp posts or parked cars along the roadside and add these objects , but with less details to the virtual scenario. The trajectories of the moving TX and RX, respectively, are reproduced using the GPS coordinates logged during the measurement runs. Finally, the snapshot-based CIRs at a time resolution of 10 ms are calculated by the ray tracing model. A post-processing algorithm that exploits knowledge about the positions of the TX, RX and scatterers as well as the driving speed of the vehicles interpolates the obtained CIR data between two adjacent snapshots leading to a final time resolution of 100 μs. As an example, Fig. 3 illustrates the virtual scenario and visualizes the calculated propagation paths of an arbitrary snapshot.

5   Analysis

The main objective is to perform a validation of the ray-tracing simulation results for the V2X channel by means of a comparison with measured channel data. In the simulations, we have restricted the order of specular reflections to second order in order to keep the complexity low. Moreover, non-specular reflection of order higher than one and the diffuse scattering are not included either. Given these restrictions and limitations, the goal is to find out how well the channel properties can be described using ray tracing simulations under those conditions. Signal reception is significantly different in LOS and NLOS situations, we thus characterize the channel metrics separately for LOS and NLOS situations.

5.1   Power Delay Profile and Doppler Spectral Density

The time-variant APDP is calculated by using the time-variant 4×4 MIMO channel transfer function $H(t, f)$ obtained from the measurement data as well as from the simulations as follows,

$$P_\tau(t_k, \tau) = \frac{1}{N_{avg}} \sum_{n=0}^{N_{avg}-1} |h(t_k + n\Delta t, \tau)|^2, \qquad (3)$$

for $t_k = 0, N_{avg}\Delta t, ..., \lfloor N_t/N_{avg} - 1 \rfloor N_{avg}\Delta t$, where the $P_\tau(t_k, \tau) \in \mathbb{R}^{M_R \times M_T}$ is averaged over a window of N_{avg} time snap-shots such that $N_{avg}\Delta t = 57$ ms corresponding to TX/RX movement of a distance of about 10 wavelengths at

a speed of approximately 10 m/s. Furthermore, the processing includes noise reduction of the measurement data as described in [13].

The resulting APDP of the measurements and the simulations are depicted in Fig. 4(a) and 4(c) for $M1$ and in Fig. 4(b) and 4(d) for $M2$. At first sight, we find a good agreement when comparing the simulated APDP against the measurement data. Several MPC can be identified in both figures. However, there are individual discrete scatterers as well as diffuse scatterers that can be found in the measured APDP but not in the simulated one and vice versa. In the following, the observed differences will be discussed in more detail.

In the very first few seconds the TX and RX were far from the street intersection and the LOS between them was blocked by the buildings at the corners in both the scenarios, the LOS components (c) and (f) appear at approximately 6.8 s and 7.9 s in $M1$ and $M2$, respectively. The number of MPCs originating from discrete as well as diffuse scatterers in the measured APDP is much higher than in the simulated APDP because of the incomplete building data. In the simulations, the faces of each building are assumed to be plane surfaces with a single reflection coefficient, and the effects of doors, windows and balconies have not been taken in to account. Moreover, in the simulations MPCs with first and second order reflections from the static objects are considered only. In urban environments reflections of much higher order up to 12 was shown in [17], exist. However, the reflections with order higher than two in LOS and four in NLOS do not have significant contribution to the received power at 5.9 GHz frequency as shown in [9].

The group of arrows (d) and (g) in Fig. 4 point at several specular and non-specular MPCs that possibly originate from nearby buildings and are captured in measurements as well as in simulations. There are power contributions (e) and (h) originating from the same building which has a metallic sheet on its walls but it does not act as perfect metallic surface in reality. However, in the simulations that building is considered as a metallic object which results in a slightly higher power contribution in contrast to the measurements for that component. This example, and other similar cases points to the need for a very detailed description of the environment if one aims for an almost ideal match between measurements and simulations. But as seen, for the considered scenario, a reasonable match can be achieved with reasonable complexity using available building database.
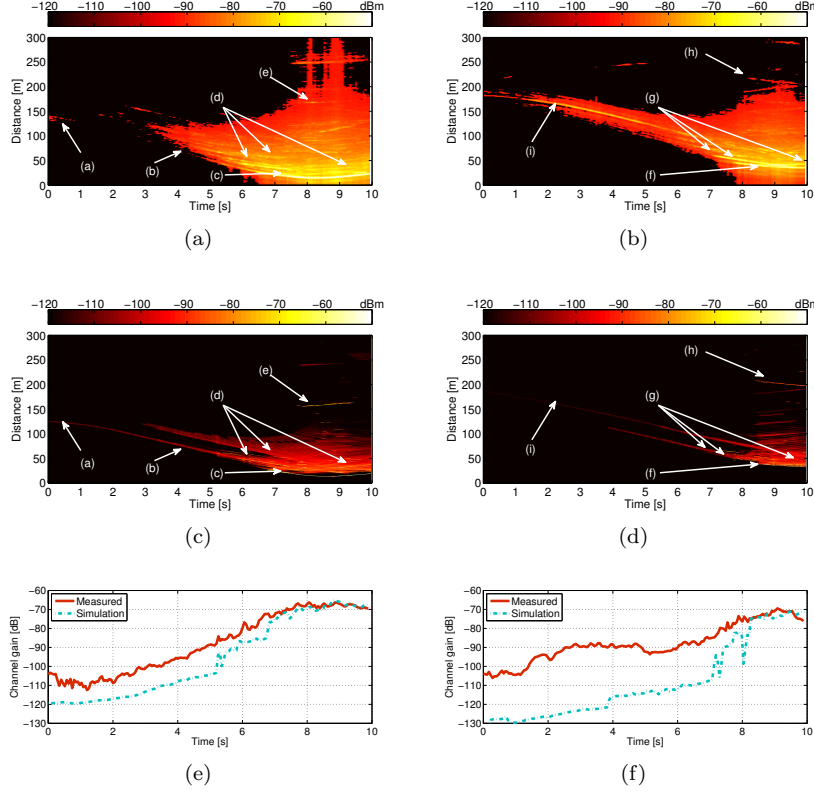
(a)

(b)

(c)

(d)

(e)

(f)

Figure 4: Averaged time-varying power delay profile obtained from the channel sounder data, the predicted CIRs using the ray-tracing channel model, and measured versus simulated channel gain from; $M1$ in (a), (c) and (e), and $M2$ in (b), (d) and (f), respectively. The first and second order reflections from the static objects are considered only.

5.2 Channel Gain

Based on the APDP, we calculate the time-variant channel gain, which includes the impact of the used antennas and the system loss, as

$$G(t_k) = \sum_{\tau} P_{\tau}(t_k, \tau). \tag{4}$$

However, for the measured channel gain the impact of noise has been removed by setting any component below the noise threshold plus $3\,\mathrm{dB}$ to zero in the APDPs. Similar noise thresholding has been performed when calculating the delay and Doppler spreads. The noise power is estimated from the regions where no signal is present in the APDPs. Figures 4(e) and 4(f) present the predicted channel gains obtained from ray-tracing simulations and measurement data for both scenarios. The simulated channel gains correspond to a plain scenario, where static objects like buildings, street signs and lamp posts are included, but all the parked and moving vehicles have been removed in order to reduce the simulation time. Note that we have also compared the simulation results of the full scenario including everything mentioned above with the plain scenario and have found only a marginal differences in the channel gain values.

In Fig. 4(e), a very good agreement is found between measurement and simulation results in the LOS region ($t \geq 6.8\,\mathrm{s}$) and in the transition region from NLOS to LOS ($6.8\,\mathrm{s} \geq t \geq 5.7\,\mathrm{s}$). In Fig. 4(f), a very good agreement is found between measurement and simulation results mainly in the LOS region ($t \geq 7.9\,\mathrm{s}$) and the region $1\,\mathrm{s}$ before the LOS. The most significant power contribution arises from the LOS component and the first order specular and non-specular reflections that are captured by the ray-tracer. There is a noticeable difference of about $8-10\,\mathrm{dB}$ during the NLOS periods ($t \leq 5.7\,\mathrm{s}$) and $6-40\,\mathrm{dB}$ during the NLOS periods $t \leq 7.9\,\mathrm{s}$) in Fig. 4(e) and Fig. 4(f), respectively.

As it is evident from the APDPs that in the NLOS situation the ray tracer underestimates the channel gain. We have found two reasonable explanations for this huge gap in NLOS situations of both scenarios: 1) The buildings in the four corners of the investigated intersections feature a lot of glass or metallic surfaces (e.g. windows and balcony elements) that yield strong power contributions at the receiver caused by specular and non-specular reflections. Especially, in scenario $M2$ we find a significant reflection (cf. arrow (i) in Fig. 4(b)) that is present even at the beginning of the scenario where both TX and RX are far away from the intersection. The same measurement was analyzed in [12], where the results were compared against a measurement based NLOS pathloss model. It was found that the NLOS model too was unable to capture such a strong reflection coming from metallic surface on the wall which is not typical for NLOS situations in urban intersections. Please note that a similar strong reflection can be identified in scenario $M1$ (cf. arrow (a) in Fig. 4(a)) which is blocked by earlier mentioned the left-turning bus for $0.5\,\mathrm{s} < t \leq 3\,\mathrm{s}$. The corresponding MPCs can also be found in the simulation-based PDPs (cf. arrows (b) and (i) in Fig. 4(c) and Fig. 4(d), respectively). However, the ray tracer treats the walls of the buildings as homogeneous and concrete surfaces which explains why the power contribution is too small in the simulations.

The inclusion of individual objects, like windows or balconies, with different material parameters need further implementation efforts, leading also to an increased computational complexity of the model but should of course also result in better accuracy.

The second reasonable explanation is: 2) The ray tracer does not capture the effects of higher-order non-specular reflections at all since these phenomena are not implemented in the mathematical model. Especially, the metallic and glass element on the buildings close to the intersection provide good conditions for multi-bounce interactions of the transmitted waves on the way to the receiver. This fact leads to an additional mismatch between measurement and simulation for the investigated intersection.

The results are summarized by presenting the mean error

$$\mu = \mathrm{E}\{\epsilon(t)\} \tag{5}$$

and the standard deviations

$$\sigma = \sqrt{\mathrm{E}\left\{|\mu - \epsilon(t)|^2\right\}} \tag{6}$$

between simulated and measured channel gains where the error ϵ is given by

$$\epsilon(t) = G_{meas}(t) - G_{sim}(t). \tag{7}$$

The values are given in Table 1 for both the measurements $M1$ and $M2$, separately for the LOS and NLOS.

5.3   Delay and Doppler Spreads

In a multipath propagation environment the signal spreads both in the delay and the Doppler domains. A number of delayed and scaled copies of the transmitted signal arrive at the receiver, and the effect of motion of the TX, RX or scatterers induce frequency and time selective fading that can be characterized by the root mean square (RMS) delay and Doppler spreads, respectively. These measures inversely proportional to the coherence bandwidth and coherence time of the channel, respectively [18]. The instantaneous RMS delay spread is the normalized second-order central moment of the time-variant PDP $P_\tau(t_k, \tau)$ and is defined as

$$S_\tau(t_k) = \sqrt{\frac{\sum_i P_\tau(t_k, \tau_i)\tau_i^2}{\sum_i P_\tau(t_k, \tau_i)} - \left(\frac{\sum_i P_\tau(t_k, \tau_i)\tau_i}{\sum_i P_\tau(t_k, \tau_i)}\right)^2}. \tag{8}$$

The measured and simulated RMS delay spreads are shown in Fig. 5(a) for $M1$ and in Fig. 5(b) for $M2$. The delay spread of the simulated data is mostly
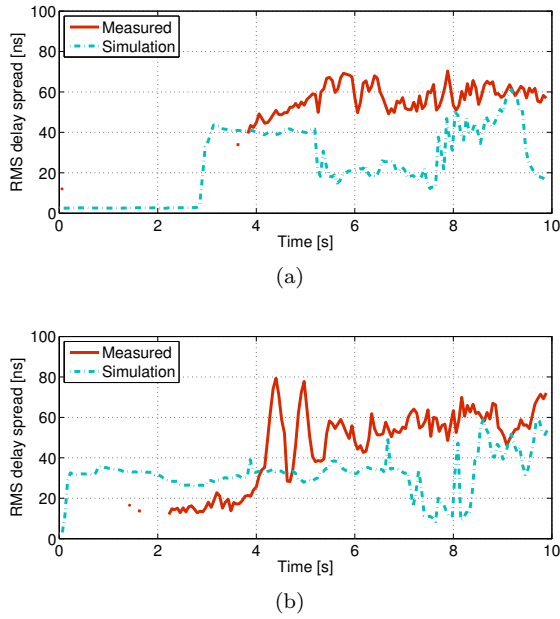
(a)

(b)

Figure 5: Measured versus simulated time-varying RMS delay spread
of: (a) $M1$, and (b) $M2$.

smaller than the delay spread of measured data because the number of specular
MPCs captured by the ray tracer are much smaller than of the measurements
due to the limited information about the scattering environment. In addition
to the aforementioned discrete MPCs that are missing, parts of the diffuse
scattering that can be observed in the measured PDP with large delays do
not appear in the simulations. The mean error and standard deviation are
obtained by (5) and (6), respectively, whereas $\epsilon(t)$ refers to the error between
the measured and simulated RMS delay spread as a function of time. The
values are summarized in Table 1. We find a reasonable agreement, with a
mean error of around 24 ns mean error in the LOS and approximately the
same in the NLOS situation for both $M1$ and $M2$. As a result, we notice the
capability of the deterministic channel model to provide reliable information
about the time-dispersive behavior of the urban channel, though with some
underestimation

Similarly, the instantaneous RMS Doppler spread is the normalized second-
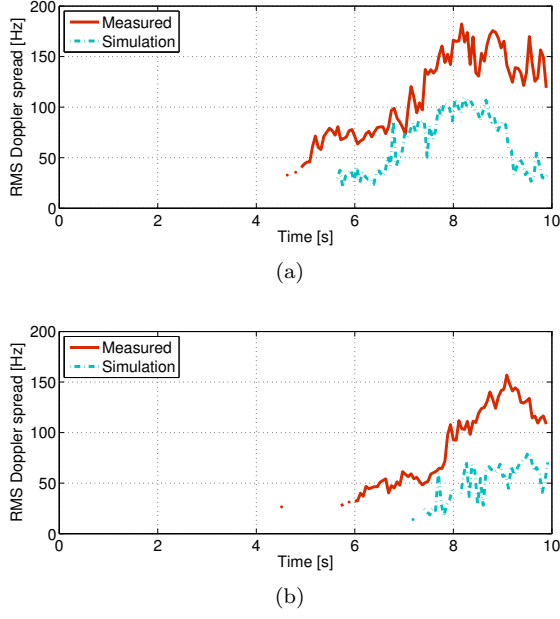order central moment of the time-variant Doppler spectral density (DSD). The

(a)

(b)

Figure 6: Measured versus simulated time-varying RMS Doppler spread of: (a) $M1$, and (b) $M2$.

DSD $P_\nu(t_k, \nu)$ is calculated analogous to PDP by taking the Fourier transform in the time domain over a sliding window of N_{avg} snapshots and averaged over the delay domain. The Doppler spread can be computed as

$$S_\nu(t_k) = \sqrt{\frac{\sum_i P_\nu(t_k, \nu_i)\nu_i^2}{\sum_i P_\nu(t_k, \nu_i)} - \left(\frac{\sum_i P_\nu(t_k, \nu_i)\nu_i}{\sum_i P_\nu(t_k, \nu_i)}\right)^2}. \qquad (9)$$

The measured and simulated RMS Doppler spreads are shown in Fig. 6(a) for $M1$ and in Fig. 6(b) for $M2$. The mean error and standard deviation are obtained by (5) and (6), respectively, whereas $\epsilon(t)$ here refers to the error between the measured and simulated RMS Doppler spread and are summarized in Table 1. As mentioned above, only static objects are considered in the simulations and the number of MPCs captured by the ray tracer is smaller than what can be identified from the measurements. Although the Doppler spread of the simulated data is smaller than that of the measured data, the ray tracing model is able to capture most of the significant MPCs. The higher

Doppler spread in the measured data is due to many incoming waves from all directions (angles) at the receiver, originating from scatterers such as moving and parked vehicles, details at the building walls, etc. The ray tracing model does not capture all of these details, in turn results in a smaller spread in the Doppler domain.

5.4   Antenna Diversity

Random fluctuations in the signal power due to multipath propagation caused by scattering impair the wireless channel across space, time or frequency. This is commonly known as channel fading. Diversity techniques are developed to combat fading by combining several independently faded version of the same transmitted signal at the receiver to improve link reliability by improving the signal-to-noise ratio (SNR). Thus, diversity is an important metric to be analyzed in order to validate the performance of ray-tracing channel simulations for MIMO V2V systems.

Among the diversity techniques, here spatial, or antenna, diversity is of particular interest in which multiple antennas at the TX and/or RX are used to exploit the diversity gain. In order to evaluate antenna diversity captured in the ray-tracing simulations we compare two metrics, the eigenvalue distribution and antenna correlation in the following.

Eigenvalue distribution and array gain

The eigenvalues (EVs) and their distributions obtained from ray-tracing simulations are compared against the ones obtained from the measurement data as they capture important properties of the array and the medium [19]. An SVD expansion of the normalized channel matrix $H \in \mathbb{C}^{M_R \times M_T}$ can be written as,

$$H = U \cdot S \cdot V^*, \tag{10}$$

where U is an $M_R \times M_R$ unitary matrix, S is a diagonal matrix of real non-negative singular values σ_m where $m = 1, 2, ..., \min\{M_R, M_T\}$, and V^* (the conjugate transpose of V) is an $M_T \times M_T$ unitary matrix. Singular values of H are the square roots of the eigenvalues of $H \cdot H^*$.

In Fig. 7(a) and 7(b), the time evolution of the eigenvalues, λ_m where $m = 1, 2, ..., \min\{M_R, M_T\}$, of the measured and simulated data are compared for both $M1$ and $M2$. The markers represent measured eigenvalues whereas the lines represent simulated eigenvalues. It is interesting to notice that the eigenvalues of the measured and simulated data are very similar. For the first $5\,\mathrm{s}$ in both $M1$ and $M2$ the eigenvalues look the same, but the scenario is NLOS and the available signal power is very weak. In such a situation the noise, which
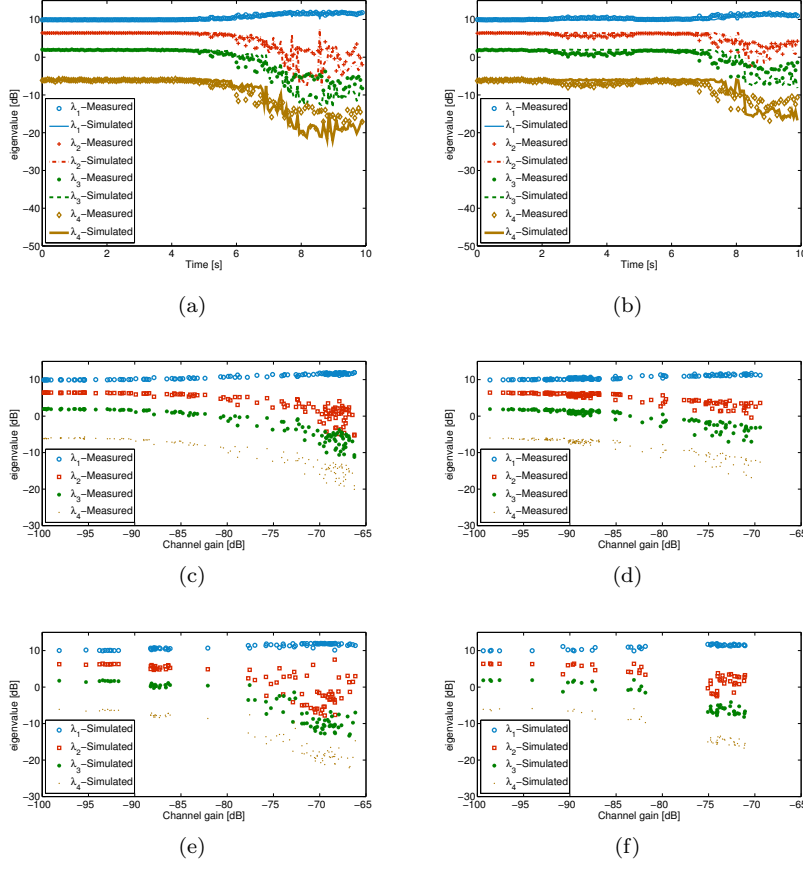
(a)   (b)

(c)   (d)

(e)   (f)

Figure 7: Measured versus simulated eigenvalues: Figs. 7(a), 7(c), and 7(e) represent $M1$ and Figs. 7(b), 7(d), and 7(f) represent $M2$.

is approximately i.i.d. Gaussian in both the measurements as well as in the simulations, is dominating. This in turn gives the same eigenvalues. However, in Fig. 7(b) the are some differences in the eigenvalues between $2 - 5\,$s because of the presence of the dominating MPC in the NLOS in $M2$ as discussed before.

In Fig. 7(c)-7(f) the eigenvalues are plotted as a function of channel gain. The eigenvalues are shown only for the samples where the channel gain is higher than $-100\,$dB, for the region in time where signal is dominating the noise. As

the ray tracing simulations do not extract all MPCs and thus provides lower
channel gain, we see some gaps in the plots where the eigenvalues correspond
to lower channel gain than in reality. The mean and standard deviation of the
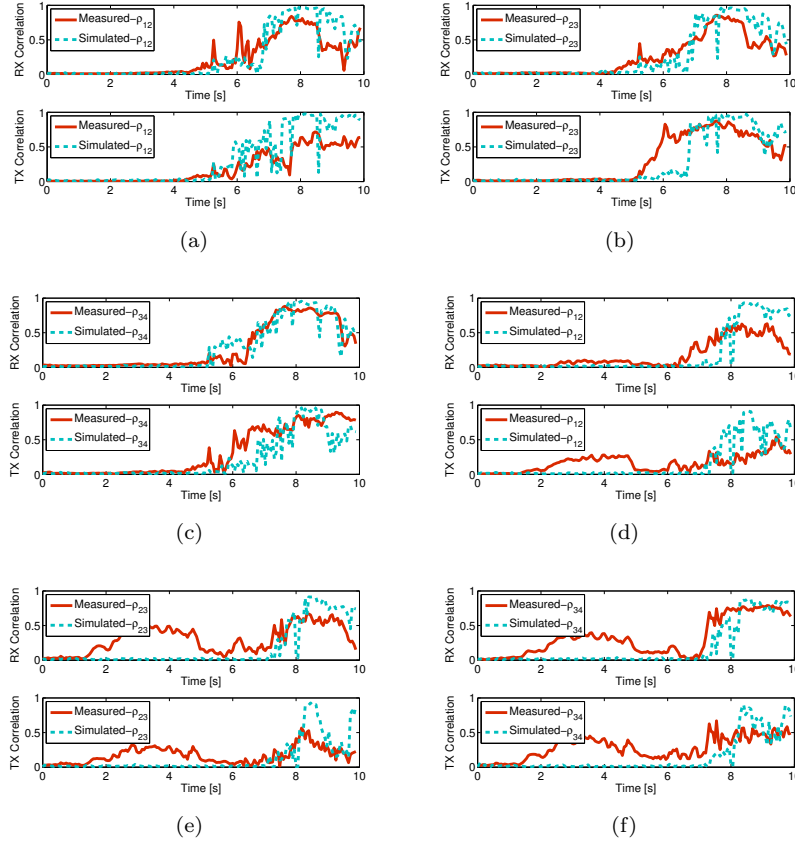error in the eigenvalues are listed in Table 1.

Figure 8: The correlation between the antenna elements $1-2$, $1-3$,
and $1-4$ is shown as a function of time. Figs. 8(a), 8(b), and 8(c)
represent $M1$ and Figs. 8(d), 8(e), and 8(f) represent $M2$.

Antenna correlations

Multiple antennas at the TX or at the RX can improve the system performance through diversity arrangements, but their benefits can only be fully utilized if the correlation between signals at different antenna elements is low [20]. Thus, antenna correlation for both the TX and the RX array is an important parameter to study. The time-variant antenna correlation $\rho_{ij}^{RX}(t_k)$ between the RX elements i and j is calculated as

$$\rho_{ij}^{RX}(t_k) = \sum_{n_t=1}^{N_{avg}} \sum_{n_f=1}^{N_f} \frac{\sum_{m=1}^{M_T} H_{i,m} H_{j,m}^*}{\sqrt{\sum_{m=1}^{M_T} |H_{i,m}|^2 \sum_{m=1}^{M_T} |H_{j,m}|^2}}. \tag{11}$$

Similarly, the correlation $\rho_{ij}^{TX}(t_k)$ between the TX elements i and j is calculated as,

$$\rho_{ij}^{TX}(t_k) = \sum_{n_t=1}^{N_{avg}} \sum_{n_f=1}^{N_f} \frac{\sum_{n=1}^{M_R} H_{n,i}^* H_{n,j}}{\sqrt{\sum_{n=1}^{M_R} |H_{n,i}|^2 \sum_{n=1}^{M_R} |H_{n,j}|^2}}, \tag{12}$$

where H is a block matrix for each time instant t_k such that $H \in \mathbb{C}^{N_{avg} \times N_f}$ and H^* is conjugate transpose of H.

In Fig. 8, the correlation between the antenna elements is shown as a function of time. The correlation between the elements is almost zero as the i.i.d. Gaussian noise dominates in that region, which result in zero correlation. In the absence of LOS, and it increases as the vehicle gets close to the intersection. The correlation between all elements is higher when there is LOS between the TX and RX in both $M1$ and $M2$. The antenna correlation coefficients for consecutive antenna elements $1-2$, $2-3$, and $3-4$ of both the RX and TX arrays for $M1$ are shown in Figs. 8(a), 8(b), and 8(c). The measured and simulated correlation coefficients are not exactly the same but show a similar trend over the time. Similarly, the antenna correlation coefficients for antenna elements $1-2$, $2-3$, and $3-4$ of both the RX and TX arrays for $M2$ are shown in Figs. 8(d), 8(e), and 8(f). For $M2$, again the correlation between $2-5\,$s is higher for measurement than that in simulations. However, in the presence of LOS the correlation of the TX and RX from the simulation and measurement show similar trend. The mean and standard deviation of the error in correlations is listed in Table 1.

Table 1: Mean μ and standard deviation σ of the error in the estimated parameters obtained from the simulated data with respect to measurement data for both $M1$ and $M2$.

Parameters	LOS		NLOS	
	M1	**M2**	**M1**	**M2**
	(μ_1, σ_1)	(μ_2, σ_1)	(μ_1', σ_1')	(μ_2', σ_1')
G_h [dB]	(0.87, 1.66)	(3.12, 5.43)	(11.2, 2.75)	(26.2, 6)
S_τ [ns]	(24.5, 13.5)	(23.2, 17.2)	(24, 17.5)	(9.3, 20)
S_ν [Hz]	(64.8, 28.9)	(62.7, 20.1)	(40.4, 10.2)	(34.4, 6.34)
λ_1 [dB]	(-0.07, 0.38)	(-0.07, 0.49)	(0.104, 0.19)	(0.28, 0.26)
λ_2 [dB]	(1.88, 4.26)	(0.92, 2.5)	(-0.21, 0.51)	(-0.49, 0.59)
λ_3 [dB]	(2.41, 3.36)	(1.55, 3.18)	(-0.37, 0.76)	(-0.69, 0.75)
λ_4 [dB]	(2.41, 3.1)	(1.08, 3.23)	(-0.52, 0.98)	(-0.77, 0.82)
ρ_{12}^{TX}	(-0.31, 0.23)	(-0.31, 0.24)	(-0.032, 0.11)	(0.1, 0.1)
ρ_{13}^{TX}	(-0.12, 0.3)	(-0.11, 0.33)	(0.07, 0.108)	(0.117, 0.12)
ρ_{14}^{TX}	(-0.12, 0.23)	(-0.14, 0.26)	(0.02, 0.106)	(0.17, 0.13)
ρ_{23}^{TX}	(-0.12, 0.17)	(-0.18, 0.27)	(0.1, 0.19)	(0.12, 0.1)
ρ_{24}^{TX}	(-0.13, 0.27)	(-0.14, 0.25)	(0.03, 0.12)	(0.17, 0.14)
ρ_{34}^{TX}	(0.11, 0.23)	(-0.07, 0.23)	(0.07, 0.14)	(0.21, 0.13)
ρ_{12}^{RX}	(-0.22, 0.21)	(-0.27, 0.27)	(0.043, 0.11)	(0.07, 0.09)
ρ_{13}^{RX}	(-0.20, 0.33)	(0.02, 0.2)	(-0.002, 0.104)	(0.04, 0.07)
ρ_{14}^{RX}	(-0.03, 0.19)	(0.026, 0.15)	(-0.007, 0.08)	(0.06, 0.09)
ρ_{23}^{RX}	(-0.18, 0.18)	(-0.17, 0.23)	(0.05, 0.09)	(0.21, 0.16)
ρ_{24}^{RX}	(0.008, 0.33)	(-0.21, 0.33)	(0.02, 0.09)	(0.16, 0.15)
ρ_{34}^{RX}	(-0.01, 0.16)	(0.03, 0.21)	(-0.01, 0.103)	(0.17, 0.14)

6   Conclusion

The characterization of an urban intersection for V2V channel is non-trivial, as many details of the environment may have a huge impact on the experienced radio channel. This includes material, position and alignment of buildings, street width, location and density of road side objects etc. An accurate modeling is required for safety-critical system design, which in turn requires a full understanding of these physical effects. Deterministic models such as those achieved with a ray tracer are anticipated to be good candidates to model such complex scenarios.

In this paper, we have presented an accuracy analysis of ray tracing based simulation of V2V channels in an urban intersection scenario with the help of real channel measurements. We have compared important channel metrics, namely channel gain, delay and Doppler spreads, eigenvalue decomposition and antenna correlations, that are obtained from both channel sounder measurements and simulation results using a ray-optical channel model. We have found a good accuracy of the simulation results in the sense that the present physical phenomena of wave propagation are captured by the ray tracer. Variations between measurements and simulations are consistent and can be explained with the microscopic features of the investigated scenario. We have identified limitations of the ray tracing model in terms of higher-order non-specular reflections that are currently not included in the model. By analyzing the aforementioned metrics, both tools are analyzed on their accuracy and possible flaws of the underlying channel models are identified. Based on the results obtained from this analysis the end goal is develop a channel model for the intersection scenario that can easily be integrated in network simulators and provide better approximation of a deterministic channel model for V2X communications in street intersection.

Acknowledgment

References

[1] A. F. Molisch, F. Tufvesson, J. Karedal, and C. F. Mecklenbräuker, "A survey on vehicle-to-vehicle propagation channels," in *IEEE Wireless Commun. Mag.*, vol. 16, no. 6, 2009, pp. 12–22.

[2] R. Santos, A. Edwards, and V. Rangel-Licea, *Wireless Technologies in Vehicular Ad Hoc Networks: Present and Future Challenges.* Hershey, PA: IGI Global (701 E. Chocolate Avenue, Hershey, Pennsylvania, 17033, USA), 2012.

[3] I. Sen and D. W. Matolak, "Vehicle-vehicle channel models for the 5 GHz band," *IEEE Trans. Intell. Transp. Syst.*, vol. 9, no. 2, pp. 235–245, Jun. 2008.

[4] A. Paier, L. Bernado, J. Karedal, O. Klemp, and A. Kwoczek, "Overview of vehicle-to-vehicle radio channel measurements for collision avoidance applications," in *Vehicular Technology Conference (VTC 2010-Spring), IEEE 71st, Taipei, Taiwan*, May 2010, pp. 1–5.

[5] J. Nuckelt, M. Schack, and T. Kürner, "Deterministic and stochastic channel models implemented in a physical layer simulator for Car-to-X communications," *Advances in Radio Science*, vol. 9, pp. 165–171, Sept. 2011.

[6] T. Mangel, O. Klemp, and H. Hartenstein, "5.9 GHz inter-vehicle communication at intersections: a validated non-line-of-sight path-loss and fading model," *EURASIP Journal on Wireless Communications and Networking*, vol. 2011, no. 1, p. 182, 2011.

[7] J. Maurer, T. Fugen, T. Schafer, and W. Wiesbeck, "A new inter-vehicle communications (ivc) channel model," in *Vehicular Technology Conference, 2004. VTC2004-Fall. 2004 IEEE 60th*, vol. 1, 2004, pp. 9–13 Vol. 1.

[8] C. Sommer, D. Eckhoff, R. German, and F. Dressler, "A computationally inexpensive empirical model of IEEE 802.11p radio shadowing in urban environments," in *Wireless On-Demand Network Systems and Services (WONS), 2011 Eighth International Conference on*, 2011, pp. 84–90.

[9] J. Nuckelt, T. Abbas, F. Tufvesson, C. F. Mecklenbräuker, L. Bernado, and T. Kürner, "Comparison of ray tracing and channel-sounder measurements for vehicular communications," in *2013 IEEE 77th Vehicular Technology Conference: VTC2013-Spring, Dresden, Germany*, June 2013, pp. 1–5.

[10] Google   earth   v7.1.1.1888   (2013).   [Online].   Available:
     http://www.google.com/earth/index.html [Accessed: 2013/08/15]

[11] M. Schack, J. Nuckelt, R. Geise, L. Thiele, and T. Kürner, "Comparison of
     path loss measurements and predictions at urban crossroads for C2C com-
     munications," in *5th European Conference on Antennas and Propagation
     (EuCAP), Rome, Italy*, April 2011.

[12] T. Abbas, A. Thiel, T. Zemen, C. F. Mecklenbräuker, and F. Tufvesson,
     "Validation of a non-line-of-sight path-loss model for V2V communications
     at street intersections," in *13th International Conference on ITS Telecom-
     munications, Tampere, Finland*.   IEEE, November 2013.

[13] J. Karedal, F. Tufvesson, T. Abbas, O. Klemp, A. Paier, L. Bernadó,
     and A. F. Molisch, "Radio channel measurements at street intersections
     for vehicle-to-vehicle safety applications," in *IEEE VTC 71st Vehicular
     Technology Conference (VTC 2010-spring), Taipei, Taiwan*, May 2010,
     pp. 1–5.

[14] A. Thiel, O. Klemp, A. Paier, L. Bernadó, J. Karedal, and A. Kwoczek,
     "In-situ vehicular antenna integration and design aspects for vehicle-to-
     vehicle communications," in *Antennas and Propagation (EuCAP), 2010
     Proceedings of the Fourth European Conference on, Barcelona, Spain*, Apr.
     2010, pp. 1–5.

[15] M. Schack, "Integrated simulation of communication applications in ve-
     hicular environments," Ph.D. dissertation, Technische Universität Braun-
     schweig, 2013.

[16] J. Nuckelt, D. Rose, T. Jansen, and T. Kurner, "On the use of open-
     streetmap data for v2x channel modeling in urban scenarios," in *Antennas
     and Propagation (EuCAP), 2013 7th European Conference on*, 2013, pp.
     3984–3988.

[17] Z. Li, R. Wang, and A. Molisch, "Shadowing in urban environments with
     microcellular or peer-to-peer links," in *Antennas and Propagation (EU-
     CAP), 2012 6th European Conference on*, 2012, pp. 44–48.

[18] A. Molisch and M. Steinbauer, "Condensed parameters for characteriz-
     ing wideband mobile radio channels," *International Journal of Wireless
     Information Networks*, vol. 6, no. 3, pp. 133–154, 1999.

[19] R. Vaughan and J. B. Andersen, *Channels, Propagation and Antennas for
     Mobile Communications (IEE Electromagnetic Waves Series, 50)*.   Insti-
     tution of Engineering and Technology, Feb. 2003.

[20] A. Molisch, *Wireless Communications.*   Chichester, West Sussex, UK:
     IEEE Press-Wiley, 2005.

Paper IV

Validation of a Non-Line-of-Sight Path-Loss Model for V2V Communications at Street Intersections

In this paper a non-line-of-sight (NLOS) path-loss and fading model developed for vehicle-to-vehicle (V2V) communication at 5.9 GHz is validated with independent and realistic measurement data. The reference NLOS model is claimed to be flexible and of low complexity, and incorporates specific geometric aspects in a closed-form expression. We validated the accuracy of the model with the help of realistic channel measurements performed in selected street intersections in the city of Lund and Malmö, Sweden. The model fits well, with a few exceptions, to the measurements. Those are in turn made in different intersections having variable geometries and scattering environments. It is found that the model can be made more general if an intersection dependent parameter, that depends on the property and number of available scatterers in that particular intersection, is included in the model.

1 Introduction

Intelligent transportation systems (ITS) have gained considerable attention in recent years, because they have the potential to enhance location awareness and safety of vehicles. Safety-related applications, e.g., cross-traffic assistance and traffic condition warnings, will help to reduce the rate of accidents. The idea is to utilize vehicle-to-vehicle (V2V) and vehicle-to-infrastructure (V2I) communications for such applications.

A lot of research efforts and field trails focusing on V2V safety applications have been done and are still ongoing both in academia and the vehicular industry. There are a number of challenges and use cases that are not yet completely understood and require further investigation. Among those, cross-traffic assistance in urban street intersections is one of the most critical use cases as visual line-of-sight (LOS) is often blocked by buildings at the corners of the streets. When the LOS is not available then scattering, i.e., reflection, diffraction and refraction, of radio waves can enable signal reception.

There exist a number of V2V measurement and ray-tracing simulation based studies to characterize the radio channel in urban street intersections [1–6]. In these studies it was found that the geometry of the street intersections, i.e., street width and alignment, structure of buildings, and antenna height have great impact on the NLOS reception in an urban intersection at 5.9 GHz frequency. Moreover, it is found that V2V ray-tracing simulation models often underestimate channel parameters like, e.g., delay spread and Doppler spread, for certain streets due to limited geographical information. Thus, a generalized and well validated NLOS model is needed for urban intersections.

Based on an extensive channel measurement campaign Mangel *et al.* in [7] have developed a flexible and generalized NLOS path-loss model named *VirtualSource11p* at 5.9 GHz. The channel measurements were performed in many different street intersections in the city of Munich, Germany, which were selected carefully such that they may represent a majority of urban street intersections. However, it is anticipated that the given *VirtualSource11p* NLOS path-loss model can be limited in its validity to the intersections where the measurements were conducted. Thus, it would be interesting to validate the model using an independent measurement data set and study the generalizability of the model.

In this paper, we validate the afore-mentioned NLOS path-loss model using independent and realistic channel measurement data recorded in a measurement campaign called DRIVEWAY [8]. To the author's best knowledge there has been no such validation studies of the NLOS path-loss model and large-scale fading of [7] using independent measurement data.

The DRIVEWAY measurements were conducted in various traffic situations

that are of particular interest for safety-related ITS applications. All test sites
are located in and around the cities of Lund and Malmö in southern Sweden.
The aim of our measurements was to understand and model the properties
of V2V radio channels with a realistic measurement setup in realistic traffic
conditions. However, in this paper, the measurement data recorded only at
urban street intersections is used for the analysis.

The rest of the paper is organized as follows; section 2 summarizes the
DRIVEWAY V2V measurement campaign where the measurement setup, sce-
narios description and measurement data evaluation are discussed. Section 3
explains very briefly the *VirtualSource11p* NLOS path-loss model followed by
Section 4 in which the model is validated using measurement data. Finally,
section 5 summarizes the whole discussion and concludes the paper.

2   V2V Measurement Campaign

The measurements were performed using standard hatch-back style cars with
roof mounted four-element antenna arrays, specifically designed for V2V com-
munication [10]. During the measurements the channel transfer function
$H(f,t)$ was recorded using the RUSK Lund channel sounder that performs
switched-array MIMO measurements [11]. Each transmitter (TX) and receiver
(RX) vehicle logged their GPS coordinates, and videos were taken through
the windshield of the TX/RX cars. In the post-processing these data were
also used in combination with the measurement data. The most important
measurement parameters are listed in Table 1.

2.1   Scenarios

During the DRIVEWAY measurement campaign several measurements were
recorded in many different propagation environments. The selected measure-
ment scenarios are of particular interest for many safety related intelligent
transport systems (ITS) applications [8]. In this paper we are mainly inter-
ested in NLOS propagation, especially in the intersection scenario. The refer-
ence NLOS path-loss model takes into account the inter-building distance, i.e.,
the street widths w_t and w_r, on the transmitter as well as on the receiver side,
distance of the TX and RX from the intersection center and TX position on
the street relative to side walls. To be able to analyze the effect of these varia-
tions, we have selected 9 measurements (2 suburban and 7 urban) recorded in
the four different street intersections of variable street widths and propagation
condition, shown in Fig. 1. The speed of the TX and RX cars were varying
between $7-11\,\mathrm{m/s}$ $(25-40\,\mathrm{km/h})$, depending on the street intersection and

Table 1: Measurement parameters configuration

| Parameter	Value
Center frequency [GHz], f_c	5.6
Measurement bandwidth [MHz], BW	240
Test signal length [μs], τ_{max}	3.2
Snapshot repetition time [μs], t_{rep}	307.2
Number of snapshots in time, N_t	32500 or 65000
Number of samples in frequency, N_f	769
Recording time [s], t_{rec}	10 or 20
Number of TX antenna elements	4
Number of RX antenna elements	4
TX/RX antenna height [m]	1.73
Average TX plus RX antenna gain [dB]	6.7
Approximate system loss [dB]	4

yield signs.

Intersection-1: (N 55°42′26″, E 13°9′39″) can be described as suburban in which the buildings are situated to the left, to the right is an open surrounding with some vegetation and a power line. In both measurements the TX and RX vehicles are approaching the intersection, in 18 m and 20 m wide orthogonal streets, from south-to-north and from west-to-east, respectively (see Fig. 1(a)).

Intersection-2: (N 55°35′56″, E 13°0′30″) can be described as urban with wider geometry where multi-story buildings are situated at each corner of the intersection. In the measurement the TX and RX vehicles are approaching the intersection, in 43 m and 23 m wide orthogonal streets, from southwest-to-northeast and from northwest-to-southeast, respectively (see Fig. 1(b))

Intersection-3: (N 55°42′37″, E 13°11′15″) can be described as urban with relatively narrow geometry where $3 - 4$ story buildings are situated at each corner of the intersection. In both measurements the TX and RX vehicles are approaching the intersection, in 20 m and 24 m wide streets, from west-to-east and from south-to-north, respectively. Streets are not perfectly orthogonal. (see Fig. 1(c)).

Intersection-4: (N 55°42′37″, E 13°11′15″) is the same as intersection-3. The only difference is that the TX and RX vehicles are approaching the intersection, in 24 m and 23 m wide, from north-to-south and east-to-west, respectively. (see Fig. 1(d)).
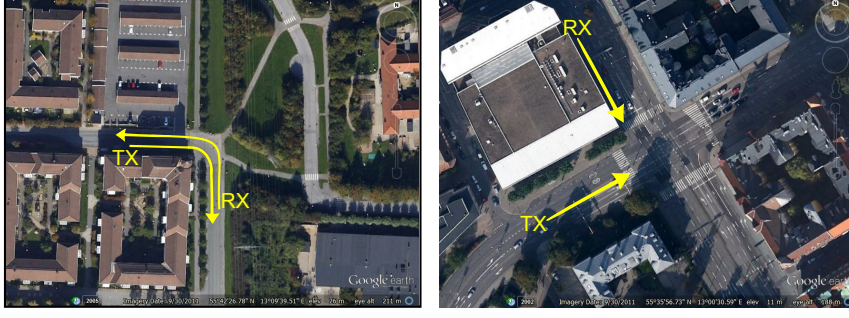
(a) Intersection-1 (N 55°42′26", E 13°9′39")

(b) Intersection-2 (N 55°35′56″, E 13°0′30″)
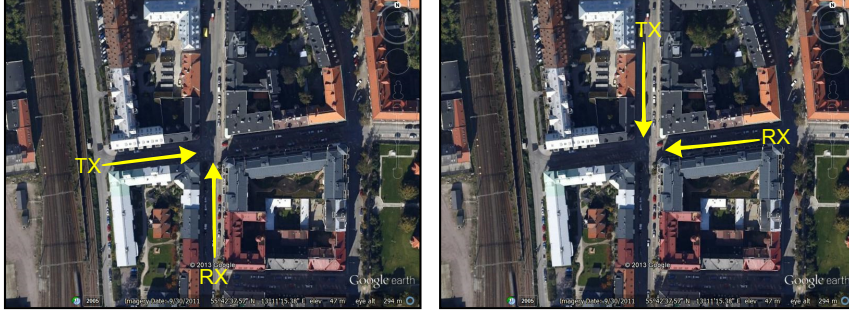
(c) Intersection-3 (N 55°42′37″, E 13°11′15″)

(d) Intersection-4 (N 55°42′37″, E 13°11′15″)

Figure 1: Google Earth$^{\text{TM}}$ [9] aerial image of the four measured street intersections in Lund and Malmö. In each intersection the TX and RX vehicles were approaching the intersection center while driving along the yellow lines. All the images have same map scale.

2.2 Data Evaluation and Results

To analyze the measurement data we first derive the instantaneous time-varying power-delay-profile (PDP) of each measurement using the channel transfer functions at each time instant. These PDPs are averaged over the time samples that correspond to a movement of 10 wavelengths in order to remove the effect of small scale fading (for details see [1]). The temporal variations, impact of scatters as a function of propagation distance, the LOS component and other specular/non-specular components can be visualized in the averaged-PDP

(APDP) plots. APDPs of two selected measurements taken at the intersection-1 and intersection-2 are shown in Figs. 2(a) and 2(b). From the APDP plot it is evident that the scattering environment is very different in both intersection-1 and 2. Intersection-2 has many MPCs including a couple of strong MPCs, due to wider streets and presence of buildings at the corners. Whereas in intersection-1 an open surrounding to one side result in fewer MPCs with less received power in the NLOS. This difference in the received power due to the geometry of the intersections can be best appreciated by looking at Fig. 2(c), in which the received power is plotted as a function of combined distance from TX to RX via the intersection center (d_{dc}). The negative and positive d_{dc} indicate that the TX and RX vehicles are approaching and leaving the intersection center, respectively. The effect of the antenna gain and cable losses have been removed from the measured channel gains. Moreover, the transmit power (P_{TX}) of $23\,$dBm is used that is added in the measured channel gain in order to calculate the received power (P_{RX}).

To observe the overall difference in the received power due to the variable geometry and the scattering environment the received powers of the measurements at each intersection are presented together in Fig. 3. As a first observation, it can be seen that the smallest power is received at the Intersection-1 which is logical as it has an open surrounding and fewer scatterers available that can aid NLOS reception.

Moreover, Intersection-2 (wider), 3 and 4 (narrow) have $3-4$ story buildings at each corner of the intersection with more or less similar traffic conditions, which means similar scattering environments. Ideally, the received power in a wide intersection should be higher than that in a narrow intersection given that the scattering environment is similar. However, this is not always the case, the received power in a narrow intersection can be higher than that in a wide intersection if the scattering environment in the narrow intersection is rich. This can be seen in Fig. 3 where Intersection-2, which is wider, has lower received power than Intersection-4. After a detailed investigation of the measurement results and having a close look at the geography of the intersections it is found that there are a couple of very strong reflected MPCs in Intersection-4 unlike in Intersection-2. These strong reflections arise from the metallic window structures of a building at one corner of the intersection and give rise to the received power. Such an unexpected behavior in the power depends not only on the number of scatterers but on their material properties and geographic location. If we wish a model to be universal or most generalized then it should be able to reflect such unexpected behavior. In the subsequent analysis we would like to find out how well the NLOS path-loss model fits our measurement data and possible underlying limitations.

It is specified in the IEEE 802.11p standard [12] that a $10\,$MHz frequency

(a) APDP of Intersection-1

(b) APDP of Intersection-2
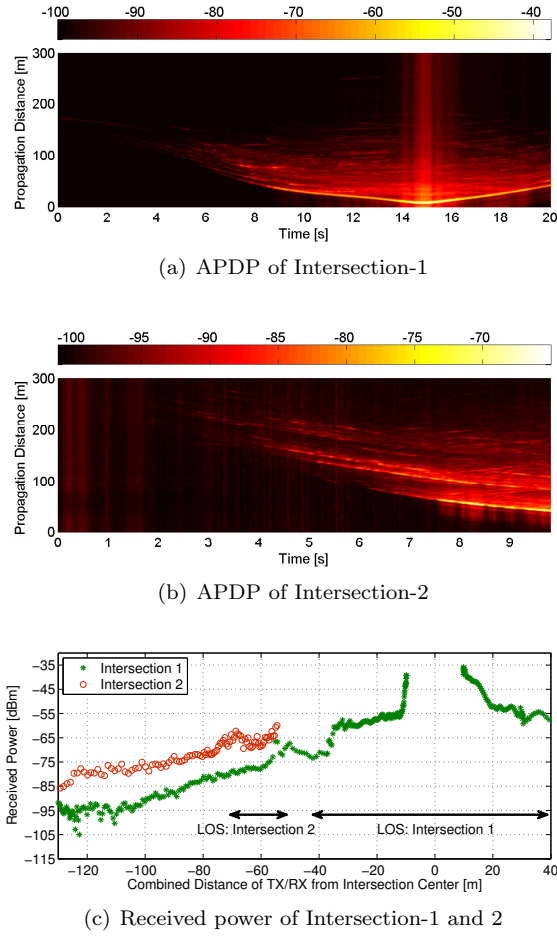

(c) Received power of Intersection-1 and 2

Figure 2: APDP of the 2 selected measurements at Intersection-1 in (a) and 2 in (b). The color bar indicates the received power in dBm. Received power as a function of combined distance of TX/RX from the intersection center (d_{dc}) for both measurements is shown in (c).

bandwidth will be used at $5.9\,$GHz for V2V communication systems but the DRIVEWAY channel measurements were performed over a $240\,$MHz bandwidth. For the measurements this larger bandwidth was selected to get a fine
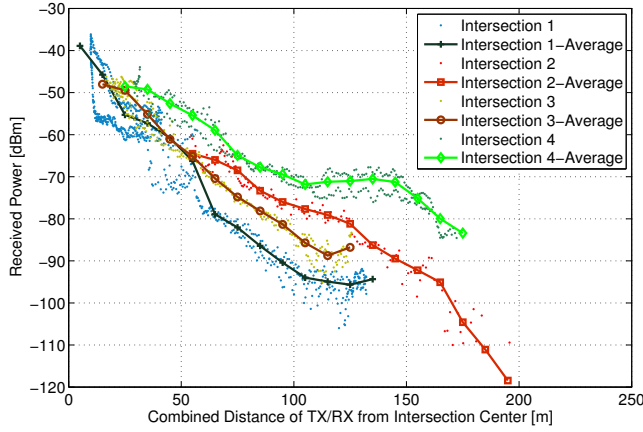
Figure 3: Received power as function of d_{dc} and curves showing their
mean power averaged over every 10 meters for all four intersection in-
tersection.

resolution in delay and to get better statistics of the channel, which is impor-
tant for a detailed understanding. In the analysis of the measurement data, no
difference in the received power is found when considering the total 240 MHz
of measured bandwidth or selected portions of 10 MHz measured bandwidth.

3   Reference NLOS path-loss model

Before the comparison it is important to explain briefly the reference NLOS
path-loss model. Mangel *et. al.* in [7] has performed an extensive measurement
campaign and presented a realistic and a well validated NLOS path-loss model
at 5.9 GHz frequency named *VirtualSource11p*. The model is considered to
be of low complexity, thus, enabling large-scale packet level simulations in
intersection scenarios. The *VirtualSource11p* model is obtained from a NLOS
path-loss model proposed in [13] for cellular communications, which is slightly
modified to correspond well to V2V measurements. The derivation of the
VirtualSource11p model can be found in [7] where the corresponding NLOS
path-loss equation to calculate the received power at a certain distance is given
as follows,

$$PL(d_r, d_t, w_r, x_t, i_s) = C + i_s L_{SU}$$

$$
+ \begin{cases} 10 \log_{10} \left(\left(\frac{d_t^{E_T}}{(x_t w_r)^{E_S}} \frac{4\pi d_r}{\lambda} \right)^{E_L} \right), & \text{if } d_r \leq d_b \\ 10 \log_{10} \left(\left(\frac{d_t^{E_T}}{(x_t w_r)^{E_S}} \frac{4\pi d_r^2}{\lambda d_b} \right)^{E_L} \right), & \text{if } d_r > d_b \end{cases} \tag{1}
$$

where d_t/d_r denotes the distance of the TX/RX to the intersection center, w_r is width of the RX street, and x_t is the distance of the TX to the wall, respectively.

As the NLOS path-loss at a certain distance can be calculated by the model, the NLOS received power $P_{RX}(d)$ for a certain $P_{TX}(d)$ can be calculated using the following expression,

$$
P_{RX}(d) = P_{TX}(d) - S_{Loss} + G_a - PL(d_r, d_t, w_r, x_t, i_s) \tag{2}
$$

where S_{Loss} and G_a are the system loss and the combined TX/RX antenna gain, respectively. For the comparison both of these parameters are assumed to be zero as the effect of averaged antenna gain and cable losses have been removed from the measured channel gains before calculating the received powers. The NLOS model parameters and their values are listed in Table 2.

Table 2: NLOS path-loss model parameters

| Parameters	Values
Curve shift, C (dB)	3.75
Sub-urban loss, L_{SU} (dB)	2.94
Urban loss factor, i_s	0
Sub-urban loss factor, i_s	1
Loss exponent, E_L	2.69
Small-scale fading, σ (dB)	4.1
Street exponent, E_S	0.81
TX distance exponent, E_T	0.957
Break even distance, d_b (m)	180

4   Validation of the NLOS model

In this section, the NLOS path-loss model is compared to the channel measurements data. It is desired to investigate whether the overall behavior of the received power in NLOS, both for the model and measurements, changes in accordance to the geometry of the respective intersection.
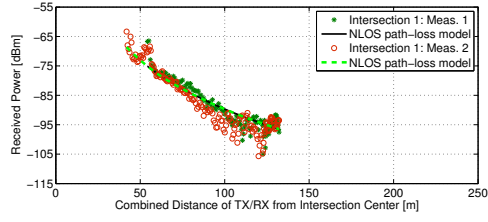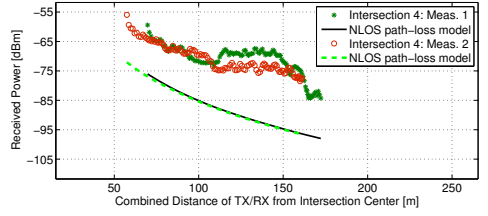
(a) Intersection-1
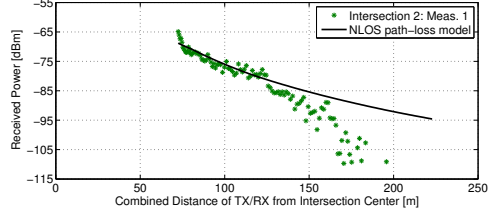
(b) Intersection-2
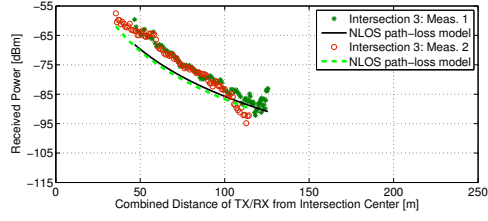
(c) Intersection-3

(d) Intersection-4

Figure 4: Received power $P_{RX}(d)$ as a function of combined distance of TX/RX from the intersection center (d_{dc}) for Intersection-1 to Intersection-4: measurement and model.

The NLOS $P_{RX}(d)$, obtained from the measurements and model, as a function of d_{dc} for Intersections-1 to 4 are presented in Fig. 4(a) to 4(d). The $P_{RX}(d)$ from the model is calculated by using the measured distances. Thus, the powers from each measurement and their respective powers from the model are plotted together to find out the difference.

From Figs. 4(a), 4(b) and 4(c), it can be seen that the measurement data fit very well to the NLOS model for Intersection-1, 2 and 3. However, in Intersection-2, the difference in the model and measurement starts to grow for $d_{dc} > 130$ m. The reason behind this is the curved TX street. The TX street start to bend at an approximate distance of 60 m from the intersection center (see Fig. 1(b)). Due to that many significant MPCs, which are visible at $d_{dc} < 130$ m, and start to disappear gradually for $d_{dc} > 130$, which in turn continuously reduce the total P_{RX}. On the other hand, the model assumes the intersecting streets to be straight and perpendicular to each other, thus we do not see such power degradation in the model curve in Fig. 4(b) and that is one of the limitations in the model, urban streets are not always straight and perpendicular.

Another, interesting difference can be found in Fig. 4(d), where the difference in the measurement data and the model is quite large. After taking a closer look at the intersection and doing some visual inspection with the help of video recordings it is found that there are metallic window structures at the corner of the buildings that are situated at the corner of the street intersection right in front of the TX and RX. The strength of the reflected MPCs from these metallic window frames is very large, giving an unexpected rise to the received power. From the Fig. 4(d) we can see that the NLOS model is unable to capture this unusual behavior in the received power which is due to the material properties and the placement of scatterers. Although Mangel *et. al.* in [7] tried to select most representative street intersection in the city of Munich but still they may not be representative enough for many other cities. This causes another limitation in the model that the NLOS model cannot capture unusual behaviors due to the variety in the scattering environment of street intersections.

From this validation study it is found that it could be beneficial to add another intersection dependent gain parameter (G_{ID}) in the model of (6) to compensate for the loss or gain in the power due to variations in the scattering as follows,

$$PL(d_r, d_t, w_r, x_t, i_s) = C + i_s L_{SU} + G_{ID}$$

$$+ \begin{cases} 10 \log_{10}\left(\left(\dfrac{d_t^{E_T}}{(x_t w_r)^{E_S}} \dfrac{4\pi d_r}{\lambda}\right)^{E_L}\right), & \text{if } d_r \leq d_b \\[3ex] 10 \log_{10}\left(\left(\dfrac{d_t^{E_T}}{(x_t w_r)^{E_S}} \dfrac{4\pi d_r^2}{\lambda d_b}\right)^{E_L}\right), & \text{if } d_r > d_b \end{cases} \tag{3}$$

To find the correct values of such a parameter, available measurement data is not sufficient thus it is left for future investigations. After this investigation a need of new and larger amount of measurement data is felt to find a better and more generalized model for urban intersections.

In the comparison plots in Fig. 4(a) to 4(d) measured P_{RX} data points deviated slightly from the model curves, which is due to the large-scale fading. Whereas the model curves are showing a distance dependent mean path-loss only, without effect of any fading. As mentioned earlier in the APDP derivation, the effect of small-scale fading has been removed by averaging the APDP but the effect of large-scale fading is not removed and thus the measured P_{RX} data points fluctuate around a distance dependent path-loss curves. Therefore, variations in the large scale fading for all intersections with respect to the model are investigated. The large-scale fading for each intersection is approximated as log-normal and the standard deviation (σ) of zero mean Gaussian distributed large-scale fading is parameterized in Table 3.

Table 3: Large-scale fading parameter

Large-scale fading	σ
Intersection-1 (dB)	6.26
Intersection-2 (dB)	5.5
Intersection-3 (dB)	4.16
Intersection-4 (dB)	3.2

5 Summary and Conclusions

We present a validation of the NLOS path-loss model named *VirtualSource11p* developed for vehicle-to-vehicle communications at 5.9 GHz. A large amount of measurement data collected at selected intersections in the city of Munich Germany is used to develop the model. In this paper the model is validated with the help of an independent measurement data set, recorded during the DRIVEWAY measurement campaign in the city of Lund and Malmö in southern Sweden. It is intended to test the model for its accuracy and flexibility. It is found that the model is very flexible and fits well to most of our measurements

in different intersections. However, there are some cases in which the model does not fit well to the measurements due to rich scattering in some intersections. The results in this study suggest to introduce an intersection dependent gain parameter in the reference NLOS such that it can cope with the varying richness of scattering.

References

[1] J. Karedal, F. Tufvesson, T. Abbas, O. Klemp, A. Paier, L. Bernadó, and A. F. Molisch, "Radio channel measurements at street intersections for vehicle-to-vehicle safety applications," in *IEEE VTC 71st Vehicular Technology Conference (VTC 2010-spring)*, May 2010.

[2] T. Mangel, M. Michl, O. Klemp, and H. Hartenstein, "Real-world measurements of non-line-of-sight reception quality for 5.9 GHz IEEE 802.11p at intersections," *Communication Technologies for Vehicles, Springer Berlin Heidelberg*, vol. 6596, pp. 189–202, 2011.

[3] M. Schack, J. Nuckelt, R. Geise, L. Thiele, and T. Kürner, "Comparison of path loss measurements and predictions at urban crossroads for C2C communications," in *5th European Conference on Antennas and Propagation (EuCAP)*, April 2011.

[4] T. Abbas, F. Tufvesson, and J. Karedal, "Measurement based shadow fading model for vehicle-to-vehicle network simulations," *ArXiv e-prints*, Mar. 2012.

[5] J. Nuckelt, T. Abbas, F. Tufvesson, C. F. Mecklenbräuker, L. Bernado, and T. Kürner, "Comparison of ray tracing and channel-sounder measurements for vehicular communications," in *2013 IEEE 77th Vehicular Technology Conference: VTC2013-Spring, 2013-06-2.* IEEE, 2013.

[6] T. Abbas, J. Kredal, and F. Tufvesson, "Measurement-Based Analysis: The Effect of Complementary Antennas and Diversity on Vehicle-to-Vehicle Communication," *IEEE Antennas and Wireless Propagation Letters*, vol. 12, no. 1, pp. 309–312, 2013. [Online]. Available: http://lup.lub.lu.se/record/3516482/file/3555826.pdf

[7] T. Mangel, O. Klemp, and H. Hartenstein, "5.9 GHz inter-vehicle communication at intersections: a validated non-line-of-sight path-loss and fading model," *EURASIP Journal on Wireless Communications and Networking*, vol. 2011, no. 1, p. 182, 2011.

[8] A. Paier, L. Bernado, J. Karedal, O. Klemp, and A. Kwoczek, "Overview of vehicle-to-vehicle radio channel measurements for collision avoidance applications," in *Vehicular Technology Conference (VTC 2010-Spring), 2010 IEEE 71st*, 2010, pp. 1–5.

[9] Google earth v7.1.1.1888 (2013). [Online]. Available: http://www.google.com/earth/index.html [Accessed: 2013/08/15]

[10] A. Thiel, O. Klemp, A. Paier, L. Bernadó, J. Karedal, and A. Kwoczek, "In-situ vehicular antenna integration and design aspects for vehicle-to-vehicle communications," in *EUCAP*, Apr. 2010.

[11] R. Thoma, D. Hampicke, A. Richter, G. Sommerkorn, A. Schneider, U. Trautwein, and W. Wirnitzer, "Identification of time-variant directional mobile radio channels," *Instrumentation and Measurement, IEEE Transactions on*, vol. 49, no. 2, pp. 357 –364, apr 2000.

[12] IEEE, "Part 11: Wireless lan medium access control (MAC) and physical layer (PHY) specifications: Amendment 7: Wireless access in vehicular environment," *IEEE 802.11p,2010*, 2010.

[13] H. El-Sallabi, "Fast path loss prediction by using virtual source technique for urban microcells," in *IEEE 51st Vehicular Technology Conference Proceedings (VTC 2000-Spring) Tokyo.*, vol. 3, 2000, pp. 2183 –2187 vol.3.

Paper V

A measurement Based Shadow Fading Model for Vehicle-to-Vehicle Network Simulations

The vehicle-to-vehicle (V2V) propagation channel has significant implications on the design and performance of novel communication protocols for vehicular *ad hoc* networks (VANETs). Extensive research efforts have been made to develop V2V channel models to be implemented in advanced VANET system simulators for performance evaluation. The impact of shadowing caused by other vehicles has, however, largely been neglected in most of the models, as well as in the system simulations. In this paper we present a shadow fading model targeting system simulations based on real measurements performed in urban and highway scenarios. The measurement data is separated into three categories, line-of-sight (LOS), obstructed line-of-sight (OLOS) by vehicles, and non line-of-sight due to buildings, with the help of video information recorded during the measurements. It is observed that vehicles obstructing the LOS induce an additional attenuation of about $10\,\mathrm{dB}$ in the received signal power. An approach to incorporate the LOS/OLOS model into existing VANET simulators is also provided. Finally, system level VANET simulation results are presented, showing the difference between the LOS/OLOS model and a channel model based on Nakagami-m fading.

1   Introduction

Vehicle-to-Vehicle (V2V) communication allows vehicles to communicate directly with minimal latency. The primary objective with the message exchange is to improve active on-road safety and situation awareness, e.g., collision avoidance, traffic re-routing, navigation, etc. The propagation channel in V2V networks is significantly different from that in cellular networks because V2V employs an *ad hoc* network topology, both transmitter (TX) and receiver (RX) are highly mobile, and TX/RX antennas are situated on approximately the same height and close to the ground level. Thus, to develop an efficient and reliable system a deep understanding of V2V channel characteristics is required [1].

A number of V2V measurements have been performed to study the statistical properties of V2V propagation channels [2–6]. Signal propagation over the wireless channel is often divided by three statistically independent phenomena named deterministic path loss, small-scale fading, and large-scale or shadow fading [7]. Path loss is the expected (mean) loss at a certain distance compared to the received power at a reference distance. The signal from the TX can reach the RX via several propagation paths or the multi-path components (MPC), which have different amplitudes and phases. The change in the signal amplitude due to constructive or destructive interference of the different MPCs is classified as small-scale fading. Finally, obstacles in the propagation paths of one or more MPCs can cause large attenuation and the effect is called shadowing. Shadowing gives rise to large-scale fading and it occurs not only for the line-of-sight (LOS) component but also for any other major MPC. Understanding all of these phenomena is equally important to characterize the V2V propagation channel.

In real scenarios there can be light to heavy road traffic, involving vehicles with variable speeds and heights, and there are sometimes buildings around the roadside. Hence, it might be the case that the LOS is partly or completely blocked by another vehicle or a house. The received power depends very much on the propagation environment, and the availability of LOS. Moreover, in [8] it is reported that, in the absence of LOS, most of the power is received by single bounce reflections from physical objects. Therefore, for a realistic simulation and performance evaluation it is important that the channel parameters are separately characterized for LOS and non-LOS conditions.

A number of different V2V measurement based studies with their extracted channel parameters are summarized in [9]. For most of the investigations mentioned in [9], it is assumed that the LOS is available for the majority of the recorded snapshots. Thus, the samples from both the LOS and non-LOS cases are lumped together for modeling, which is somewhat unrealistic, especially for larger distances. The LOS path being blocked by buildings greatly impacts the

reception quality in situations when vehicles are approaching the street intersection or road crossings. The buildings at the corners influence the received signal not only by blocking the LOS but also they act as scattering points which helps to capture more power in the absence of LOS [10]. A few measurement results for a non-LOS (NLOS) environment are available [11–15] in which the path loss model is presented for different types of street crossings.

In addition to the NLOS situation, the impact of neighboring vehicles can not be ignored. In [5], it is reported that the received signal strength degrades on the same patch of an open road in heavy traffic hours as compared to when there is light traffic. These observed differences can only be related to other vehicles obstructing LOS since the system parameters remained the same during the measurement campaign. Similarly, Zhang *et al.* in [16] presented an abstract error model in which the LOS and NLOS cases are separated using a thresholding distance. It is stated that the signals will experience more serious fading in crowded traffic scenario when the distance between the TX and RX is larger than the thresholding distance.

In [17] and [18], it is shown that the vehicles (as obstacles) have a significant impact on LOS obstruction in both dense and sparse vehicular networks, implying that shadowing caused by other vehicles cannot be ignored in V2V channel models. To date, in majority of the findings for V2V communications except [17] and [18], the shadowing impact of vehicles has largely been neglected when modeling the path loss. It is important to model vehicles as obstacles, ignoring this can lead to an unrealistic assumptions about the performance of the physical layer, both in terms of received signal power as well as interference levels, which in turn can effect the behavior of higher layers of V2V systems.

In order to characterize the channel parameters separately for LOS and non-LOS conditions V2V communication links in this paper are categorized into following three groups:

- Line-of-sight (LOS) is the situation when there is an optical line-of-sight between the TX and the RX.

- Obstructed-LOS (OLOS) is the situation when the LOS between the TX and RX is obstructed completely or partially by another vehicle.

- Non-LOS (NLOS) is the situation when a building between the TX and RX completely block the LOS as well as many other significant MPCs.

The channel properties for LOS, OLOS and NLOS are distinct, and their individual analysis is required. No path loss model, except a geometry based channel model published recently [19], is today available dealing with all three cases in a comprehensive way.

The main contribution of this paper is a shadow fading channel model
(LOS/OLOS model) based on real measurements in highway and urban sce-
narios distinguishing between LOS and OLOS. The model targets vehicular
ad hoc network (VANET) system simulations. We also provide a solution
on how to incorporate the LOS/OLOS model in a VANET simulator. We
model the temporal correlation of shadow fading as an auto-regressive pro-
cess. Finally, simulation results are presented where the results obtained from
the LOS/OLOS model are compared against the Cheng's model [20], which is
also based on an outdoor channel sounding measurement campaign performed
at 5.9 GHz. The reason to choose Cheng's model for comparison is that the
Cheng's model do not classify measured data as LOS, OLOS and NLOS, but it
represents both the small-scale fading, and the shadowing by the Nakagami-m
model.

The remainder of the paper is organized as follows. Section 2 outlines the
outdoor V2V measurements and explains the methods for separating LOS,
OLOS and NLOS data samples which serves as first step to model the effects
of shadow fading. It also includes the derivation of path loss and modeling of
shadow fading in LOS and OLOS cases as log-normal distribution. The channel
model is provided in section 3. First, the extension in traffic mobility models
is suggested to include the effect of large-scale fading, and then the path loss
model is presented and parameterized based on the measurements. VANET
simulation results are discussed in Section 4. Finally, section 5 concludes the
paper.

2   Methodology

2.1   Measurement Setup

Channel measurement data was collected using the RUSK-LUND channel
sounder, which performs multiple-input multiple-output (MIMO) measure-
ments based on the switched array principle. The measurement bandwidth
was 200 MHz centered around a carrier frequency of 5.6 GHz and a total
$N_f = 641$ frequency points. For the analysis the complex time-varying channel
transfer function $H(f, t)$ was measured for two different time durations: short
term (ST), 25 s, and long term (LT), 460 s. The short-term and long-term
channel transfer functions were composed of total $N_t = 49152$ and $N_t = 4915$
time samples, sampled with a time spacing of $\Delta t = 0.51$ ms and $\Delta t = 94.6$ ms,
respectively. The test signal length was set to 3.2 μs.

Two standard 1.47 m high station wagons, Volvo V70 cars, were used during
the measurement campaign. An omni-directional antenna was placed on the

roof of the TX and RX vehicles, taped on a styrofoam block that in turn was taped sideways to the shark fin on the center of the roof, and 360 mm from the back edge of the roof. Videos were taken through the windscreen of each TX/RX car and GPS data was also logged during each measurement. Video recordings and GPS data together with the measurement data were used in the post processing to identify the LOS, OLOS and NLOS conditions, important scatterers, and to keep track of the distance between the two cars. The videos were synchronized to the measurements.

2.2   Measurement routes

Eight routes in two different propagation environments were chosen with differences in their traffic densities, roadside environments, number of scatterers, pedestrians and houses along the road side. All measurements were conducted in and between the cities Lund and Malmö, in southern Sweden.

Highway: Measurements were performed when both the TX and RX cars were moving in a convoy at a speed of $22-25$ m/s ($80-90$ km/h), on a 2 lane (in each direction) highway, between the cities of Lund and Malmö, Sweden. The traffic density was varying on both sides of the road from low to high traffic. Along the roadside there were trees, vegetation, road signs, street lights and few buildings situated at random distances. The direction of travel was separated by a (≈ 0.5 m tall) concrete wall whereas the outer boundary of the road was guarded by a metallic rail.

Urban: Measurements were performed when both the TX and RX cars were moving in a convoy as well as in the opposite directions, in densely populated areas in Lund and Malmö. The TX and RX cars were moving with different speeds, between $0-14$ m/s ($0-50$ km/h), depending on the traffic situation. The streets were either single or double lane ($12-20$ m wide) lined with $2-4$ storied buildings. There were trees on either side and sidewalks on both sides of the streets. Moreover, there were road signs, street lights, bicycles and many parked cars, usually on both sides of the street. The streets were occupied with a number of moving vehicles as well as few pedestrians walking on the sidewalks.

In total 3 ST and 2 LT measurements for highway, and, 7 ST and 4 LT measurements for urban-convoy were performed. During each measurement, the LOS was often obstructed by other cars, taller vans, trucks, buses or houses at the street corners.

2.3   LOS, OLOS and NLOS separation

The measured channel transfer functions were first separated as LOS, OLOS and NLOS for all the measurements. The geometric information available form
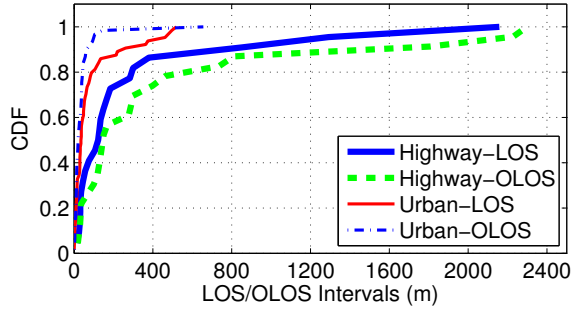
Figure 1: Cumulative Distribution Function (CDF) of LOS and OLOS
distance intervals for all measurements; (a) highway scenario, (b) urban
scenarios.

the video recording from the measurements has served as the foundation for
the separation process. To distinguish the LOS samples from OLOS and NLOS
samples, we define LOS condition as when it is possible for one of the cameras
to see the middle of the roof of the other vehicle. Otherwise, the LOS is
categorized as blocked. The blocked LOS situation is further categorized into
two groups as defined above; OLOS and NLOS. The recorded videos contain
25 frames per second and are synchronized to the measurements. Therefore, a
frame-by-frame evaluation of video data is performed to separate the data for
LOS, OLOS and NLOS cases.

During the whole measurement run, the TX-RX link transited between
LOS, OLOS and NLOS states a number of times, i.e., LOS-to-OLOS: 61 times
in urban and 23 times in highway scenario, similarly, LOS-to-NLOS: 4 times in
urban and 0 times in highway scenario. Each time the TX-RX pair is in either
LOS, OLOS or NLOS state, it remains in that state for some time interval and

Table 1: Distance traveled in LOS, OLOS and NLOS conditions.

	Scenario	Total	Min	Max	Mean	Median
LOS (m)	Highway	6622	24.4	2157	299	125
	Urban	5477	0.95	519	84.6	35.3
OLOS (m)	Highway	10752	18.6	2298	467	150
	Urban	2429	2.4	656	39.8	20.5
NLOS (m)	Urban	415	-	-	-	-

travel a certain distance relative to the speed vehicles. In Table 1 the traveled distances for both the scenarios; urban and highway, are tabulated together with the distances where TX/RX were in LOS, OLOS and NLOS, respectively. The Cumulative Distribution Function (CDF) of these LOS/OLOS distance intervals are shown in Fig. 1. No transition took place from OLOS-to-NLOS. The NLOS does not usually occur on highways, and the data samples for NLOS data in urban measurements are too few to be plotted as a CDF.

2.4   Pathloss Derivation

The time varying power-delay-profile (PDP) is derived for each time sample in order to determine the path loss. The effect of small scale fading is eliminated by averaging the time varying PDP over N_{avg} number of time samples, the averaged-PDP (APDP) is given by [21] as

$$P_h(t_k, \tau) = \frac{1}{N_{avg}} \sum_{n=0}^{N_{avg}-1} |h(t_k + n\Delta t, \tau)|^2, \tag{1}$$

for $t_k = 0, N_{avg}\Delta t, ..., \lfloor N_t/N_{avg} - 1 \rfloor N_{avg}\Delta t$, where $h(t_k + n\Delta t, \tau)$ is the complex time varying channel impulse response derived by an inverse Fourier transform of a channel transfer function $H(f, t)$ for a single-input single-output (SISO) antenna configuration. The N_{avg} corresponds to the movement of the TX and RX by $s = 15\lambda$ and is calculated by $N_{avg} = \frac{s}{v\Delta t}$, where Δt is the time spacing between snapshots and v is the velocity of TX and RX given in each scenario description. $N_{avg}\Delta t$ equals $32\,\mathrm{ms}$ and $71\,\mathrm{ms}$ for highway and urban scenarios, respectively, and they are chosen such that the wide-sense stationary (WSS) assumption is valid over N_{avg} snapshots [22].

The noise thresholding of each APDP is performed by suppressing all signals with power below the noise floor, i.e., noise power plus a $3\,\mathrm{dB}$ additional margin, to zero. The noise power is determined from the part of PDP, at larger delays, where no contribution from the transmitted signal is present. Thus, the zeroth order moment of the noise thresholded, small-scale averaged APDPs gives the averaged channel gain for each link as,

$$G_h(t_k) = \sum_{\tau} P_h(t_k, \tau), \tag{2}$$

where τ is the propagation delay.

Finally, the antenna influence and other implementation losses such as cable attenuation and the effect of the low-noise-amplifier (LNA) were removed from the measured gains. The azimuth antenna pattern was almost omni-directional
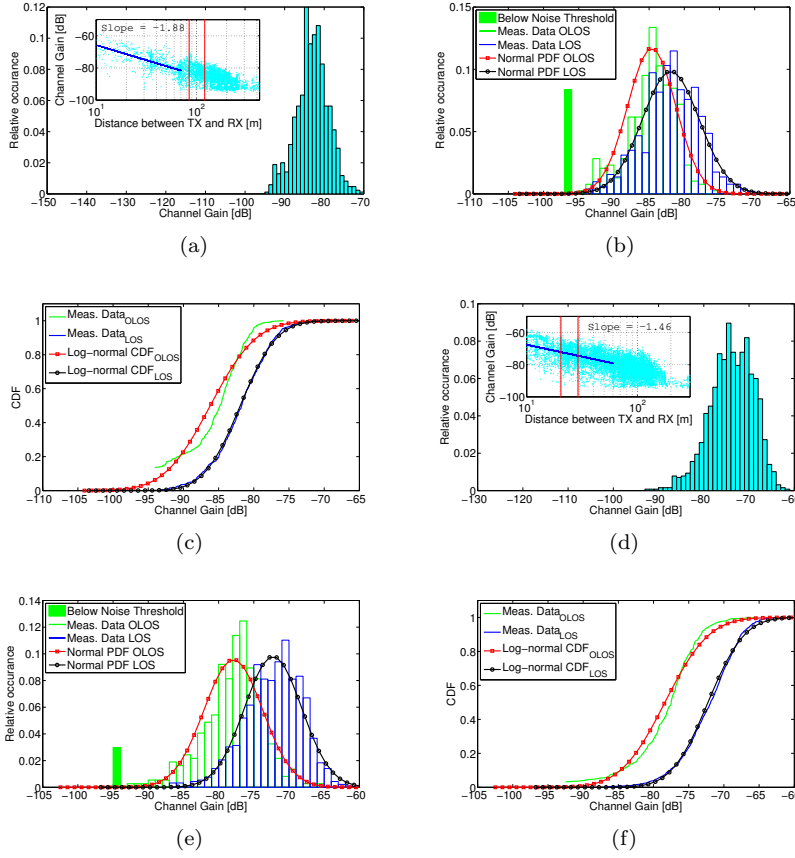
Figure 2: Figures (a), (b), (c) represent highway data, and (d), (e), (f)
represent urban data: In (a) and (d) inset plots shows channel gain for
the overall measurement data as a function of direct distance between
TX and RX. The slopes are provided up to the distance where no sample
is below the noise. Large plot is the histogram of channel gains taken
from log spaced distance bin, $20.4-29.1$ m in (a) and $84.6-121$ m in (d),
marked by vertical lines in the inset plot. The LOS and OLOS data is
treated together in these figure; (b) and (e) show histogram of the same
channel gains shown in (a) and (d), when separated as LOS and NLOS,
pdf fitting the Gaussian distribution; (c) and (f) show CDF fitting the
log-normal distribution with 95% confidence interval.

with variations of about 2 dB and peak gain of about 3.7 dBi, which was measured in an anechoic chamber. The distance dependent path-loss $PL(d)$ is then calculated using the following equation,

$$PL(d) = 2G_a - P_{IL} - 10\log_{10} G_h(d), \tag{3}$$

where $G_h(d)$ is the distance dependent channel gain, which is obtained by matching the time dependent channel gain $G_h(t_k)$ to its corresponding distance d between TX and RX at time instant t_k, G_a is the antenna gain, and P_{IL} is the implementation loss.

GPS data, recorded during the measurements, was used to find the distance between TX and RX, which corresponds to the propagation distance of first arriving path for each time sample in the presence of LOS. The time resolution of the GPS data was limited to one GPS position/second. Thus, to make GPS data sampling rate equal to the time snapshots, interpolation of the GPS data was performed with a cubic spline method. The distance obtained from the GPS data was further validated, later, by tracking the first arrived MPC, in the presence of LOS, with a high resolution tracking algorithm [23].

2.5   Large-scale or shadow fading

As explained earlier the effect of small scale fading is removed by averaging the received signal power over a distance of $15\,\lambda$. The averaged envelope is a random variable due to the large-scale variations caused by the shadowing from large objects such as building, and vehicles. The most widely accepted approach is to model the large-scale variations with a log-normal distribution function [7, 24].

For the analysis of large-scale variations the distance dependent channel gain $G_h(d)$ is divided into log-spaced distance bins and the distribution of the data associated to each bin is studied independently with and without the separation of LOS, OLOS, and NLOS data. Before the data separation it was observed that a log-normal distribution does not provide a good approximation of the data, as often anticipated, as shown in Fig. 2(a) and 2(d). Moreover, an additional attenuation was observed, which made the spread in the channel gain large and the spread was different for different distance bins. The conclusion was drawn that the attenuation could possibly be associated to the LOS obstruction. Therefore, it was important to separate the data for the LOS, OLOS and NLOS situations. The analysis of the separated data sets showed that the large-scale variations for both LOS and OLOS can be modeled as log-normal distribution (see, e.g., Fig. 2(b), 2(f)) with an offset of almost 10 dB in their mean. In highway and open scenarios even higher losses are expected due to obstructed LOS especially when the two cars have communication distance

less than 80 m. This observation is in line with the independent observations presented in [18]. In which it is found that a single obstruction at the communication distance of about 10 m can cause an additional attenuation of about 20 dB.

The channel gain in the OLOS condition momentarily falls below the noise floor of the channel sounder and power levels of samples below the noise threshold can not be detected correctly. However, the OLOS data in each bin for shorter distances, with no missing samples, fits well to a log-normal distribution, and the assumption is made that the data continues to follow a log-normal distribution for larger distance bins where the observed data is incomplete. Moreover, the exact count of missing samples is also available, which can be used to estimate the overall data distribution. To get the mean and variance of Gaussian distributed LOS and OLOS data, the maximum likelihood estimates (MLE) of scale and position parameters from incomplete data were computed by using the method in [25], in which Dempster *et al.* presented a broadly applicable algorithm that iteratively computes MLE from incomplete data via expectation maximization (EM).

3   Channel Model

In this section a shadow fading model (LOS/OLOS model) for VANET simulations is provided. This model targets network simulation, where there is a need for a realistic model taking shadowing effects into account but still with a reasonable complexity.

3.1   Pathloss Model

The measurement data is split into three data sets; LOS, OLOS and NLOS. The parameters of the path loss model are extracted only for the LOS and the OLOS data sets, whereas, not enough data is available to model the path loss for the third data set, NLOS.

The measured channel gain for LOS and OLOS data for the highway and the urban scenario is shown as a function of distance in Fig. 3 and 4, respectively. A simple log-distance power law [7] is often used to model the path loss to predict the reliable communication range between the transmitter and the receiver. The generic form of this log-distance power law path loss model is given by,

$$PL(d) = PL_0 + 10n \log_{10}\left(\frac{d}{d_0}\right) + X_\sigma, \tag{4}$$

where d is the distance between TX and RX, n is the path loss exponent estimated by linear regression and X_σ is zero-mean Gaussian distributed random variable with standard deviation σ and with some time correlation. The PL_0 is the path loss at a reference distance d_0 in dB.

In practice it is observed that a dual-slope model, as stated in [20], can represent measurement data more accurately. We thus characterize a dual-slope model as a piecewise-linear model with the assumption that the power decays with path loss exponent n_1 and standard deviation σ until the breakpoint distance (d_b) and from there it decays with path loss exponent n_2 and standard deviation σ. The dual-slope model is given by,

$$PL(d) = \begin{cases} PL_0 + 10n_1 \log_{10}\left(\frac{d}{d_0}\right) + X_\sigma, & \text{if } d_0 \leq d \leq d_b \\ PL_0 + 10n_1 \log_{10}\left(\frac{d_b}{d_0}\right) + & \text{if } d > d_b \\ 10n_2 \log_{10}\left(\frac{d}{d_b}\right) + X_\sigma. \end{cases} \tag{5}$$

Table 2: Parameters for the dual-slope path loss model.

	Scenario	n_1	n_2	PL_0	σ
LOS	Highway	-1.66	-2.88	-66.1	3.95
	Urban	-1.81	-2.85	-63.9	4.15
OLOS	Highway	-	-3.18	-76.1	6.12
	Urban	-1.93	-2.74	-72.3	6.67

The distance between TX and RX is extracted from the GPS data, which can be unreliable when TX-RX are very close to each other. Moreover, there are only a few samples available for $d < 10\,\text{m}$, thus the validity range of the model is set to $d > 10\,\text{m}$ and let $d_0 = 10\,\text{m}$. The typical flat earth model consider d_b as the distance at which the first Fresnel zone touches the ground or the first ground reflection has traveled $d_b + \lambda/4$ to reach RX. For the measurement setup the height of the TX/RX antennas was $h_{TX} = h_{RX} = 1.47\,\text{m}$, thus, d_b can be calculated as, $d_b = \frac{4h_{TX}h_{RX} - \lambda^2/4}{\lambda} = 161\,\text{m}$ for $\lambda = 0.0536\,\text{m}$ at 5.6 GHz carrier frequency. A d_b of $104\,\text{m}$ was selected to match the values with the path loss model presented in [20], implying a somewhat better fit to the measurement data.

The path loss exponents before and after d_b in (5) are adjusted to fit the median values of the LOS and OLOS data sets in least square sense and are shown in Fig. 3 and 4. The extracted parameters are listed in Table 3. For the highway measurements, OLOS occurred only when the TX/RX vehicles
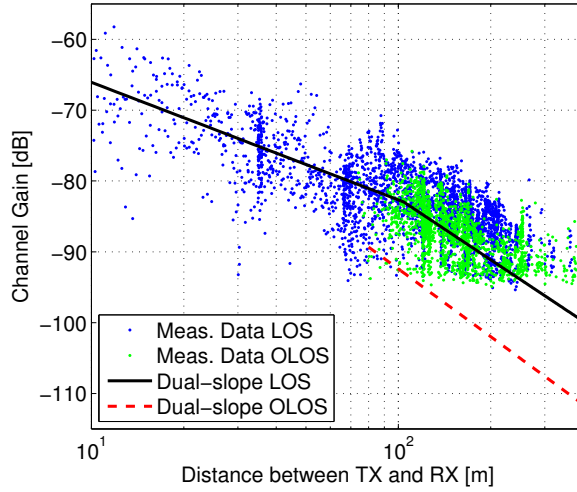
Figure 3: Measured channel gain for the highway environment and the
least square best fit to the deterministic part of (4).

were widely separated, i.e., when $d > 80$ m, which means that there are too
few samples to model the path loss exponent in OLOS for shorter distances.
Thus, the path loss exponent for OLOS for shorter distances is not modelled.
Whereas in practice, this is not always the case, the OLOS can occur at shorter
distances if there is traffic congestion on a highway with multiple lanes.

It is interesting to notice that there is an offset ΔPL_0 in the channel gain
for the LOS and OLOS data sets, which is of the order of $8.6 - 10$ dB, and
is very similar to the results that have previously been reported. In [17] an
additional attenuation of 9.6 dB is attributed to the impact of vehicle as an
obstacle. Meireles *et al.* in [18] stated that the OLOS can cause $10 - 20$ dB
of attenuation depending upon traffic conditions, as the congested traffic cause
large attenuation. Moreover, it is important to mention that the path-loss
exponents less than 2 have also been found in many other studies [9, 20, 21,
26, 27]. It is mainly due to the effect of two-ray reflection model in open and
highway scenarios or due to wave-guiding in urban scenarios.

It is highly important to model the pathloss in the NLOS situation because
power level drops quickly when the LOS is blocked by buildings. As mentioned
above, the available measured data in NLOS is not sufficient to model the
pathloss, therefore it is derived from available models specifically targeting
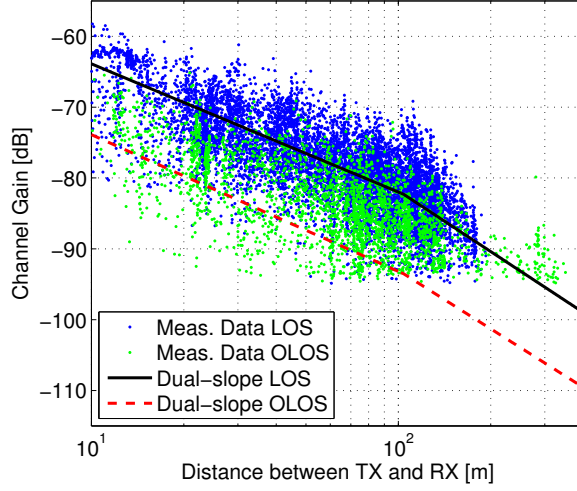similar scenarios, such as, [12, 13, 28] and COST 231-Welfish-Ikegami model

Figure 4: Measured channel gain for the urban environment and the least square best fit to the deterministic part of (4).

(Appendix 7.B in [7]). Among these, Mangel *et al.* in [13] presented a realistic and a well validated NLOS pathloss model which is of low complexity, thus, enabling large-scale packet level simulations in intersection scenarios. The basis for the pathloss equation in [13] is a cellular model proposed in [28], which is slightly modified to correspond well to V2V measurements. Validation of the NLOS model using independent V2V measurement data is done in [29], the results show that the model is a good candidate for modeling the pathloss in NLOS. For completeness Mangel's model [13] used for the NLOS situation is given as follows,

$$PL(d_r, d_t, w_r, x_t, i_s) = 3.75 + i_s 2.94$$

$$+ \begin{cases} 10 \log_{10} \left(\left(\frac{d_t^{0.957}}{(x_t w_r)^{0.81}} \frac{4\pi d_r}{\lambda} \right)^{n_{NLOS}} \right), & \text{if } d_r \leq d_b \\ 10 \log_{10} \left(\left(\frac{d_t^{0.957}}{(x_t w_r)^{0.81}} \frac{4\pi d_r^2}{\lambda d_b} \right)^{n_{NLOS}} \right), & \text{if } d_r > d_b \end{cases} \quad (6)$$

where d_r/d_t are distance of TX/RX to intersection center, w_r is width of RX street, x_t is distance of TX to the wall, and i_s specifies suburban and urban with $i_s = 1$ and $i_s = 0$, respectively. In a network simulator, the road topology and TX/RX positions are known, thus, these parameters can be obtained easily. The pathloss exponent in NLOS is provided in the model as $n_{NLOS} = 2.69$ and
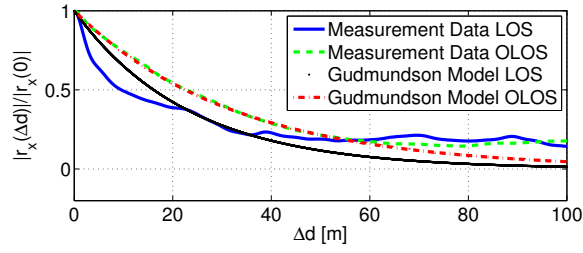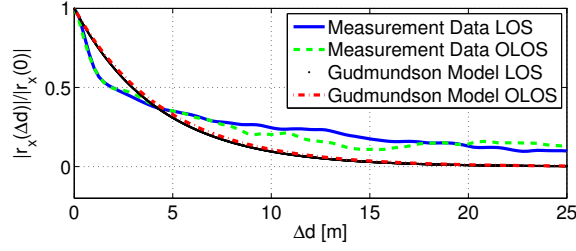
Figure 5: Measured auto-correlation function and model according to
(8) for LOS and OLOS data; (a) highway scenario, (b) urban scenarios.

Gaussian distributed fading with $\sigma = 4.1\,\mathrm{dB}$.

For larger distances $(d_r > d_b)$ the model introduces an increased loss due
to diffraction, around the street corners, being dominant. The NLOS model
is developed for TX/RX in intersecting streets. If the TX/RX are not in
intersecting streets but in parallel streets with buildings blocking the LOS
then this NLOS model is not advisable. The direct communication in such
setting might not be possible or not required but these vehicles can introduce
interference for each other due to diffraction over roof tops. This propagation
over the roof top can be approximated by diffraction by multiple screens as
it is done in the COST 231 model. However, in [30] simulation results are
shown which state that the pathloss in parallel street is always very high,
$> 120\,\mathrm{dB}$. The value is similar to the one obtained with theoretical calculations
for diffraction by multiple screens. As the losses for the vehicles in parallel
streets are high, interference from such vehicles can simply be ignored.

3.2   Spatial Correlation of Shadow Fading

Once a vehicle goes into a shadow region, it remains shadowed for some time interval implying that the shadowing is a spatially correlated process. If a vehicle is in a shadow region there is possibility that its existence may not be noticed for some time. Hence, it is important to study the spatial correlation of the shadow fading as part of the analysis to find the average decorrelation distances.

The large-scale variation of shadow fading can be well described as a Gaussian random variable (discussed in section III). By subtracting the distance dependent mean from the overall channel gain, the shadow fading can be assumed to be stationary process. Then the spatial auto-correlation of the shadow fading can be written as,

$$r_x(\Delta d) = E\{X_\sigma X_\sigma(d + \Delta d)\}. \tag{7}$$

The auto-correlation of the Gaussian process can then be modeled by a well-known analytical model proposed by Gudmundson [31], which is a simple negative exponential function,

$$r_x(\Delta d) = e^{-|\Delta d|/d_c}, \tag{8}$$

Table 3: Decorrelation distances d_c for highway and urban scenarios.

Scenario	LOS	OLOS
Highway	23.3	32.5
Urban	4.25	4.5

where Δd is an equally spaced distance vector and d_c is a decorrelation distance being a scenario-dependent real valued constant. In the Gudmundson model, d_c is defined as the value of Δd at which the value of the auto-correlation function $r_x(\Delta d)$ is equal to $1/e$. The value of the decorrelation distance d_c is determined from both the LOS and OLOS measured auto-correlation functions and are given in Table 3, for both the highway and urban scenarios, respectively. The estimated correlation distance is thus used to model the measured auto-correlation functions using (8), and is shown in Fig. 5(a) and 5(b).

Looking at decorrelation distance d_c, the implementation of shadow fading in a simulator can, if desired, be simplified by treating it as a block shadow fading, where d_c can be assumed as a block length in which the signal power will remain, more or less, constant.

3.3   Extension in the Traffic Mobility Models

The mobility models of today implemented in VANET simulators are very advanced, SUMO (Simulation of Urban Motility) [32] is one example of such an open source mobility model. These advanced models are capable of taking into account vehicle positions, exact speeds, inter-vehicle spacings, accelerations, overtaking attitudes, lane-change behaviors, etc. However, the ability to treat the vehicles as obstacles and model the intensity at which they obstruct the LOS for other vehicles is currently missing. Therefore, an extension for including shadowing effects in network simulators is provided herein, as stated in [33]. Since the vehicular mobility models implemented in the simulators give instantaneous information about each vehicle, the state of TX and RX vehicles can be identified by a simple geometric manipulation in the existing traffic mobility models as follows.

- Model each vehicle or building as a rectangle in the simulator.

- Draw a straight line starting from the antenna position of each TX vehicle to the antenna position of each RX vehicle.

- If the line does not touch any other rectangle, TX/RX has LOS.

- If the line passes through another rectangle, the LOS is obstructed by a vehicle or by a building, the two cases are distinguied by using the geographical information available in the simulator.

- Once the propagation condition is identified, the simulator can simply use the relevant model to calculate the power loss.

The impact of an obstacle is usually assessed qualitatively by the concept of the Fresnel ellipsoids. Only the visual sight does unfortunately not promise the availability of LOS, it is required that the Fresnel zone is free of obstacles in order to have the LOS [7]. The availability of LOS based on Fresnel ellipsoids depends very much on the information about the height of the obstacle, its distance from TX and RX, the distance between TX and RX as well as the wavelength λ. The information, if available in the traffic mobility simulator, should be utilized for the characterization of LOS and OLOS situation.

4   Network simulations

Finally, networks simulations are provided to show the difference between Cheng's Nakagami model [20] and the channel model presented herein distinguishing between LOS and OLOS. The simulation scenario is a 10 km long
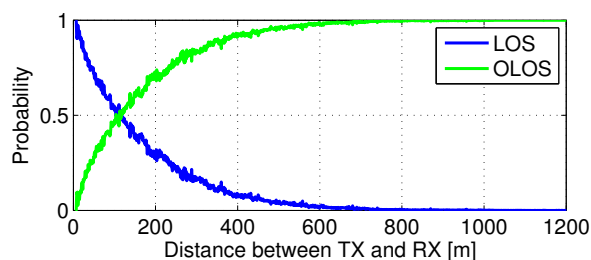
Figure 6: The probabilities of being in LOS and OLOS, respectively, depending on distance between TX and RX.

highway with four lanes (two in each direction). The vehicles appear with a Poisson distribution with three different simulation settings for the mean inter-arrival time; 1 s, 2 s, and 3 s. The three different mean inter-arrival times yield three different vehicle densities, where 1 s corresponds is ≈ 100 vehicles/km, 2 s corresponds to 60 vehicles/km, and 3 s corresponds to 40 vehicles/km. Every vehicle broadcasts 400 byte long position messages at 10 Hz (10 messages/sec) using a transfer rate of 6 Mbps and an output power of 20 dBm (100 mW). The channel access procedure is carrier sense multiple access (CSMA), that has been selected as medium access control (MAC) for VANETs supporting road traffic safety applications. The vehicle speeds are independently Gaussian distributed with a standard deviation of 1 m/s, with different means (23 m/s and 30 m/s) depending on lane. The vehicles maintain the same speed as long as they are on the highway. More details about the simulator can be found in [34]. The shadowing based channel model LOS/OLOS model presented herein has been compared against Cheng's Nakagami model [20] in the network simulations, where the latter is not capable of distinguishing between LOS and OLOS. Cheng's Nakagami model is also based on an outdoor channel sounding campaign, performed at 5.9 GHz in which the small-scale fading and the shadowing are both represented by the Nakagami-m model [20]. The fading intensities, represented by the m parameter of the Nakagami distribution, are different depending on the distance between TX and RX. The m values and the path loss exponents are taken from data set 1 in [20] to compute the averaged received power for Cheng's Nakagami model.

The averaged received power for the LOS/OLS and Cheng's Nakagami model is depicted in Fig. 7. At shorter distances there is a little chance that another vehicle is between two communicating vehicles but as the distance increases the chances of being under OLOS either by vehicle, object, or due to the curvature of the earth, increases. The probabilities of being in LOS,
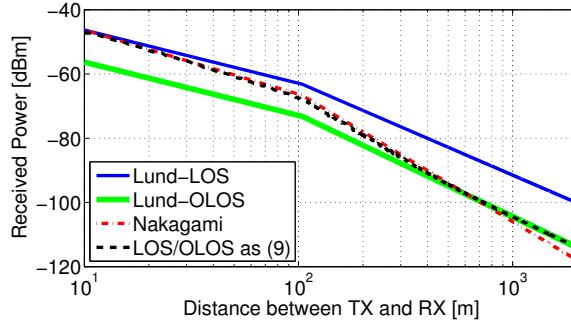
Figure 7: The averaged received power for the LOS/OLOS model and
the Cheng's Nakagami model, respectively.

$Prob(LOS|d)$, and being in OLOS, $Prob(OLOS|d)$, have been calculated from
the network simulator for the highway scenario, as a function of distance and
are depicted in Fig. 6. To receive the averaged power as a function of distance
similar to Cheng's model, these probabilities can be multiplied with the av-
eraged received power for LOS, $P_{RX,LOS}(d)$, and OLOS, $P_{RX,OLOS}(d)$, using
the following equation:

$$P_{RX}(d) = Prob(LOS|d)P_{RX,LOS}(d)$$
$$+Prob(OLOS|d)P_{RX,OLOS}(d) \qquad (9)$$

By using (9) the averaged received power from the LOS/OLOS model coincides
with Cheng's Nakagami model, see Fig. 7, which is very interesting to notice.
In Fig. 8, the packet reception probability is depicted for the two channel
models; LOS/OLOS model and Cheng's Nakagami model, respectively, and
for three different vehicle densities. On the x-axis, the distance between TX
and RX is shown. For detailed analysis six pairs of vehicles, three pairs in
each direction are studied in the simulations. Each pair travels in the same
direction in different lanes with different speeds, where the vehicle with high
speed will pass by the vehicle with the low speed. The selection of pairs where
done to study individual performance of the vehicles. It should be noted that
exactly the same number of communicating vehicles has been used for the
different vehicle densities for every channel model, i.e., the same TX-RX pair
are studied using both channel models. When TX and RX are close to each
other, i.e., within 100 m, the two channel models perform equal. As the distance
increases to $200 - 400$ m, the vehicles exposed to the Nakagami model are
experiencing a better packet reception probability. The vehicles exposed to
the Nakagami model reach a packet reception probability of zero at around
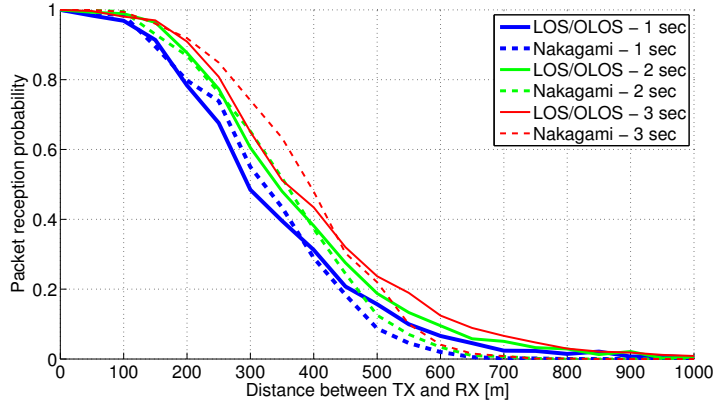
Figure 8: Packet reception probability for the two different channel models and for three different vehicle densities.

700 m, whereas this is reached above 1000 m for the LOS/OLOS model. Real measurements [35] also show such a behaviour with occational successful packet transmission at larger distances. This also implies that the LOS/OLOS model contributes to interference at stations situated further away, which is in line with what is seen on the averaged received power in Fig. 7. Here the OLOS part has a stronger signal than Cheng's Nakagami model above 700 m.   In Fig. 9, the CDF for packet inter-arrival time for a vehicle density of 3 seconds (40 vehicles/km) is depicted. The received packet inter-arrival time is the time that has elapsed between two successfully received packets from a specific TX that RX is listening to. Around every 100 ms, the RX is expecting a new packet from a specific TX. The period is not exactly 100 ms due to channel access delays caused by, e.g., backoff procedures [36]. The different lines in the figure represent different distance bins. When TX and RX are within 100 m of each other, the RX can expect a new packet every 100 ms and the channel models only differ slightly in performance. When distance increases to $200 - 400$ m, the vehicles under the treatment of the Nakagami model are experiencing a better packet inter-arrival times, which was also reflected in Fig. 8. In the distance bin $300 - 400$ m, studying the vehicles under Nakagami, in almost 60% of the cases there are no packets lost between two successful receptions and in about 25% of the cases, a single packet is lost between successful receptions. As the distance increases to above 400 m, stations under the LOS/OLOS model are having slightly better packet reception probabilities. The CDF for packet inter-arrival times for a vehicle density of 2 s (60 vehicles/km) is depicted in Fig. 10. Here, it
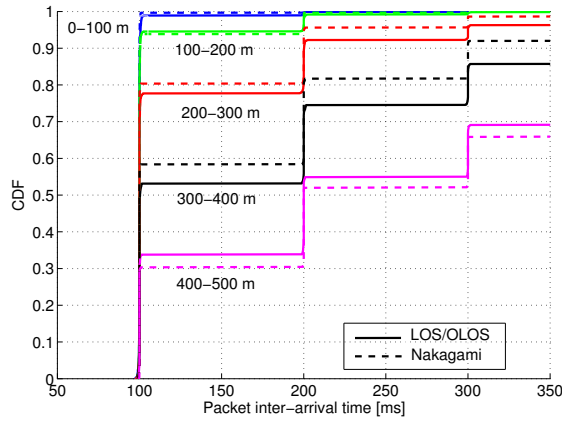
Figure 9: CDF for the packet inter-arrival time for a vehicle density of
40 vehicles/km for the LOS/OLOS and Nakagami models, respectively

is seen that the gap in performance between the two models has decreased since
there are more transmissions on the channel and the overall interference has
increased. In Fig. 11, CDF for packet inter-arrival times for the highest vehicle
density case is depicted. Still, the stations under the treatment of Nakagami
are experiencing a better packet inter-arrival pattern, especially for distances
between $200 - 300$ m.

5   Summary and Conclusions

In this paper, a shadow fading model based on measurements performed in
urban and highway scenarios is presented, where a separation between LOS,
obstructed LOS by vehicle (OLOS) and obstructed LOS by building (NLOS),
is performed. In the past, despite extensive research efforts to develop more
realistic channel models for V2V communication, the impact of vehicles ob-
structing LOS has largely been ignored. We have observed that the LOS ob-
struction by vehicles (OLOS) induce an additional loss, of about 10 dB, in the
received power. Network simulations have been conducted showing the dif-
ference between a conventional Nakagami based channel model (often used in
VANET simulations) and the LOS/OLOS model presented herein. There is
a difference in the performance of the two channel models. However, depend-
ing on the evaluated VANET application the obstruction of LOS cannot be
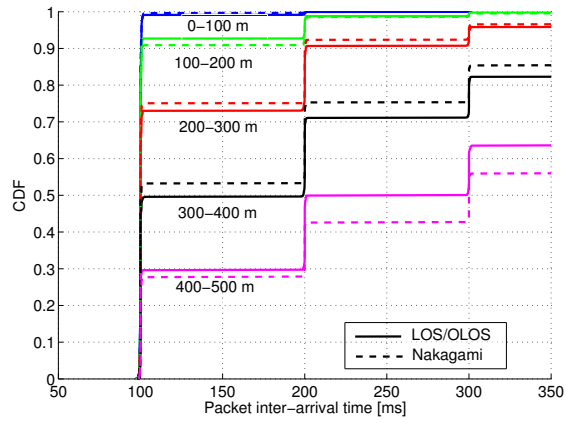ignored and there is a need for a LOS/OLOS model in VANET simulators.

Figure 10: CDF for the packet inter-arrival time for a vehicle density of 60 vehicles/km for the LOS/OLOS and Nakagami models, respectively.
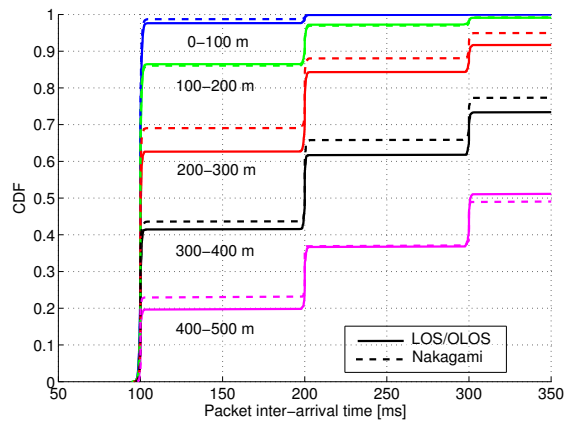

Figure 11: CDF for the packet inter-arrival time for a vehicle density of 100 vehicles/km for the LOS/OLOS and Nakagami models, respectively.

The LOS/OLOS model is easy to implement in VANET simulators due to the
usage of a dual-piece wise path loss model and the shadowing effect is modeled
as a log normal correlated variable with a mean determined by the propagation
condition (LOS/OLOS).

References

[1] J. Gozalvez, M. Sepulcre, and R. Bauza, "Impact of the radio channel mod-
    eling on the performance of VANET communication protocols," *Telecom-
    munication Systems*, pp. 1–19, Dec. 2010.

[2] G. Acosta-Marum and M. Ingram, "Six time- and frequency- selective em-
    pirical channel models for vehicular wireless LANs," *IEEE Veh. Technol.
    Mag.*, vol. 2, no. 4, pp. 4–11, 2007.

[3] I. Sen and D. W. Matolak, "Vehicle-vehicle channel models for the 5 GHz
    band," *IEEE Trans. Intell. Transp. Syst.*, vol. 9, no. 2, pp. 235–245, Jun.
    2008.

[4] A. Paier, J. Karedal, N. Czink, C. Dumard, T. Zemen, F. Tufvesson,
    A. F. Molisch, and C. F. Mecklenbräuker, "Characterization of vehicle-to-
    vehicle radio channels from measurements at 5.2 GHz," *Wireless Personal
    Commun.*, vol. 50, pp. 19–29, 2009.

[5] J. Otto, F. Bustamante, and R. Berry, "Down the block and around the
    corner the impact of radio propagation on inter-vehicle wireless communi-
    cation," in *ICDCS '09. 29th IEEE International Conference on Distributed
    Computing Systems*, June 2009, pp. 605 –614.

[6] O. Renaudin, V. M. Kolmonen, P. Vainikainen, and C. Oestges, "Non-
    stationary narrowband MIMO inter-vehicle channel characterization in the
    5 GHz band," *IEEE Trans. Veh. Technol.*, vol. 59, no. 4, pp. 2007–2015,
    May 2010.

[7] A. Molisch, *Wireless Communications*.   Chichester, West Sussex, UK:
    IEEE Press-Wiley, 2005.

[8] T. Abbas, J. Karedal, F. Tufvesson, A. Paier, L. Bernado, and A. Molisch,
    "Directional analysis of vehicle-to-vehicle propagation channels," in *2011
    IEEE 73rd Vehicular Technology Conference (VTC Spring)*, may 2011, pp.
    1 –5.

[9] A. F. Molisch, F. Tufvesson, J. Karedal, and C. F. Mecklenbräuker, "A survey on vehicle-to-vehicle propagation channels," in *IEEE Wireless Commun. Mag.*, vol. 16, no. 6, 2009, pp. 12–22.

[10] T. Abbas, L. Bernado, A. Thiel, C. F. Mecklenbräuker, and F. Tufvesson, "Radio channel properties for vehicular communications: Merging lanes vs. urban intersections," *IEEE Vehicular Technology Magazine*, Dec. 2013.

[11] T. Mangel, M. Michl, O. Klemp, and H. Hartenstein, "Real-world measurements of non-line-of-sight reception quality for 5.9 GHz IEEE 802.11p at intersections," *Communication Technologies for Vehicles, Springer Berlin Heidelberg*, vol. 6596, pp. 189–202, 2011.

[12] E. Giordano, R. Frank, G. Pau, and M. Gerla, "Corner: a realistic urban propagation model for vanet," in *Seventh International Conference on Wireless On-demand Network Systems and Services (WONS-2010)*, feb. 2010, pp. 57 –60.

[13] T. Mangel, O. Klemp, and H. Hartenstein, "5.9 GHz inter-vehicle communication at intersections: a validated non-line-of-sight path-loss and fading model," *EURASIP Journal on Wireless Communications and Networking*, vol. 2011, no. 1, p. 182, 2011.

[14] P. Paschalidis, A. Kortke, K. Mahler, M. Wisotzki, W. Keusgen, and M. Peter, "Pathloss and Multipath Power Decay of the Wideband Car-to-Car Channel at 5.7 GHz," in *IEEE 73th Vehicular Technology Conference (VTC2011-Spring)*, Budapest, Hungry, May 2011.

[15] J. Turkka and M. Renfors, "Path loss measurements for a non-line-of-sight mobile-to-mobile environment," in *8th International Conference on ITS Telecommunications (ITST-2008), Hilton Phuket, Thailand*, oct. 2008, pp. 274 –278.

[16] Y. Zang, L. Stibor, G. Orfanos, S. Guo, and H.-J. Reumerman, "An error model for inter-vehicle communications in highway scenarios at 5.9 GHz," in *Proceedings of the 2nd ACM international workshop on Performance evaluation of wireless ad hoc, sensor, and ubiquitous networks*, ser. PE-WASUN '05.   New York, NY, USA: ACM, 2005, pp. 49–56.

[17] M. Boban, T. Vinhoza, M. Ferreira, J. Barros, and O. Tonguz, "Impact of vehicles as obstacles in vehicular ad hoc networks," *Selected Areas in Communications, IEEE Journal on*, vol. 29, no. 1, pp. 15 –28, Jan. 2011.

[18] R. Meireles, M. Boban, P. Steenkiste, O. Tonguz, and J. Barros, "Experimental study on the impact of vehicular obstructions in VANETs," in *2010 IEEE Vehicular Networking Conference (VNC), New Jersey, USA*, dec. 2010, pp. 338 –345.

[19] M. Boban, J. Barros, and O. K. Tonguz, "Geometry-based vehicle-to-vehicle channel modeling for large-scale simulation," *CoRR*, vol. abs/1305.0124, 2013.

[20] L. Cheng, B. Henty, D. Stancil, F. Bai, and P. Mudalige, "Mobile vehicle-to-vehicle narrow-band channel measurement and characterization of the 5.9 GHz dedicated short range communication (DSRC) frequency band," *Selected Areas in Communications, IEEE Journal on*, vol. 25, no. 8, pp. 1501 –1516, Oct. 2007.

[21] J. Karedal, N. Czink, A. Paier, F. Tufvesson, and A. Molisch, "Path loss modeling for vehicle-to-vehicle communications," *IEEE Transactions on Vehicular Technology*, vol. 60, no. 1, pp. 323–328, 2011.

[22] L. Bernado, T. Zemen, F. Tufvesson, A. Molisch, and C. Mecklenbrauker, "The (in-) validity of the wssus assumption in vehicular radio channels," in *Personal Indoor and Mobile Radio Communications (PIMRC), 2012 IEEE 23rd International Symposium on*, 2012, pp. 1757–1762.

[23] J. Karedal, F. Tufvesson, N. Czink, A. Paier, C. Dumard, T. Zemen, C. Mecklenbräuker, and A. F. Molisch, "A geometry-based stochastic MIMO model for vehicle-to-vehicle communications," *IEEE Transactions on Wireless Communications*, vol. 8, no. 7, pp. 3646–3657, 2009.

[24] G. Stüber, *Principles of Mobile Communication*, second ed. ed. Dordrecht: Norwell, MA: Kluwer Academic Publishers, 2000.

[25] A. P. Dempster, N. M. Laird, and D. B. Rubin, "Maximum likelihood from incomplete data via the em algorithm," *JOURNAL OF THE ROYAL STATISTICAL SOCIETY, SERIES B*, vol. 39, no. 1, pp. 1–38, 1977.

[26] H. Fernãndez, L. Rubio, J. Reig, V. Rodrigo-Pearrocha, and A. Valero, "Path loss modeling for vehicular system performance and communication protocols evaluation," *Mobile Networks and Applications*, pp. 1–11, 2013. [Online]. Available: http://dx.doi.org/10.1007/s11036-013-0463-x

[27] J. Kunisch and J. Pamp, "Wideband car-to-car radio channel measurements and model at 5.9 GHz," in *Vehicular Technology Conference, 2008. VTC 2008-Fall. IEEE 68th*, 2008, pp. 1–5.

[28] H. El-Sallabi, "Fast path loss prediction by using virtual source technique for urban microcells," in *IEEE 51st Vehicular Technology Conference Proceedings (VTC 2000-Spring) Tokyo.*, vol. 3, 2000, pp. 2183 –2187 vol.3.

[29] T. Abbas, A. Thiel, T. Zemen, C. F. Mecklenbräuker, and F. Tufvesson, "Validation of a non-line-of-sight path-loss model for V2V communications at street intersections," in *13th International Conference on ITS Telecommunications, Tampere, Finland.*   IEEE, November 2013.

[30] T. Gaugel, L. Reichardt, J. Mittag, T. Zwick, and H. Hartenstein, "Accurate simulation of wireless vehicular networks based on ray tracing and physical layer simulation," in *High Performance Computing in Science and Engineering '11.*   Springer Berlin Heidelberg, 2012, pp. 619–630.

[31] M. Gudmundson, "Correlation model for shadow fading in mobile radio systems," *Electronics Letters*, vol. 27, no. 23, pp. 2145 –2146, nov. 1991.

[32] M. Behrisch, L. Bieker, J. Erdmann, and D. Krajzewicz, "SUMO - simulation of urban mobility: An overview," in *SIMUL 2011, The Third International Conference on Advances in System Simulation*, Barcelona, Spain, October 2011, pp. 63–68.

[33] T. Abbas and F. Tufvesson, "Line-of-sight obstruction analysis for vehicle-to-vehicle network simulations in a two-lane highway scenario," *International Journal of Antennas and Propagation*, vol. 2013, p. 9, 2013.

[34] K. Sjöberg, "Medium access control in vehicular ad hoc networks," Ph.D. dissertation, Chalmers University of Technology, Göteborg, Sweden, 2013.

[35] A. Paier, "The vehicular radio channel in the 5 ghz band," Ph.D. dissertation, Technische Universität Wien, Vienna, Austria, 2010.

[36] *IEEE Std. 802.11p-2010, Part 11: Wireless LAN Medium Access Control (MAC) and Physical Layer (PHY) specifications: Amendment 7: Wireless Access in Vehicular Environment*, IEEE Std., July 2010.

Paper VI

Measurement-Based Analysis: The Effect of Complementary Antennas and Diversity on Vehicle-to-Vehicle Communication

In vehicle-to-vehicle (V2V) communication systems the antennas are prone to shadowing and the antenna gain is dissimilar even for same antenna elements if mounted at different positions on the car. This paper investigates the impact of antenna placement based on channel measurements performed with four omni-directional antennas mounted on the roof, bumper, windscreen and left-side mirror of the transmitter and receiver cars. Results suggest to use antennas with complementary characteristics, e.g., antennas on each side, mounted on the roof and bumper, to exploit diversity and decrease the effect of shadowing.

1   Introduction

The research interest in vehicle-to-vehicle (V2V) communications has recently
increased and is continuously flourishing due to the diversified scope of applica-
tions of V2V communications for improving the traffic safety and management.
The effectiveness of these applications require low latency communication with
high reliability. In order to obtain a high reliability, it is necessary to have a
stable radio link. In cellular communications the base station antenna is at an
elevated position with a circular (sectorized) coverage around it. This is not
the case in V2V communications; both the transmit (TX) and receive (RX)
antennas are at the same height relatively close to ground level, at some $1-2\,\mathrm{m}$
above ground. In V2V systems, the position of the antenna is expected to have
a large impact on the radio link performance. Therefore some of the experi-
ences gained from cellular communications [1] are not directly applicable to
V2V communications. Above all, by having antennas close to the ground level,
shadowing effects from other vehicles and surrounding buildings are expected.
Therefore, experimental studies employing real-time-measurement are essential
to understand how antennas mounted at different positions on a car affect the
behavior and performance of the radio link.

In the past, a number of measurement campaigns have been conducted for
V2V systems, e.g., [2–7]. These measurements have almost exclusively been
conducted with the same type of antenna mounting: a roof-mounted antenna
(array). However, a small number of exceptions exist. In [4], an antenna was
placed inside the vehicle, next to the windshield. In [3] and [8], the effects of five
and three different roof positions, respectively, were tested. In, [9] and [10], ray
tracing based simulations have been applied for analyzing impact of three and
six antenna positions, respectively. To the authors' best knowledge, though, no
(measurement-based) investigations to study the impact of antenna placement
at different positions on the car, other than on the roof and windscreen, have
been presented in the literature.

In order to meet the need for measurement-based investigations, as de-
scribed above, a measurement campaign was conducted with four antennas
mounted at four different positions on each TX and RX car (see Fig. 1): roof
(R), bumper (B), inside-windscreen (W) and left-side mirror (M). Alternative
antenna mounts include the rear bumper as well as the right side mirror, but
those antenna positions are not measured in this campaign. The main goal
is to investigate whether there is any antenna combination that is especially
suitable for a diversity based system, i.e., if there are any two antenna elements
that complement each other well in different propagation environments.

This letter contributes to the knowledge of the impact of distributed an-
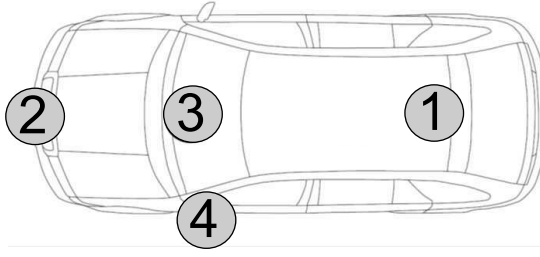tennas in V2V communication and helps to develop a better understanding by

Figure 1: The antennas were taped on a Styrofoam block that, in turn, was mounted in the following way: 1) Roof antenna (R), was mounted at the shark fin on the center of the roof, side wise, and 360 mm from the back edge of the roof: 2) Bumper antenna (B), was mounted 70 mm ahead of the registration plate; 3) Inside Windscreen antenna (W), was centered at the instrument board/dashboard at distance 1600 mm from the front of the car; 4) Left-side mirror antenna (M), was mounted at the outer edge of the mirror about 290 mm from the car side.

characterizing the propagation channel properties for antennas mounted at different positions on a car. This is achieved in four steps. First, we analyze how the overall channel gain varies over time for different antenna positions in different environments. Second, we perform the diversity combining, and present diversity gain from different antenna combinations using selection combining (SC) and maximum ratio combining (MRC). Third, we select the best antenna pair among four antennas for the TX/RX vehicles based on the maximum diversity gain. Finally, we present delay and Doppler spread for these antenna positions.

2   Measurements

2.1   Measurement setup

For the measurement campaign we measure the gain of different links between two standard Volvo V70 cars, 1.47 m high station wagons, used either as TX or RX. Each vehicle was equipped with four omni-directional (in azimuth) vertically polarized SkyCross meander line antennas mounted at four different positions (see Fig. 1), SMT-2TO6MB-A, having a frequency range between 2.3 to 5.9 GHz and an antenna gain of around 3 dBi in the used frequency band. Channel measurements were performed using the RUSK-LUND channel sounder [11], which performs multiple-input multiple-output (MIMO) measure-
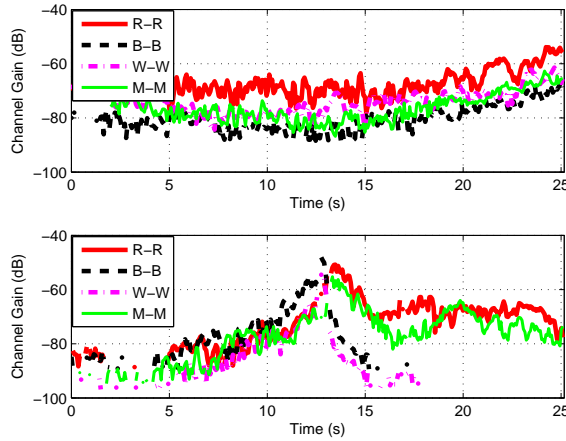
Figure 2: Example of channel gains for four SISO links between same
antenna mounts in urban convoy (top) where R-R links have higher gain.
In urban opposite (bottom) the B-B and W-W links are the stronger as
long as the vehicles are approaching, whereas R-R and M-M links have
higher gain after the cars have passed each other.

ments based on a switched array principle. The complex time-varying channel
transfer function $H(f,t)$ was measured for each TX/RX link over $200\,\mathrm{MHz}$
of bandwidth at $5.6\,\mathrm{GHz}$, the highest carrier frequency on which our channel
sounder can operate. Since $5.6\,\mathrm{GHz}$ is very close to $5.9\,\mathrm{GHz}$, the standard
frequency for 802.11 p, it is believed that the channel characteristics remain
same. Moreover, the $200\,\mathrm{MHz}$ bandwidth is chosen to achieve the high delay
resolution which is beneficial for the channel analysis. During the analysis the
transmitted power was assumed constant and was switched over the multiple
transmitted antennas. Moreover, to secure additional support in post process-
ing, videos were taken through the windscreen of each car and GPS data were
logged during each measurement run.

All measurements were conducted in and between the cities of Lund and
Malmö, in the south of Sweden. Three typical propagation environments were
chosen due to differences in the traffic densities, road-side environments, num-
ber of scatterers, pedestrians, and houses along the road side:

- **Highway** - Measurements were performed on a $4-$lane highway (E22)
  where TX/RX vehicles were moving in a convoy at a speed of $22-25\,\mathrm{m/s}$
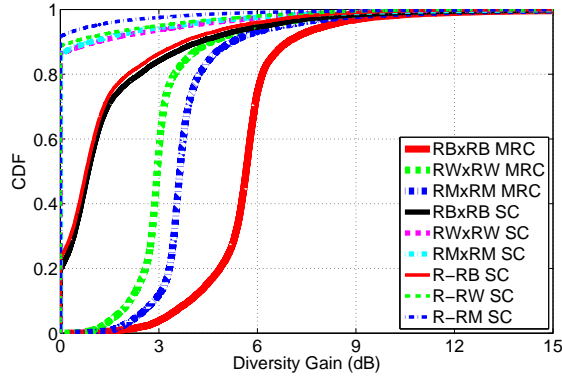 over a $10\,\mathrm{km}$ long stretch of the road. The direction of travel was sep-

Figure 3: Highway convoy: The diversity gain shown above is relative to the R-R SISO link. MRC has significant gain for all antenna combinations whereas SC does not provide any diversity gain for more than 80% of the time because the R-R link is better than the other links except for the RB×RB and R-RB links.

arated by a ($\approx 0.5\,\mathrm{m}$ tall) concrete wall whereas the outer boundary of road was guarded by a metallic rail.

- **Urban** - Measurements were performed in densely populated areas in Lund and Malmö where the streets were $12 - 20\,\mathrm{m}$ wide, either single or double lane, lined with $2 - 4$ storied buildings. The vehicles were driven over $4 - 6\,\mathrm{km}$ long loops and on a $3\,\mathrm{km}$ long stretch at varying speeds ranging $0 - 14\,\mathrm{m/s}$ while moving as a convoy or in opposite directions.

- **Rural** - Measurements were performed on a patch of road with open surroundings just outside the city of Lund at an approximate speed of $17 - 20\,\mathrm{m/s}$. There were no moving scatterers but a couple of houses at some $300\,\mathrm{m}$ distance from the measurement site. The rural scenario was measured as a reference to analyze the case when there are no or very few scatterers around.

Moreover, along the roadside there were trees, vegetation, road signs, street lights, bicycles, parked cars and often buildings situated at random distances, where the concentration of these objects depends upon the scenarios. There were other vehicles which occasionally obstructed the line-of-sight (LOS), partially or completely, for all or only for a subset of antenna combinations. In the urban environment, vehicles experience additional attenuation when buildings

around the corner block the LOS. For more details on measurement set up,
see [12].

3   Results and Discussion

Before the measurements the cable losses and the gain of the low-noise-amplifier
(LNA) were explicitly measured and their effect is removed from the measured
channel gains. Hence the channel gains presented here are the gains experienced
from TX antenna connector to the RX antenna connector of the measurement
equipment without further cables.

V2V antennas are sensitive to the shadowing effects either from other vehi-
cles or from the body of the car itself. This means, e.g, due to the shadowing
caused by the curved surface and the size of the roof of a car that the R-antenna
(roof) experiences stern degradation in the azimuth gain in the forward direc-
tion [13] whereas it has higher gain in the backward direction. The M-antenna
(left-side mirror) has the higher channel gain both in forward and backward
direction but it is sensitive to the exact alignment of the two vehicles, as also
stated in [14]. Finally, the W and B antennas, mounted next to the windscreen
and bumper respectively, are completely shadowed by the car body thus they
only have good gain in the forward direction. Thus, it is interesting to notice
that the antenna gain is dissimilar even by similar antenna elements if mounted
at different positions on the car [3].

These differences in channel gain for the links associated to same antenna
positions on the TX and RX, i.e., link for; R-R, B-B, W-W, and M-M, in urban
environment are highlighted in Fig. 2, while TX and RX are moving in a convoy
as well as in the opposite directions. It can be observed in Fig. 2 that the R-R
link has higher gain since all other antennas are somehow under the shadow of
the car body itself. On the contrary, in an opposite setting when both the TX
and RX cars are moving towards each other, the LOS between the B-B and
W-W antenna pairs will enhance the received power compared to other links.
This gain in power by the B-B link will make us detect vehicles 2 s before other
antenna pairs as if the TX/RX vehicles are moving at speed of around 17 m/s.
In other words, by having an additional antenna on the bumper, we can detect
other cars from slightly larger distance relative to the roof only antenna (see
Fig. 2). Moreover, when TX/RX are moving away from each other, we gain
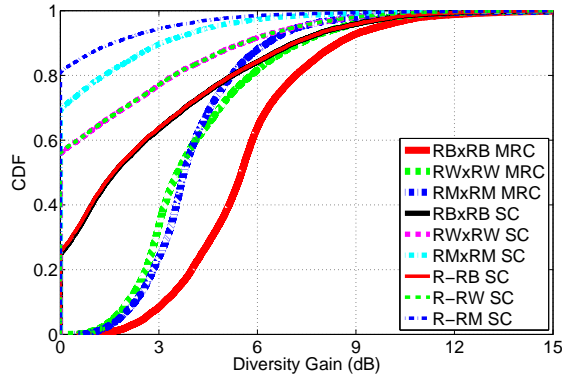similar amount of time with the roof antenna.

Figure 4: Urban convoy: For more than 50% of the time the SC diversity gain is at least 2 dB and 6 dB for the RB×RB and R-RB links, respectively. MRC performs well in all situations since it uses dominant eigen mode transmission.
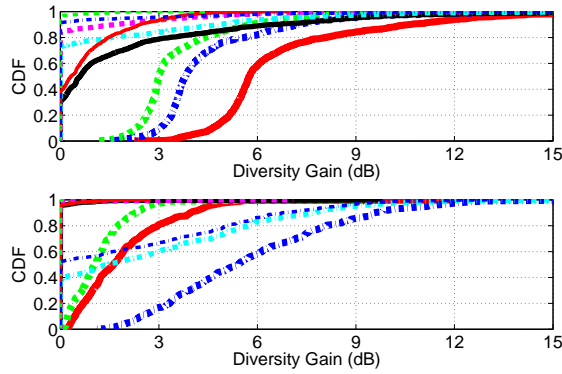

Figure 5: Urban opposite: Vehicles approaching (top) and moving away (bottom). The R and B antenna combination has the strongest gain when vehicles are approaching whereas R and M antenna combination has better gain when moving away. However, for more than 50% of time there is no diversity gain with SC for both the RB and RM combinations because the bumper or mirror antennas were often obstructed by other vehicles. Legend is the same as in the above figure.
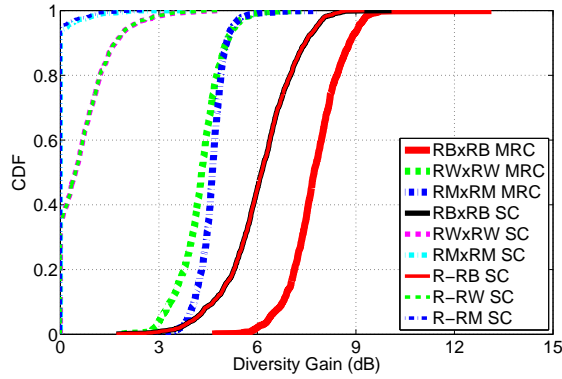
Figure 6: Rural convoy: Both TX/RX vehicles are well aligned so
the RWxRW and RMxRM links provide diversity gain also with SC.
However, the RB×RB combination has the best performance since it
provides 6 dB and 8 dB gain for SC and MRC, respectively, for more
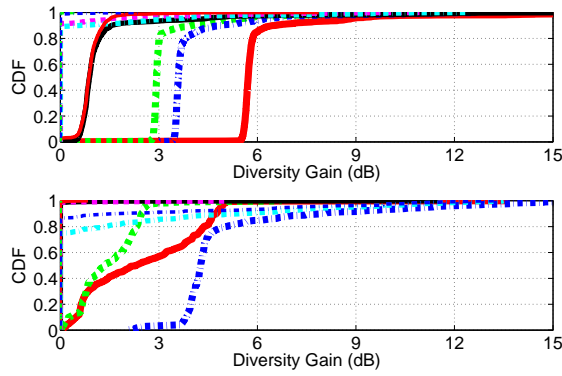than 50% of the time.

Figure 7: Rural opposite: Vehicles approaching (top) and moving away
(bottom). Similar to the urban opposite case, the R and B antenna com-
bination has best performance when vehicles are approaching, whereas
the R and M antenna combination has higher gain when moving away.
Legend is same as in above figure.

3.1   Diversity Gains

The performance differences in antenna gain for each position suggests to use multiple antennas that complement each others performance by exploiting diversity gain [10]. We thus investigate MIMO and single-input multiple-output (SIMO) diversity methods by using selection combining (SC) and maximum ratio combining (MRC) [14]. We first compute the diversity gain using both methods for all possible MIMO and SIMO combinations, i.e. 1x1, 2x2, 3x3, 4x4 and 1x2, 1x3, 1x4 antenna systems, and for all antenna mounts in all measurement scenarios, respectively. We then short list and analyze the most interesting cases, that are 2x2 MIMO diversity with SC and MRC, and 1x2 SIMO diversity with SC only. The cumulative distribution function (CDF) of the diversity gain for 5 measurement scenarios: highway convoy, urban convoy, urban opposite, rural convoy and rural opposite, are shown in Figs. 3-7. The diversity gains presented here are relative to the R-R single-input single-output (SISO) link.

As a first observation, for the given antenna arrangement the R-antenna together with the B-antenna outperform all other antenna combinations (in particular, 1x2 SIMO and 2x2 MIMO). From the results it is evident that the diversity gain for RB-RB MRC is $4 - 5$ dB higher than that for RB-RB SC. It is because there are two channels which are almost equally strong in both settings, either moving in convoy (R-B and R-R) or in opposite direction (B-B and R-R). MRC gives the best system performance [14] but for V2V systems SC could be a preferred solution. Mounting an antenna on the roof and on the bumper require $2 - 4$ m long cables connections from the on-board units (OBU), and this long RF cables will introduce $3.5 - 7$ dB extra attenuation, as a typical cable loss is 1.7 dB/m. This loss can be avoided if the processing units are placed near the antennas and the data is transfered to the OBU via an Ethernet cable. For such a setup, the SC diversity scheme could be more useful than MRC. The antenna gain can be increased $4-5$ dB by using antennas with directional beam patterns, such that the bumper antenna has its main beam in the forward direction and the roof antenna having a somewhat omni-directional antenna pattern.

3.2   Delay and Doppler Spreads

The delay and Doppler spreads are measures of the channel dispersion in time and frequency. The mirror antenna has good gain in both the forward and backward directions, whereas the roof antenna has a somewhat higher gain in the backward direction in the horizontal plane. Similarly, the bumper and windscreen antenna has a very low gain in the backward direction, thus reduc-

ing the experienced delay spread and Doppler spreads. It means that the rms
delay and Doppler spreads are affected by the antenna placement even though
it is the same kind of antenna elements that are used for all antenna positions.
Therefore, it is important to include realistic antenna patterns in simulations,
which is inherent in models such as geometry based stochastic channel mod-
els (GSCM) [15]. From the above diversity based analysis the roof antenna
together with the bumper antenna appears to be the best pair in current set-
tings. In Table 1 the 90th percentile of rms-delay and rms-Doppler spread is
given for all 4 links of the RB×RB antenna combinations. The 90th percentile
is the value for which 90% of the data points are smaller.

4   Summary and Conclusions

In this letter we have presented a measurement based analysis of the impact
of antenna placement on vehicle-to-vehicle communications. This investigation
suggests that a pair of antennas with complementary properties, e.g., a roof
mounted antenna together with a bumper antenna is a good solution for obtain-
ing the best reception performance, in most of the propagation environments.
It is because when vehicles are moving in opposite direction, approaching each
other, the roof and left-side mirror antennas can experience shadowing due to
the roof or body of the transmitter and receiver cars itself, even when there
is line-of-sight in between the cars, whereas the bumper antenna does not suf-
fer from this problem. However, the bumper or windshield antennas do not
provide good coverage to vehicles in the backward direction, which may af-
fect collision warning times severely. Therefore it is better to have a pair of
antennas placed at different positions than to have a single roof or bumper
mounted antenna. The use of these antenna positions requires, however, long
cables which introduce an additional attenuation unless some countermeasures
are taken.

Table 1: 90th Percentile of rms-delay and rms-Doppler spread for the RB×RB
links (2×2 MIMO)

Scenario	$\tau_{rms}(ns)$				$\nu_{rms}(Hz)$			
	R-R	R-B	B-R	B-B	R-R	R-B	B-R	B-B
Highway	10.0	10.8	-	7.8	30	31	-	15.5
Urban-Convoy	35	21.8	55.4	62.6	67	23.6	364	287
Urban-Opposite	21.9	28	32.2	15.2	42.2	107	59.3	26.5
Rural-Convoy	103	21.6	4.1	96	24.1	28.6	-	19.4
Rural-Opposite	12.2	8.5	9.8	10.7	196	26.2	79.7	127

References

[1] J. R. J. K Fujimoto, "Mobile antenna systems handbook," *Artech House, Boston*, 1994.

[2] G. Acosta-Marum and M. Ingram, "Six time- and frequency- selective empirical channel models for vehicular wireless LANs," *IEEE Veh. Technol. Mag.*, vol. 2, no. 4, pp. 4–11, 2007.

[3] S. Kaul, K. Ramachandran, P. Shankar, S. Oh, M. Gruteser, I. Seskar, and T. Nadeem, "Effect of antenna placement and diversity on vehicular network communications," in *4th Annual IEEE Communications Society Conference on Sensor, Mesh and Ad Hoc Communications and Networks, SECON '07*, Jun. 2007, pp. 112 –121.

[4] I. Sen and D. W. Matolak, "Vehicle-vehicle channel models for the 5 GHz band," *IEEE Trans. Intell. Transp. Syst.*, vol. 9, no. 2, pp. 235-245, Jun. 2008.

[5] A. Paier, J. Karedal, N. Czink, C. Dumard, T. Zemen, F. Tufvesson, A. F. Molisch, and C. F. Mecklenbräuker, "Characterization of vehicle-to-vehicle radio channels from measurements at 5.2 GHz," *Wireless Personal Commun.*, vol. 50, pp. 19–29, 2009.

[6] O. Renaudin, V. M. Kolmonen, P. Vainikainen, and C. Oestges, "Non-stationary narrowband MIMO inter-vehicle channel characterization in the 5 GHz band," *IEEE Trans. Veh. Technol.*, vol. 59, no. 4, pp. 2007–2015, May 2010.

[7] A. Thiel, O. Klemp, A. Paier, L. Bernadó, J. Karedal, and A. Kwoczek, "In-situ vehicular antenna integration and design aspects for vehicle-to-vehicle communications," in *EUCAP*, Apr. 2010.

[8] T. Mangel, M. Michl, O. Klemp, and H. Hartenstein, "Real-world measurements of non-line-of-sight reception quality for 5.9 GHz IEEE 802.11p at intersections," *Communication Technologies for Vehicles, Springer Berlin Heidelberg*, vol. 6596, pp. 189–202, 2011.

[9] M. Schack, D. Kornek, E. Slottke, and T. Kürner, "Analysis of channel parameters for different antenna configurations in vehicular environments," in *IEEE 72nd Vehicular Technology Conference (VTC 2010-Fall)*, Sept. 2010, pp. 1 –5.

[10] L. Reichardt, T. Fugen, and T. Zwick, "Influence of antennas placement
     on car to car communications channel," in *3rd European Conference on
     Antennas and Propagation, EuCAP 2009*, March 2009, pp. 630 –634.

[11] R. Thoma, D. Hampicke, A. Richter, G. Sommerkorn, A. Schneider,
     U. Trautwein, and W. Wirnitzer, "Identification of time-variant directional
     mobile radio channels," *Instrumentation and Measurement, IEEE Trans-
     actions on*, vol. 49, no. 2, pp. 357 –364, apr 2000.

[12] T. Abbas, F. Tufvesson, and J. Karedal, "Measurement based Shadow Fad-
     ing Model for Vehicle-to-Vehicle Network Simulations," *ArXiv e-prints*,
     Mar. 2012.

[13] O. Klemp, "Performance considerations for automotive antenna equipment
     in vehicle-to-vehicle communications," in *URSI International Symposium
     on Electromagnetic Theory (EMTS)*, Aug. 2010, pp. 934 –937.

[14] R. Vaughan and J. B. Andersen, *Channels, Propagation and Antennas for
     Mobile Communications (IEE Electromagnetic Waves Series, 50)*. Insti-
     tution of Engineering and Technology, Feb. 2003.

[15] J. Karedal, F. Tufvesson, N. Czink, A. Paier, C. Dumard, T. Zemen,
     C. Mecklenbräuker, and A. F. Molisch, "A geometry-based stochastic
     MIMO model for vehicle-to-vehicle communications," *IEEE Transactions
     on Wireless Communications*, vol. 8, no. 7, pp. 3646–3657, 2009.